Oceanic, Climatic and Vegetation Variability in Western Equatorial Africa since the Penultimate Glaciation

Thesis submitted in accordance with the requirements of the University of Liverpool for the degree of Doctor in Philosophy

by

Rachael Elizabeth Lem

24th October 2018

Oceanic, Climatic and Vegetation Variability in Western Equatorial Africa since the Penultimate Glaciation

Global temperatures are expected to rise by 2 – 2.5 °C by the middle of the 21st century, posing a significant threat to human populations and the natural environment. Tropical West Africa has been classified as a highly vulnerable region; naturally-driven multi-decadal droughts are predicted to become more frequent and intense 20 years ahead of the global average. Examination of past records of large scale climate change is critical in order to validate climate models and mitigate against future global warming. This thesis examines the land-ocean interactions of a small-scale Western Equatorial African (WEA) river catchment and explores its potential as a record of regional and global climatic change during the Late Quaternary Period.

Previous research has documented large-scale WEA climate change using marine cores offshore the Niger and Congo Rivers, however the response of the smaller, medially positioned, Ogooué River catchment remains to be investigated. In 2003, the IMAGES programme recovered 34 m of sediment, spanning the last 150 ka, from the Ogooué Fan, offshore Gabon. Geochemical, sedimentological, isotopic ($\delta^{18}O$ and $\delta^{13}C$), trace element and palynological analyses were carried out. Three research objectives were established: (1) reconstruct the hydrological variability of the Ogooué River catchment through the identification of terrigenous fluvial discharge events; (2) explore the glacial and interglacial control of surface and bottom water $\delta^{13}C$ in the Eastern Equatorial Atlantic (EEA); and (3) examine WEA vegetation biome changes in order to infer the drivers of past regional hydrological and climatic change.

Sedimentological and geochemical investigations demonstrated the strong potential of using a Fe/Ti ratio and foraminiferal planktic $\delta^{18}O$ as proxies for Ogooué River discharge variability. Ogooué discharge events were synchronous with the neighbouring Sanaga and Congo Rivers and were also concomitant with precessional maxima. A preliminary sea surface temperature (SST) reconstruction evidenced coeval SST and salinity responses to riverine discharge variability and highlights an opportunity to undertake further trace element analysis on the study material.

Planktic and benthic $\delta^{13}C$ stratigraphies were constructed in order to produce the first $\Delta\delta^{13}C$ gradient record from a region of EEA not dominated by upwelling. Thermocline – bottom water $\Delta\delta^{13}C$ evidenced an alternation of nutrient-poor North Atlantic Deep

Water influx during glacial periods and nutrient-rich Antarctic Intermediate Water masses during interglacial periods. Locally, planktic $\delta^{18}O$ data support that precessionally driven riverine discharge events contributed to the $\delta^{13}C$ of the planktic foraminifera *Globigerinoides ruber* (white variety).

Finally, vegetation change in the Ogooué River catchment, and wider WEA, was documented through palynomorph reconstructions. Pollen data evidences a transition from grassland vegetation in glacial marine isotope stage (MIS) 6, through to more precipitation dependent lowland rainforest and swamp biomes from interglacial MIS 5 (~ 100 ka) to present day. High abundances of rainforest taxa in MIS 4-2 suggests rainforests remained as refugia facilitated by a weaker monsoon. The mangrove pollen, *Rhizophora,* is interpreted as an indicator of sea level change, with high abundances in MIS 5 and 1 evidencing sea level rise. Lastly, the Afromontane pollen *Podocarpus,* shows a strong correspondence with precession minima, suggesting alternating dominance of trade wind and monsoon intensity over the 23 ka precessional cycle.

Acknowledgements

My PhD journey has been a remarkable four years defined by new challenges and immense rewards, made possible by the kindness and backing of my family and my many colleagues and friends. First and foremost I would like to thank my funder NERC for their financial support and also the multiple opportunities to attend diverse and valuable training courses. I am indebted to my supervisor Dr Fabienne Marret for her perpetual support, encouragement and guidance and for allowing me to take full reign of my project. Fabienne has cheered me on at every opportunity and for this I am very grateful. Professor Jim Marshall has been an invaluable supervisor, offering continual direction and ideas that had not originally occurred to me, but most importantly, he has been a kind and generous constant in my times of need. I am incredibly grateful for the advice, opportunities and kindness that Professor Melanie Leng has given me; her feedback on my thesis has been instrumental and her encouragement to pursue an academic career has been greatly appreciated.

I feel extremely fortunate to have studied within and had the backing of such a diverse and encouraging physical geography research group. I cannot thank Professor Richard Chiverrell and Dr John Boyle enough for their continuous guidance and patience; their knowledge and input has transformed my sedimentological and geochemical analyses. I would also like to thank Dr Barbara Mauz for her subject guidance, Professor Andreas Lang and Dr Hugh Smith for their career advice, and Professors Andy Plater and Janet Hooke for providing me with demonstrating opportunities, but more importantly jovial chats at lunch time.

I am appreciative of the support and time extended to me by the School of Environmental Sciences' technical staff: Mike O'Connor, Alan Henderson, Chris Cakebread, Jenny Bradley, Danny Jones, Mhari Birchall, Steven Crowley, James Utley, Carmel Pinnington and Sabena Blackbird. I am also indebted to the Stable Isotope Facility team at the British Geological Survey, Keyworth; the insight from Professor Melanie Leng and Dr Sev Kender and the continual laboratory assistance from Hilary Sloane and Chris Kendrick have been invaluable. Thanks also go to Drs Jonathan Dean, Andi Smith and Keely Mills for always being ready to have lunch and tea breaks on my visits. I am also grateful for the instruction and friendly support given to me by Drs Lydie Dupont and Ilham Bouimetarhan during my two weeks of pollen training in

Bremen and similarly to Dr Leon Clarke for his thorough training in Mg/Ca analysis at Manchester Metropolitan University.

I am incredibly grateful for the number of students that assisted with my research by undertaking partnership analysis on the MD03-2708 sediment core. Thanks go to Laura Merij for her stoic work during the very hot summer of 2014; to Michael Davies for his enduring approach to foraminiferal assemblage analysis in 2015; and also to the BSc students who gave up parts of their holiday to undertake summer internships with me in 2016 – their hard work and knowledge was remarkable.

For the last four years, the 'Roxby Tower' has been a comfortable and familiar constant for me. The morale and friendship of my fellow PhD and postdoctoral students cannot be overstated - (in office order) – thanks go to Dan, Onema, Soeren, Ben, Ai, Chris Feeney, Jen Clear, Tim, Bev, Fiona, Karen, Charlotte, Matt Benwell, Veronica, Thea, Maddy, Hazel, Sion, Simon, Sally, Celestine, Sam, Chris Oldknow, Phil, Amy, Matt Wallace, Cai, Kush, Madeleine, Josh, Maddie Brasier, Lee, Heather and Matt Burke.

Along with Amy Lennard, Cai Bird and Poonperm (Ai) Vardhanabindu, undertaking the NERC Environment YES competition in the autumn of 2014 was a milestone in my PhD experience. Not only did we come away from the final with a trophy that has been a vital window prop for the Roxby 805C office for the last three years, but the experience created a friendship between the four of us that shall last a life time. I shall miss our laughs, jokes and shared experiences, but I shall not miss being the 'financial expert' of the group!

Finally, I would like to thank my close friends and family for their perpetual reassurance and belief. I am eternally grateful for the love and dedication of my Mom and Dad who have supported me emotionally, financially and academically throughout my life. It has been a long, and at times, rocky journey, but with their encouragement I have kept on travelling and for that I am truly grateful.

Table of Contents

1 Introduction

1.1. Rationale and Research Objectives

Evidence that present day climate is changing is overwhelming (IPCC, 2014). In recent decades, significant changes in the global climate system have been detected (e.g. Beniston, 2004; Meehl and Tebaldi, 2004; O'Gorman and Schneider, 2009). Impacts of climate extremes such as heatwaves, droughts, floods and cyclones are predicted to become more regular and widespread, posing a significant threat to many vulnerable human populations and ecosystems (IPCC, 2014). Africa is the most susceptible continent to climate change (IPCC, 2014), with its vulnerability exacerbated by existing socio-economic challenges, poor infrastructure and ecosystem degradation (IPCC, 2007). Despite its physical and social fragility, little research has been undertaken into the implications of climate change scenarios for Africa (Brown, 2012).

Developing a rigorous understanding of the past environment and climate of the tropics is critical to ensure the validation of climate models and ultimately the mitigation of extreme climate change. Tropical West Africa (TWA) in particular has been identified as an unprecedented hotspot of climate change (Diffenbaugh and Giorgi, 2012). TWA is a region of global ecological importance (Myers *et al.,* 2000) that is undergoing unprecedented human population growth (Shanahan *et al.*, 2013). The naturally driven multi-decadal drought that is experienced in the region (Shanahan *et al.*, 2012) is predicted to become more frequent and intense as early as the late 2030s, a number of decades ahead of the global average (IPCC, 2007).

1.1.1 Late Quaternary Climate Variation

Palaeoclimate archives from polar ice cores (e.g. Petit *et al.,* 1999; Johnsen *et al.,* 2004), terrestrial records (e.g. Roberts *et al.*, 2008; Lamb *et al.*, 2016) and marine sediment sequences (e.g. Cita *et al.*, 1977; Zachos *et al.,* 2001) evidence that global climate has varied in the past without anthropogenic intervention. The principal drivers of past climatic changes are variations in precession (~ 23 ka cycle), obliquity (~ 41 ka cycle) and eccentricity (~ 100 ka cycle) of the Earth's orbit around the Sun. The oscillation of these orbital parameters has resulted in global temperature fluctuations of ~ 5°C (Delcourt and Delcourt, 1991), causing the Earth to transition between a series of warm (interglacial) and cold (glacial) periods during the Late Quaternary Period (the last ~

2.6 million years) (Berger, 1978). The precessional cycle plays a key role in controlling low-latitude climate, and in conjunction with obliquity, modulates the growth of northern hemisphere ice sheets (Martinson *et al.*, 1987). This ice sheet fluctuation forces the rest of the climate system and exerts control on the tropics and even the Southern Hemisphere.

1.2. Scientific Objectives

The main objective of this work is to formulate a high resolution reconstruction of oceanic, climatic and vegetation variability from the Eastern Equatorial Atlantic (EEA) over the past 150 ka. This work particularly aims to explore the sensitivity of a small-scale river catchment in documenting hydrological variability throughout the glacial and interglacial periods since Marine Isotope Stage 6. This palaeoclimatic study will assist in the better understanding of the tropical West African climate system and will provide data to drive and validate palaeoclimate models, which can then be applied to predict future climate change.

1.2.1 Research Aims

Within this thesis three specific research aims were addressed:

(1) Prior research (e.g. Schneider *et al.*, 1997; Marret *et al.*, 2001; Holtvoeth *et al.* 2003; Zabel *et al.*, 2001; Weldeab *et al.*, 2007) has explored the response of the EEA Ocean to the discharge variability of large scale riverine catchments (Congo, Sanaga and Niger Rivers), but the local sensitivity of smaller catchments remains to be investigated. This study aims to reconstruct the hydrological variability of the Ogooué River catchment over the last 156 ka by using sedimentary elemental ratios, planktic foraminiferal $\delta^{18}O$ and the Mg/Ca ratios of foraminifera shells as indicators of enhanced terrigenous fluvial discharge.

(2) Attention has been given to the ocean upwelling regions on the tropical West African coastline (e.g. Mulitza *et al.*, 1998; Abrantes, 2003; Subramaniam *et al.*, 2013), but little research has been undertaken on the quasi-nutrient rich intermediate waters between them. Here planktic and benthic foraminifera, as well as fine fraction carbonate $\delta^{13}C$, are examined in order to produce the first palaeo-reconstruction of $\delta^{13}C$ dynamics in the Ogooué Fan and used to

better understand the glacial and interglacial control of $\delta^{13}C$ in the surface and bottom waters of the EEA.

(3) Climate models suggest that temperature will increase in the coming decades (IPCC, 2014), altering the regional hydrological balance and precipitation regimes. How the vegetation of WEA, especially the grassland-savannah-forest complex will respond to these drivers remains unclear (Scheiter and Higgins, 2008). Fossil pollen records which span periods of global climate change of a comparable magnitude can be used to fill in current vegetation change knowledge gaps (Miller and Gosling, 2014). This thesis will develop biome reconstructions from catchment scale pollen data to infer the drivers of climate change in West Africa over the past 156 ka.

1.3. Thesis Structure

This thesis explores the sedimentology, geochemistry and micropalaeontology of a sediment core extracted from the Ogooué margin, offshore Gabon, to reconstruct land-ocean climatic interactions over the past 156 ka. This introductory chapter (Chapter 1) is followed by a summary of the environmental setting (Chapter 2), outlining the atmospheric, oceanographic and vegetation characteristics of the study region. The methods used throughout this thesis are outlined in Chapter 3 and are succeeded by an account of the sedimentology of the studied core (Chapter 4) and an overview of the formation of the age model used in this study (Chapter 5). The following three chapters represent the main findings of this thesis; they are written in a quasi-manuscript style and will be submitted for publication in international journals. The first paper (Chapter 6) examines the response of the Eastern Equatorial Atlantic to riverine discharge over the last 156 ka. The second paper (Chapter 7) explores the orbitally driven riverine control of surface and bottom water $\delta^{13}C$ in the Eastern Equatorial Atlantic. The last paper (Chapter 8) presents glacial-interglacial vegetation change in the Ogooué catchment since Marine Isotope Stage 6. The final chapter of the thesis (Chapter 9) summarises the findings from chapters 4-8, presents conclusions related to the research aims and suggests directions for future research (Section 1.2).

2 Environmental Setting

2.1. Marine Dufresne Site MD03-2708

Marine Dufresne site MD03-2708 is located at the periphery of the Ogooué Delta at approximately 920 m water depth (01° 10.33'S, 08° 19.01'60E), 72 km offshore Gabon [Figure 2-1]. Two cores were recovered during the PICABIA cruise on board the French RV Marine Dufresne in August 2003 (Beard, 2004). A composite sequence was generated comprising a giant piston core – MD03-2708 [GPC] (length: 34.20 m) and a giant gravity 'Casq' core – MD03-2708 [CQ] (length: 7.89 m). Lithologically, sediments are composed of very dark green-grey clay and silty clays (Beard, 2004). Core MD03-2708CQ has been used in this study for the construction of the age model only [Chapter 5]; all other observations and data analysis are based on core MD03-2708 GPC.

2.1.1 Previous Research at Site MD03-2708

The MD03-2708 marine sediment cores examined in this thesis were taken as part of the IMAGES programme (Beard, 2004). The International Marine Past and Global Changes Study (IMAGES) programme was developed in 1996 to quantify global palaeoceanographic and climatic changes using high-resolution oceanic sedimentary records, and in this instance, specifically to collect data to test whether intense palaeodischarge episodes from the Ogooué River were linked to the latitudinal positioning of the Intertropical Convergence Zone (ITCZ).

Previous research has been undertaken on the casq core (MD03-2708CQ) by multiple authors. Using a combined pollen and dinoflagellate cyst palaeoclimate reconstruction approach covering the last 26,000 years, Kim *et al.* (2010) demonstrated that terrestrial Gabon and the adjacent ocean were impacted synchronously by significant climate changes during the last glacial-interglacial transition and the Holocene. During the Last Glacial Maximum (LGM), pollen records indicated an expansion of open forest, savannah woodland and Afromontane forest, whilst heterotrophic dinoflagellate cysts and high Ca XRF counts, indicated increased productivity off the Ogooué River mouth (Kim *et al.,* 2010). The transition from the deglaciation to the mid Holocene is marked by a decrease in grassland and Afromontane communities, an expansion of mangrove pollen and a disappearance of heterotrophic dinoflagellates, indicating enhanced

fluvial discharge of the Ogooué River, facilitated by a strengthening of the West African Monsoon system (Kim *et al.,* 2010).

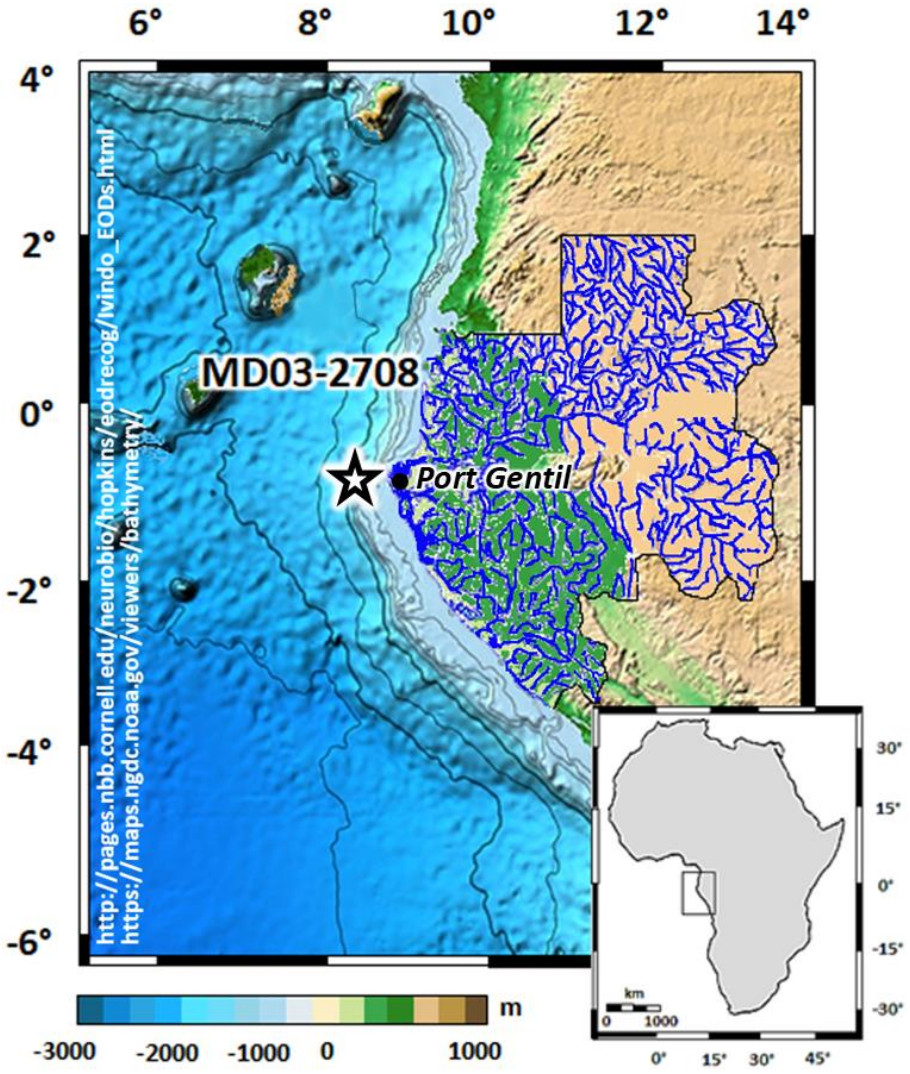

Figure 2-1: Location of Marine Dufresne Site MD03-2708 marked by a star. Ocean bathymetry and land topography are illustrated and the watershed of the Ogooué River over Gabon is given. Map adapted from NOAA bathymetric data viewer [https://maps.ngdc.noaa.gov /viewers/bathymetry] and University of Cornell online library [http://pages.nbb. cornell.edu/neurobio/hopkins/eodrecog/Ivindo_EODs. html], accessed on 30/08/2018.

Work undertaken by Jacobsen (2012) explored the sea-surface conditions of the Eastern Equatorial Atlantic Ocean, off the Ogooué River mouth, over the past 25,000 years. The author used planktonic foraminifera assemblage changes over the time period to identify the surface water control in the Ogooué Basin since the LGM. Jacobsen (2012) outlines that during the LGM surface conditions of the Eastern Equatorial Atlantic were influenced by Antarctic currents, resulting in cool and nutrient rich waters. Ocean

productivity decreased during the transition into the Holocene due a northward shift of the ITCZ and a warming of the surface waters, regulated by the South Equatorial Current.

2.1.2 Site Location Rationale

Submarine fans adjacent to large rivers draining monsoonal regions have been acknowledged as important and underexploited palaeoclimate archives (e.g. Marret *et al.,* 2001; Kim *et al.,* 2010). Prior to the acquisition of core MD03-2708, the climatic evolution of the Ogooué Basin had not been previously investigated due to a scarcity of long and continuous sedimentary records from this region (Kim *et al.,* 2010). A discharge of 4758 m^3/s attributes the Ogooué River as the third largest river in West Africa and although the water discharge is a magnitude lower than the neighbouring Congo River, the particulate load of the two rivers is analogous (Seranne *et al.,* 2008). The Ogooué Fan was therefore targeted as a coring location under the assumption that it would likely contain an integrated terrestrial and marine record of palaeoclimatic signal, similar to those documented from neighbouring deep-sea fans.

2.2. The Ogooué River and Basin

The Ogooué River is 1200 km long and is the principal river of Gabon (Scheffel *et al.* 1980). It has a catchment size of 203,000 $km^{2,}$ which is moderate in comparison to those of the Congo (3,550,000 km^2) and Niger (1,100,000 km^2) Rivers (Mahé and Olivry, 1995). The Ogooué River flows west-north-west and discharges into the Gulf of Guinea south of Port Gentil on both sides of Cape Lopez (Serrane *et al.,* 2008; Biscara *et al.*, 2011) [Figures 2.1 – 2.3]. Most parts of the river run through tropical rainforest and then mangrove forest on entering the Ogooué Delta [Figure 2-8]. Two periods of flooding are experienced in May and November, generated by the West African Monsoon (Biscara *et al.*, 2011).

The Ogooué Delta [Figures 2-2 & 2-3] is a lowland coastal plain (Serrane, 2008). Offshore, the delta grades into a fan that extends across the continental shelf and slope into the deep ocean. The Gabonese shelf is narrow, decreasing from 60 km northwards to its most narrow point of 5 km at Cape Lopez [Figure 2-3] (Biscara *et al.,* 2011). Cape Lopez is located at the northern end of the Ogooué Delta [Figure 2-3] and is created by a strong northward flowing littoral drift (Biscara *et al.,* 2011). The Western Equatorial African Margin, offshore Gabon, Angola and the Congo, presents large depocenters

[Figure 2-2] where sediments have been accumulating since Early Cretaceous rifting (Bentahaila *et al.,* 2005). Sediment accumulation is mostly derived from terrigenous flux of the coastal rivers e.g. Ogooué, Kouilou and Congo [Figure 2-2] (Bentahaila *et al.,* 2005). As can be seen from Figures 2-2 and 2-3, core MD03-2708 was deliberately positioned at the edge of the Ogooué delta in order reconstruct past terrigenous influx as well as a palaeomarine signal.

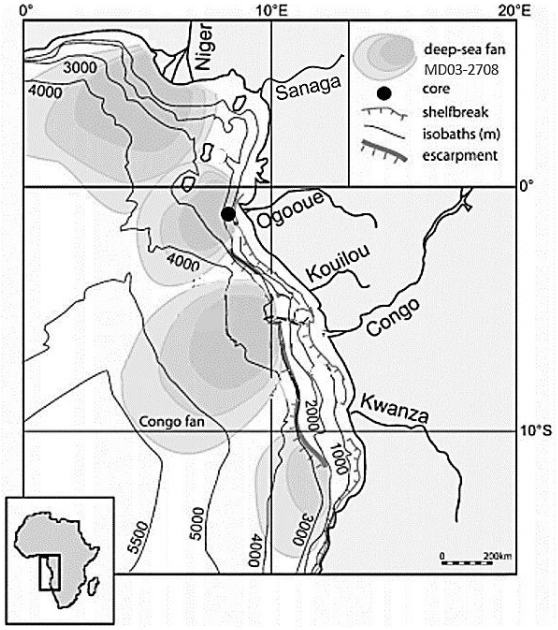

Figure 2-2: The fans and sedimentary basins of the West African rivers. After Bentahaila *et al.* (2005).

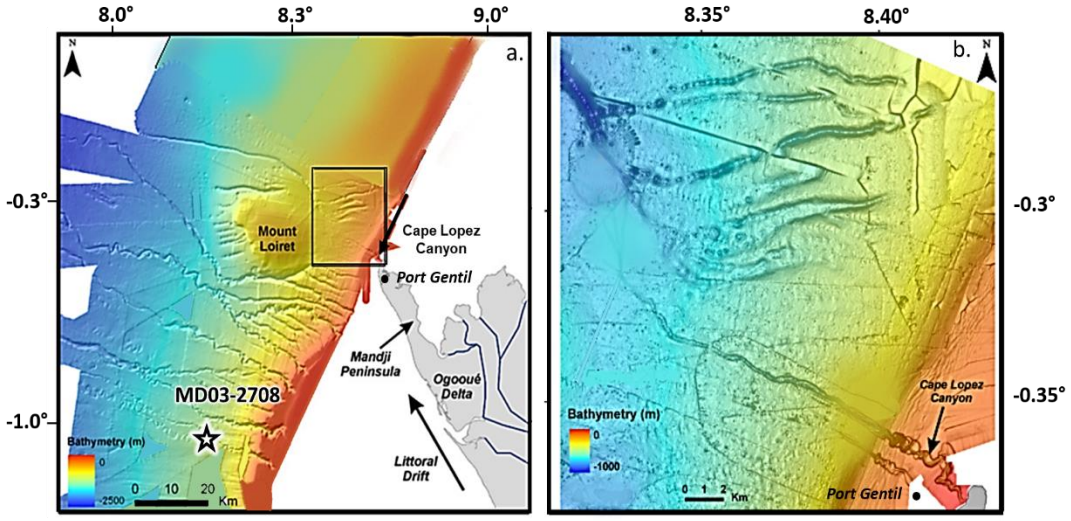

Figure 2-3: a) General bathymetric map of the Ogooué Delta and the morphology of the proximal part of the turbidite system; b) Bathymetry adjacent to Cape Lopez Canyon. [After Biscara *et al.* (2011)].

2.3. Oceanographic Setting

Locally, the Gulf of Guinea is governed by the Guinea Current (GC) - a slow warm water current that flows along the northern coast of the gulf (Henin *et al.,* 1986). The GC is characterized by areas of upwelling (Bakun, 1978) and increased biological productivity (Binet, 1997).

The Eastern Equatorial Atlantic is influenced by a number of surface and subsurface currents [Figure 2-4]. The Benguela Current (BC), an eastern boundary current of the South Atlantic tropical gyre, is the primary oceanographic feature controlling the regional surface waters (Wedepohl *et al.* 2000). Driven by the south-eastern trade winds, the BC moves north-westward along the coast of southern Africa, transporting cold, saline water into the eastern tropical Atlantic in boreal summer (Lass *et al.,* 2000).

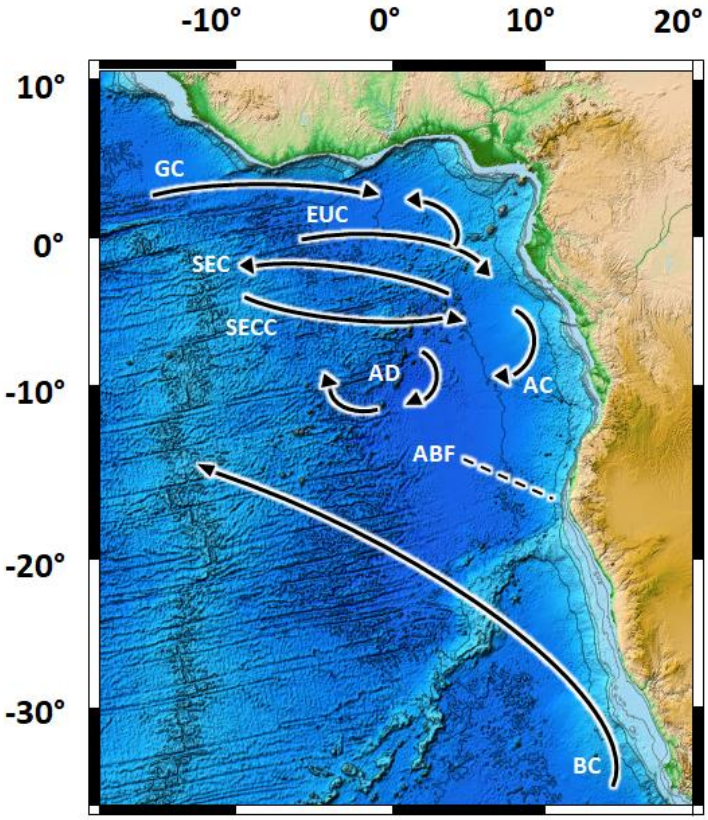

Figure 2-4: Eastern Equatorial Atlantic surface and subsurface currents. Warm currents - GC: Guinea Current; SEC: South Equatorial Current; SECC: South Equatorial Counter Current; AC: Angola Current; and AD: Angola Dome. Cold current – BC: Benguela Current. Under Current – EUC: Equatorial Under Current. Transient Angola-Benguela Front (ABF) depicted as a dashed black arrow.

The South Equatorial Current (SEC) is a broad, westward flowing current which extends from the surface to a nominal depth of 100 m below sea level (Bonhoure *et al.,* 2004). Fed by the Benguela Current (BC), the SEC crosses the equator to flow westward towards the Brazilian coast, exporting warm, tropical water into the North Atlantic (Bonhoure *et al.,* 2004; Kim *et al.*, 2010). North of the SEC, the easterly directed water masses of the South Equatorial Countercurrent (SECC) form a cyclonic gyre known as the Angola Dome (AD) which transports warm equatorial water through the Angola Current (AC) southwards (Schneider *et al.,* 1994).

The AC flows southwards along the south-east African coast and at approximately 15 °S merges with the Benguela Current to form the Angola-Benguela Front (ABF) (Meeuwis and Lutjeharms, 1990). The ABF separates the warm, nutrient-poor Angola Current water and the cold, nutrient–rich Benguela Current water, creating a transition zone between the upwelling-driven ecosystem in the south, and the tropical ecosystem in the north (Lass *et al.,* 2000). This transition is marked by the development of a sharp thermal front, characterised by a temperature transition from 27 °C to 25 ° (Moroshkin *et al.,* 1970).

Below the surface and subsurface currents, the Eastern Equatorial Atlantic is additionally influenced by Antarctic Intermediate water (AAIW) [Figure 2-5]. The AAIW is created when deep North Atlantic Water rises to the surface and is warmed and diluted by rainfall; it has a varying temperature range between 3 °C and 6 °C.

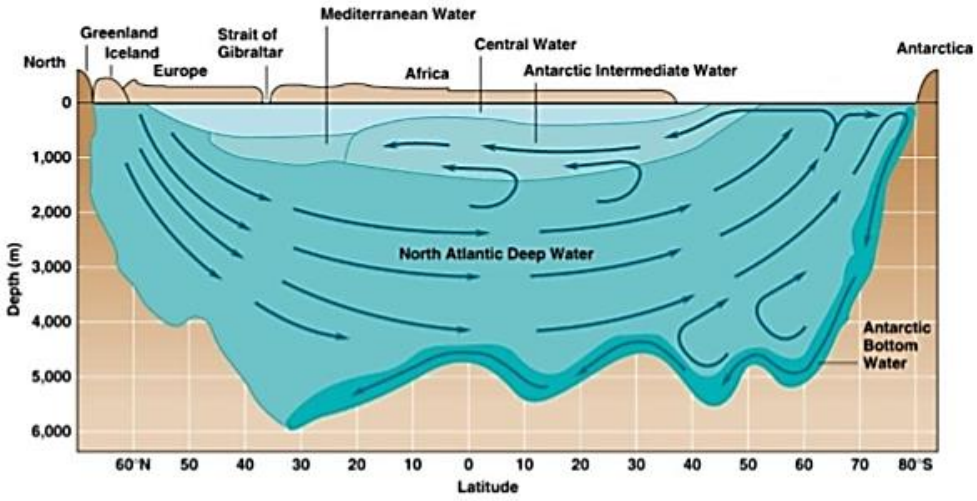

Figure 2-5: The deep water layers of the Atlantic Ocean and their flow direction (Jacobsen, 2012).

2.4. Regional Climate

Atmospheric circulation in Western Equatorial Africa is governed by the ITCZ [Figure 2-6]; an area of low pressure between the two Hadley cells. Characterised by convective precipitation, the West African rain belt is located to the south of the ITCZ and is largely facilitated by the ascending air between the Tropical Easterly Jet and the African Easterly Jet streams (Nicholson, 2009). The position of both the rain belt and the ITCZ oscillate latitudinally on a seasonal basis. The ITCZ reaches its northernmost position at about 20 °N during boreal summer (June to August) and southern limit of 5 °N during boreal winter/austral summer (December to January). Driven by the seasonal reversal of winds, the West African Monsoon (WAM) blows on land during boreal summer, and the Eastern African Monsoons [Northerly East African monsoon (NEM) and Southerly East African monsoon (SEM)] during boreal winters (Gasse *et al.*, 2008).

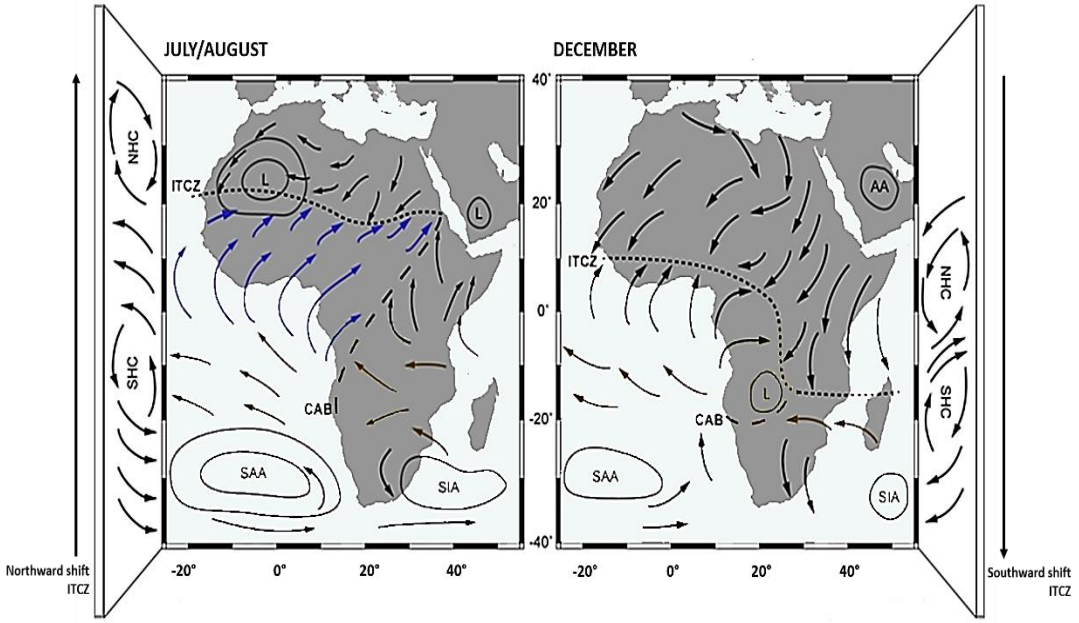

Figure 2-6: Low-level wind and pressure patterns during boreal summer (left) and boreal winter (right) [Gasse 2008; Nicholson 1996]. Some aspects of present day African climate are marked: NHC, northern Hadley Cell; SHC, southern Hadley Cell; NAA, North Atlantic Anticyclone; SAA, South Atlantic Anticyclone; SIA, South Indian Anticyclone; AA, Arabian Anticyclone; WAM, West African Monsoon; NEM, northerly East African monsoon; SEM, southerly East African monsoon; and Intertropical Convergence Zone (ITCZ).

Western Africa is also governed by two dominant surface wind systems – the north-east (NE) and south-east (SE) trade winds, which blow from high pressure regions and

converge at the Intertropical Convergence Zone (ITCZ). The high pressure cells of the North Atlantic Anticyclone (NNA) and the South Atlantic Anticyclone (SSA) intensify and shift equatorward during the corresponding winter season (Nicholson, 1996; Leroux, 2003).

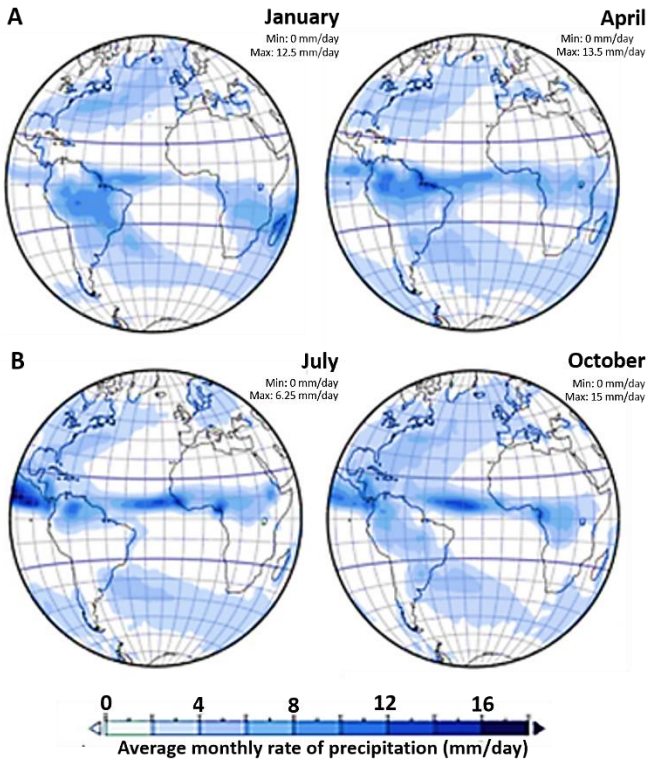

Figure 2-7: The rate of precipitation over tropical Africa. A) Boreal winter; B) Boreal summer. After Hessler *et al.* (2011).

Mean-annual precipitation extends between more than 2000 mm/yr at the equator and less than 100 mm/yr in the desert regions. Central Africa and the Western Equatorial African coastline experience two wet seasons per year, due to the rain belt crossing overhead twice, whilst peripheral regions only experience one west season (Gasse *et al.*, 2008). The present day mean monthly precipitation of Gabon is approximately 200 mm. Maximum monthly precipitations ranges from 6.25 mm/ day in July to 15 mm/ day in October [Figure 2-7].

2.5. Vegetation on the Adjacent Continent

One of the most widely used classifications of African vegetation is the map of White (1983). Grouped according to floristic regions, White (1983) defined 16 phytogeographical zones for the African continent [Figure 2-8-b]. The phytogeographical distributions are largely determined by mean annual rainfall and dry season length, although local conditions such as water availability and soil type and structure can also contribute (White, 1983). Publications focussing on the intricate

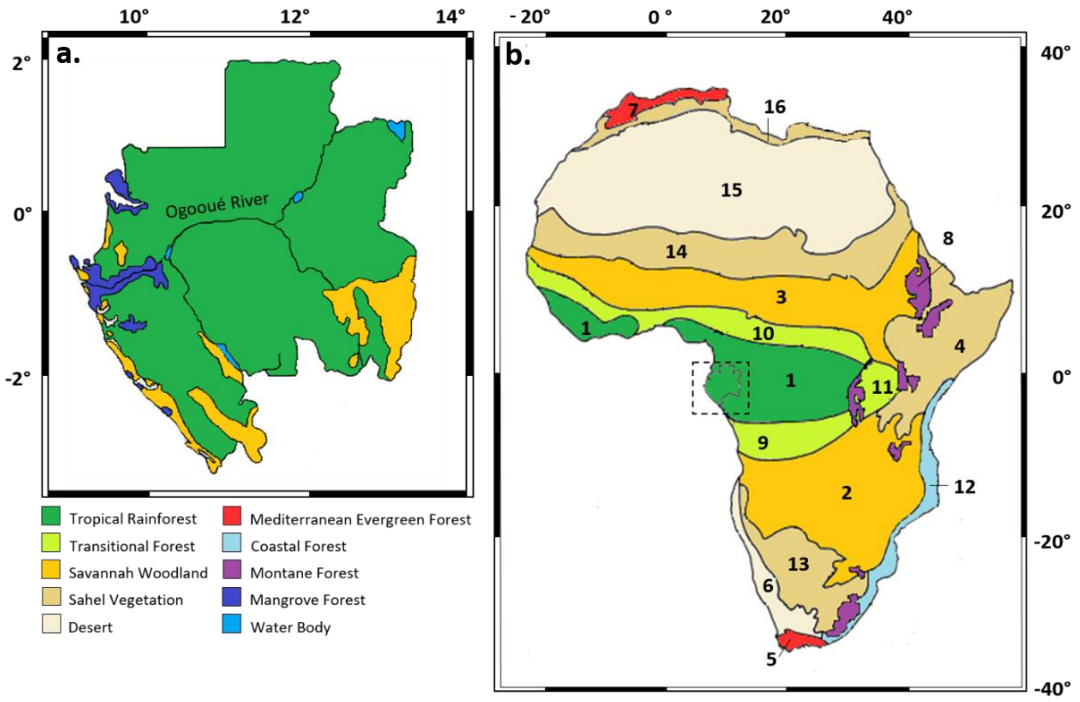

Figure 2-8: Simplified phytographic regions and vegetation biomes of Africa [after White 1983]. 1, Guinea-Congolian regional centre of endemism; 2, Zambezian regional centre of endemism; 3, Sudanian regional centre of endemism; 4, Somalia-Masai regional centre of endemism; 5, Cape regional centre of endemism; 6, Karoo-Namib regional centre of endemism; 7, Mediterranean regional centre of endemism; 8, Afromontane archipelago-like regional centre of endemism, including afro-alpine archipelago-like region of extreme floristic impoverishment; 9, Guinea Congolian/Zambezian regional transition zone; 10, Guinea-Congolian/Sudanian regional transition zone; 11, Lake Victoria regional mosaic; 12, Zanzibar-Inhambane regional mosaic; 13, Kalahari-Highveld regional transition zone; 14, Sahel regional transition zone; 15, Sahara regional transition zone; and 16, Mediterranean/Sahara regional transition zone.

vegetation composition of Gabon are rare. Consequently the following discussion is based mostly on information documented by White (1983) and will focus on the vegetation of Gabon and the surrounding phytogeographical regions.

The vegetation of Gabon is comparably uniform, consisting predominantly of tropical (Guinea-Congolian) rainforest [Figure 2-8-a]. Gabon is buffered by: transitional (Guinea-Congolian/ Sudanian) swamp and riparian forests to the north; transitional (Guinea-Congolian/ Zambezian) dry forest to the south; afromontane forest to the east; and mangrove swamps along the coastline and at the intertidal confluence of the Ogooué River (White, 1983).

2.5.1 Tropical Rainforest

Guinea-Congolian Vegetation

The Guinea-Congolian region (numbered '1' on Figure 2-8-b) extends as a broad band from 10 °N to 5 °S and consists largely of lowland rainforest and swamps (White, 1983). Regional altitude is below 1000 m, except for the Eastern Congo basin, where rainforest transitions into afromontane communities (White, 1983). Rainfall varies between 1600 and 2000 mm per year (White, 1983). The region houses an estimated 8000 species, of which roughly 80 are endemic. Three primary variants of Guinea-Congolian vegetation exist in Gabon: hygrophilous coastal evergreen rainforest (e.g. *Sacoglottis gabonensis* [Humiriaceae]) prevails along the coastline; mixed moist semi-evergreen rainforest (e.g. *Pericopsis elata* [Fabaceae]) extends over North-Eastern Gabon; and semi-evergreen forest (e.g. *Julbernardia* [Fabaceae]) occurs in small pockets across the country (White, 1983).

2.5.2 Transitional Forest

Guinea-Congolian/ Sudanian Transition Zone Vegetation

The Guinea-Congolian/ Sudanian Transition Zone (labelled '10' on Figure 2-8-b) extends from Senegal to Western Uganda. Altitude is predominantly less than 750 m and the climate is transitional between those of the wet Guinea-Congolian and drier Sudanian regions (White, 1983). Less than 2000 species prevail, of which one third are endemic. The western half of the transition zone is dominated by swamp and riparian forests (e.g. *Berlinia grandiflora* [Caesalpiniaceae]). Sudanian dry forest prevails in the

east, occurring in deep ravines and on the sandstone plateaux of western Mali (e.g. *Caesalpiniaceous* [Caesalpiniaceae]) (White, 1983).

2.5.3 Guinea-Congolian/ Zambezian Transition Zone Vegetation

The Guinea-Congolian/ Zambezian Transition Zone (numbered '9' on Figure 2-8-b) extends from the Atlantic Ocean to the high ground of the Congo-Burundi border (White, 1983). The altitude of the region extends between 1000 and 1500 m and a maximum of 800 mm of rainfall is received per year. The region comprises less than 2000 species, only a few of which are endemic. The greater part of the transition zone is occupied by secondary grassland and wooded grassland, dominated almost completely by Zambezian species (White, 1983). The region can be sub-divided into three primary groupings: drier peripheral semi-evergreen Guineo-Congolian rainforest (e.g. *Albizia zygia* [Mimosaceae]); Zambezian dry evergreen forest and transition woodland (e.g. *Marquesia macroura* [Dipterocarpacerae]); and Grassland and wooded grassland (e.g. *Aristida vanderystii* [Poaceae]) (White, 1983).

2.5.4 Afromontane Vegetation

Afromontane forests [labelled '8' on Figure 2-8-b] occur at altitudes between 1200 m and 2500 m (White, 1983). The extension of Afromontane forest is temperature and topography dependent, with forests occurring at increasing elevations with distance inland from the coast. In West Africa, Afromontane communities prevail in the mountains of Cameroon and Angola and are dominated by conifers *Podocarpus falctus, P. gracilior and P. latifolius* (Podocarpaceae) and tree ferns *Cyathea* (Cyatheaceae) (White, 1983).

2.5.5 Mangrove Vegetation

Mangrove vegetation occurs along the intertidal zone of West Africa between 19°50'N and 12°30'S (Lezine, 1991) [Figure 2-8-b]. Optimal mangrove colonisation occurs at the mouth of large rivers (e.g. the Niger and Congo Rivers), buffered from the direct influence of ocean swell and currents, and where it benefits from a combination of dilute sea water and freshwater nutrient input (Blasco, 1982). Mangrove stands can also penetrate inland river systems, as is the case for the Ogooué River [Figure 2-8-a], (Hopkins and White, 1987). Along the Gabonese coast, *Rhizophora* (Rhizophoraceae), is dominant in most areas and largely comprises three species - *R. mangle, R. harrisonii* and *R. racemosa* (Van Campo and Bengo, 2004). The species *Avicennia germinans, A.*

africana and *A. nitida,* (Avicenniaceae) and *Laguncularia racemosa* (Combretaceae) are also present (Spalding *et al.,* 1997).

3 Methodology

The work undertaken on marine core MD03-2708 can be subdivided into seven forms of laboratory analyses. This entails sedimentology, geochemistry, carbonate, isotope, micropalaeontology, trace element and palynology analyses.

3.1. Sedimentological Analyses

Marine sediments comprise three major components – detrital, biogenic and authigenic, based upon their origin. Detrital sediments reach the ocean through the air (aeolian) and riverine (fluvial) input and consist of terrigenous, volcanic and cosmogenic material (Berger and Winterer, 1974; Holz *et al.*, 2004). The authigenic component is derived from inorganic minerals (e.g. evaporates and hydrogenous ferromanganese oxides) that precipitate directly from the water column, or within the sediment after burial. Biogenic sediments are made up of the skeletal remains of marine phytoplankton and zooplankton (e.g. foraminifera, coccolithphores and diatoms), (Berger and Winterer, 1974).

The Atlantic Ocean receives a significant amount of terrigenous material from the African continent (Govin *et al.,* 2012). The proximity of core MD03-2708 to the adjacent continent is significant in that it records both the terrestrial history of the West African continent, whilst also affording a record of palaeoceanographic activity by providing data on Atlantic oceanic water movements and marine productivity (Rothwell and Croudace, 2015).

3.1.1 Particle Size Analysis

In the eastern equatorial Atlantic, oceanic (deep and surface water currents), hydrological (fresh water riverine supply) and atmospheric conditions (wind fields) determine the transport mode of terrigenous material from the West African continent to the continental shelf (Briceño-Zuluaga *et al.*, 2016). The particle size of marine sediments can be used to infer source provenance under the assumption that terrigenous sediments with a modal grain size larger than 6 μm are attributed to aeolian dust fallout, whereas hemipelagic deposition is assumed for particles smaller than 6 μm (Sarnthein *et al.*, 1981; Stuut *et al.*, 2002; Holz *et al.,* 2004; Mulitza *et al.*, 2010). Before the particle size distribution of the terrigenous fraction is determined,

equivalent sized marine components (e.g. calcium carbonate tests and diatom biogenic silica) need to be considered and either removed prior to analysis (calcium carbonate) or considered during the PSA data interpretation (biogenic silica) (Maiklem, 1968; Busseler *et al.,* 2001).

Particles size distributions were determined upon weighed freeze dried sediments using laser granulometry. Measurements were made using a Beckman Coulter™ LS 200 and a LS I3 320 at the University of Liverpool. To remove the calcium carbonate and organic content respectively samples (~ 5 g) were pre-treated with 20 ml hydrochloric acid (HCl) (6 %) until the sample stopped reacting, diluted with 40 ml double distilled water (DD H_2O), and then heated on a hot plate until the liquid had evaporated. The dried sample was rehydrated in 20 ml of hydrogen peroxide (H_2O_2) (6 %) and once again heated until the liquid had evaporated. Prior to measurement, between two and five ml of sodium hexametaphosphate ($NaPO_3$) was added to each sample to aid the dispersal of particles, and then the samples were run under sonicating conditions. Final results were averaged from three runs to ensure that intra-sample variability remained low. Particle size frequency statistics were calculated using the geometric formulae of Folk and Ward (1957) with the GRADISTAT 8.0 software (Blott and Pye, 2001).

3.1.2 Magnetic Susceptibility Analysis

Environmental magnetism involves the application of mineral magnetic techniques (e.g. magnetic susceptibility) to situations in which the transport, deposition, or transformation of magnetic grains has been influenced by environmental processes in the lithosphere, hydrosphere and atmosphere (Verosub and Roberts, 1995). Marine sediments with high terrigenous content provide high quality palaeomagnetic records (Stoner and St-Onge, 2007) and further help to determine aeolian and terrigenous source provenances.

Low field magnetic susceptibility (χ) was measured on archive plates of the core sediment at a resolution of two mm using an 'ITRAX XRF Corescanner' on board the Marine Dufrense (Beard, 2004). Background measurements were taken after each measurement to correct for instrumental drift.

3.2. Geochemical Analysis

High-resolution studies of continuous sedimentary archives are key to understanding climate change on sub-annual to millennial time scales (Jansen *et al.,* 1998). Marine sediments can provide detailed palaeoenvironmental archives through the interpretation of element proxy data. X-ray fluorescence scanning (XRF), with its rapid and non-destructive analytical capability, allows the quick acquisition of bulk geochemical data at a high resolution (Bertrand *et al.,* 2015) and can provide detailed insights into oceanographic and climatic processes when applied to marine sediments. XRF data, which are expressed as relative elemental counts or peaks, are mainly related to elemental concentrations, but they are also influenced by a series of sediment physical properties that vary with depth, such as bulk density, water content, endogenic and authigenic content and grain size (Bertrand *et al.,* 2015).

A Geotek MSCL-XZ, with a combined Olympus Delta XRF, was used at the University of Liverpool to obtain XRF geochemistry data. Plaques of the wet sediment cores (length 1.5 m) were covered with polypropelene film to ensure a homogenous and smooth measurement surface (Weltje and Tjallingii, 2008) and measurements were taken at 1 cm intervals. The XRF was run in two modes: the first, 'Soil' mode, used three beam conditions: 40 kV, 40 kV (filtered) and 15 kV for 20 seconds each to optimise beam conditions and to account for possible sediment sections in which heavier elements were embedded within a matrix of lighter elements. For the second mode, 'MiningPlus', the spectrometer performed two measurements: 40 kV and 15 kV each for 20 seconds.

Despite the advantages of rapid, non-destructive data acquisition that XRF core scanning devices provides, there are a number of potential impediments that may introduce artefacts into the dataset (Schillereff, 2015): surface irregularities and gaps in the sediment series (Weltje and Tjallingii, 2008); non-homogenous mineral and grain size composition (Hennekam and Lange, 2012); and variable down-core water and organic content (Boyle *et al.,* 2015).

To calibrate the XRF data obtained from the Geotek a training-set was subsampled from the core. Analyses were performed on a dry-mass basis at the University of Liverpool using a handheld Thermo Scientific Niton XL3t GOLDD+ in 'TestAllGeo' mode (50 kV beam for 80 seconds), to ensure a comparable suite of elements to those

registered in the Soil and MiningPlus modes of the Geotek was obtained. Samples were homogenized using a pestle and mortar and the powder was compressed into plastic pots and sealed with polypropylene film.

3.2.1 Mineralogical Analysis

Mineralogical analysis of Atlantic Ocean sediments is an indicator of sediment provenance (Biscaye, 1965). The clay mineral distribution within these sediments is attributed to the climatic and weathering zonation of the adjacent land masses and implies that the predominance of the clay is of terrigenous origin (Kolla *et. al,* 1979; Charnley, 1989; Petschick *et al.,* 1996). The ability of marine sediments to provide accurate palaeoclimatic histories can be adversely affected by the post-depositional diagenesis of magnetic minerals (Housen *et al.,* 1996). In this instance X-ray diffraction (XRD) was not only undertaken to determine the mineralogical content of core MD03-2708, but also to ensure that the particularly iron rich horizons present had not been affected by diagenesis.

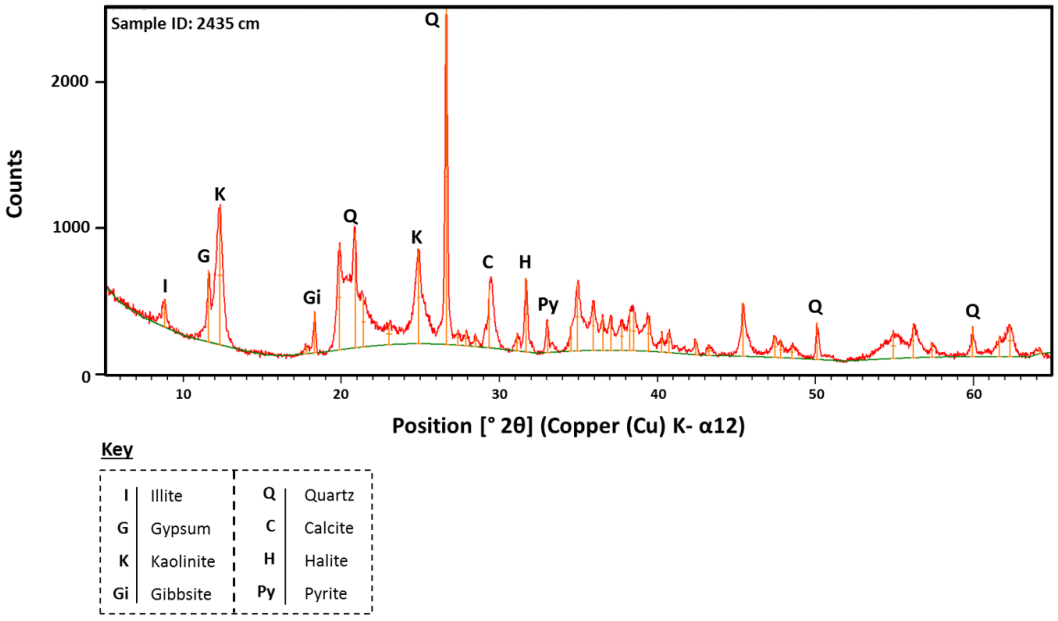

Figure 3.1 Diffractogram output for core MD03-2708, sample 2435 cm, generated using the Relative Intensity Ration method with the *HighScore Plus*® software. Red peaks are associated with particular minerals; eight key minerals are labelled here, as denoted by James Utley at the University of Liverpool.

Approximately 2 g of dry bulk sediment was hand-crushed to a fine powder (<45 μm) in an agate pestle and mortar and transferred to a side-loading aluminium cavity sample holder to produce randomly oriented particle mounts. Diffraction patterns for each sample were recorded from 5 to 65 °2 θ using a Siemens D-500 X-ray power diffractometer and Ni-filtered Cu Kα radiation at the University of Liverpool. Analysis of the diffractogram data [e.g. Figure 3.1], utilising the 'Relative Intensity Ration' method of the *HighScore Plus*® software and reference patterns from the 'International Centre for Diffraction Data, Powder Diffraction File-2 (Release 2008), was undertaken by James Utley (University of Liverpool).

3.2.2 Elemental Analysis

The total carbon (TC) within soils and sediment is the sum of the total organic (TOC), total inorganic (TIC) and elemental carbon components. TIC can be measured directly, or as was the case in this study, can be determined by the difference between TC and TOC. In a marine setting, naturally occurring TOC is derived from the decomposition of terrestrial and aquatic plants and aqueous organisms (e.g. algae) and through the biogeochemical cycling and upwelling of nutrients (Müller, 1977; Prahl *et al.*, 1994; Raymond and Bauer, 2001; Bianchi *et al.,* 2002). TIC is largely derived from marine calcium carbonate [$CaCO_3$] organisms and endogenic precipitates (Schumacher, 2002). Elemental carbon originates from geological sources and fires and shall not be considered in this study.

Aliquots of freeze-dried sediments (5–10 mg) were decarbonated using 12N Analar Grade HCl vapour (Yamamuro and Kayanne, 1995). This procedure eliminates the loss of acid-soluble organic matter during carbonate dissolution and thus allows the TOC content (%) of the dry sediment to be accurately determined. Non-decarbonated aliquots were used to determine TN and TC. The difference between TC and TOC was used to calculate the carbonate content of the sediment as a weight percent [$CaCO_3$ = (TC - TOC) x 8.33], assuming that all carbonate was $CaCO_3$ (Kiriakoulakis *et al.*, 2011). All carbon and nitrogen elemental analyses were carried out using a CEInstruments NC 2500 CHN analyser in duplicate (mean value used; all values were within 10 % of the mean) by Sabena Blackbird at the University of Liverpool.

3.3. Marine Carbonate Analyses

The biogenic carbonate component of marine sediments is one of the most important archives used in palaeoceanographic reconstructions (Farrell and Prell, 1989). Both the isotope and trace element compositions of marine carbonate convey information about variations in palaeoceanographic conditions which are key to understanding past changes in climate, particularly across glacial-interglacial transitions (Elderfield and Ganssen, 2000).

Biogenic sediments comprise the remnants of tests and shells produced by planktic (surface dwelling) and benthic (bottom dwelling) calcareous or siliceous organisms, or phosphatic particles (Fütterer, 2006). Marine organisms are abundant and diverse, but only a small number of groups contain the hard parts that are suitable for the formulation of sediment. Calcifying organisms participate in highly productive ecosystems and therefore contribute greatly to the build-up of biogenic sediments. The tests of calcitic foraminifera (amoeboid protist) and coccolithphores (eukaryotic phytoplankton) form the main focus of this study.

3.3.1 The Oxygen Isotope $\delta^{18}O$

Naturally occurring oxygen comprises three stable isotopes: ^{16}O, ^{17}O and ^{18}O, with ^{16}O being the most prevalent (99.76 % natural abundance) (Hessler, 2011). Through temperature-dependent kinetic fractionation, water evaporating from the sea surface is depleted in the 'heavier' isotope ^{18}O relative to the remaining ocean, meaning that precipitation is enriched in ^{16}O (Dansgaard, 1964). The isotope composition of precipitation varies latitudinally and is highest in the tropics and depleted with both an increase in latitude and altitude. During glacial periods, large continental ice sheets preferentially store the lighter ^{16}O, resulting in an increase of ^{18}O in the oceans. This ^{18}O to ^{16}O ratio ($\delta^{18}O$) is uniquely preserved within ice cores, whilst also being applicable to water and terrestrial (speleothems) and marine carbonates (coral reefs, coccolithphores, foraminifers, pteropods, molluscs, and calcareous dinoflagellates). Its wide applicability and ability of oxygen isotope ratios to clearly define glacial and interglacial periods has established the technique as a unique and important palaeoclimatic tool (Shackleton, 1967).

The $\delta^{18}O$ of marine $CaCO_3$ is widely used to reconstruct: sea surface temperature [SST] (e.g. Epstein *et al.*, 1953; Sikes and Keigwin, 1994; Thunell *et al.*, 1999); sea surface

salinity [SSS] (e.g. Watanabe *et al.,* 2001; Lea *et al.*, 2002; Zachos *et al.,* 2001); continental ice volume (e.g. Broecker and van Donk, 1970; Waelbroeck *et al.*, 2002); and freshwater input into the ocean (e.g. Schmidt *et al.*, 2012; Schefuβ *et al.,* 2005; Weldeab *et al.*, 2007).

Variations in the proportion of oxygen isotopes within marine $CaCO_3$ is dependent upon: the isotope composition of seawater; the temperature of the seawater during life; and vital effects (Murray, 1991). The isotopic composition of seawater is influenced by dilution from surface runoff and the ratio of evaporation to precipitation. Marine carbonate is additionally sensitive to changes in sea water temperature; a change in water temperature of 1 °C alters the $\delta^{18}O$ by 0.25 ‰ (Epstein *et al.,* 1953). Often biogenic calcite is not secreted in isotope equilibrium with the ambient seawater, leading to carbonates that have a different $\delta^{18}O$ relative to equilibrium conditions. The variety of life processes responsible for this disequilibrium are referred to as vital effects and include: habitat specific characteristics not representative of the water column as a whole; growth or calcification rate (e.g. Spero and Lea, 1993); the uptake of metabolic CO_2 during calcification; ontogenetic physiological changes; and the photosynthetic activity of symbionts (Murray, 1991; Bemis *et al.,* 1998).

3.3.2 The Carbon Isotope Ratio $\delta^{13}C$

Carbon has three isotopes, of which ^{12}C and ^{13}C are stable. The carbon composition of calcareous marine fossils reflects the dissolved carbon content of the water in which organisms precipitated their shells (Berger and Vincent, 1986). Photosynthesis takes place within the surface waters of the global ocean; ^{12}C is used preferentially in photosynthesis by plants, resulting in surface dwelling organisms becoming more enriched in ^{13}C (isotopically heavier) as the ^{12}C enriched plants are moved from the environment after death by sinking through the water column. As particles of organic matter sink into deeper water they may become oxidised, which results in bottom waters containing more ^{12}C rich CO_2 (Murray, 1991).

The $^{12}C/^{13}C$ ratio ($\delta^{13}C$) preserved within fossilised marine organisms is a key tool in palaeoceanographic reconstructions as it reflects a mixture of: global and regional changes in surface water productivity; internal shifts in circulation and water mass structures; and organism-specific fractionation effects due to changes in microhabitat (Grossman, 1987) and vital effects (Berger and Vincent, 1986; Murray, 1991). The enrichment of surface waters in ^{13}C relative to bottom water varies with changes in

productivity and ocean circulation. This enrichment oscillates as a function of time, deeming $\delta^{13}C$ to be a useful tool for examining palaeoceanographic transitions over tens to hundreds of thousands of years (Berger and Vincent, 1986).

3.3.3 Trace Element Palaeothermometry

Determining the past record of ocean surface water temperature is an important tool for understanding past climate conditions (Elderfield and Ganssen, 2000). During the precipitation of planktonic foraminiferal calcite, the incorporation of the trace element magnesium is affected by the temperature of the surrounding seawater, so that the magnesium to calcium ratio (Mg/Ca) of the foraminiferal calcite increases with increasing temperature (Lea *et al.,* 1999). The sensitivity of the Mg/Ca thermometer (~9 % per °C) (Hessler,2011), along with its global application, means the technique forms an important proxy in the reconstruction of seawater temperature (e.g. Nürnberg *et al.,* 2000; Weldeab *et al.*, 2007).

3.4. Micropalaeontological Analyses

3.4.1 Planktonic Foraminifera

Changes in the near-surface water conditions of the eastern equatorial Atlantic are reflected by the surface-dweller species *Globigerinoides ruber* [*G. ruber*] (Healey and Thunnell, 2004). *G. ruber* is a warm water species that exhibits one of the widest sea surface temperature ranges of planktonic foraminifera (9.7 – 31 °C) (Žarić *et al.*, 2005). It prevails in oligotrophic (nutrient poor) and mesotrophic (intermediate level of productivity) conditions and has dinoflagellate symbionts which make it light dependent (Hemleben *et al.,*1989). The wide temperature and micro-habitat range of *G. ruber* attribute it as a key specimen that can be used globally to reconstruct palaeoclimate.

3.4.2 Benthic Foraminifera

As a result of its epibenthic (seafloor surface dwelling) microhabitat preference and stable isotopic signatures, *Cibicidoides wuellerstorfi* [*C. wuellerstorfi*] is widely used in palaeoceanographic studies. *C. wuellerstorfi* resides above the sediment-water interface in temperatures ≤ 5 °C (Lear *et al.,* 2002), and is attached to rocks and biogenic materials (Lutze and Thiel, 1989). The benthic positioning of *C. wuellerstorfi* provides a good reconstruction of bottom water movements and productivity during the Late Quaternary period.

3.4.3 Foraminiferal Sample Preparation

For isotope and Mg/Ca analyses, 238 oven dried (40 °C) sediment samples (~10 g) were washed using DD water over a 75 μm mesh sieve. The remnant sample was then dried and further divided into size fractions by dry sieving. The 175 – 250 μm fraction of each sample was placed on a black tray under an XTL-3 stereo microscope and tests were identified using (Hayward, 2014), picked using a fine paintbrush and mounted into gridded cardboard microscope slides. Where counts of tests were high enough, ≥ 20 specimens of the benthic foraminifera *Cibicidoides wuellerstorfi* [144 horizons] and ≤ 30 specimens of the planktic foraminifera *Globigerinoides ruber* (white) [182 horizons] were picked from each sample for stable isotopic analysis. An additional ≥ 30 specimens of *G. ruber* were picked for trace element analysis [26 from the same horizons used in isotope analysis & 16 new horizons].

The isotope composition of carbonate shells remains largely unchanged unless the shell material recrystallizes during diagenesis (Bickert and Wefer, 1996). This modification usually occurs after deposition during early burial, or even before this due to CO_2 enriched, corrosive deep ocean or pore waters in the water column. To evaluate whether the MD03-2708 foraminifera had been affected by diagenesis, the microstructure of a selection of foraminifera spanning the length of the core was examined using a Philips XL30 Scanning Electron Microscope (SEM) at the University of Liverpool. Specimens were inspected for two signs of diagenesis: 'neomorphism' – the replacement of biogenic calcite with a different crystal form; and 'cementation' – the growth of inorganic calcite crystals either within the pore space of tests, or the infilling of test chambers (Sexton *et al.,* 2006). All foraminifera examined showed no signs of diagenesis [Plate 3-1].

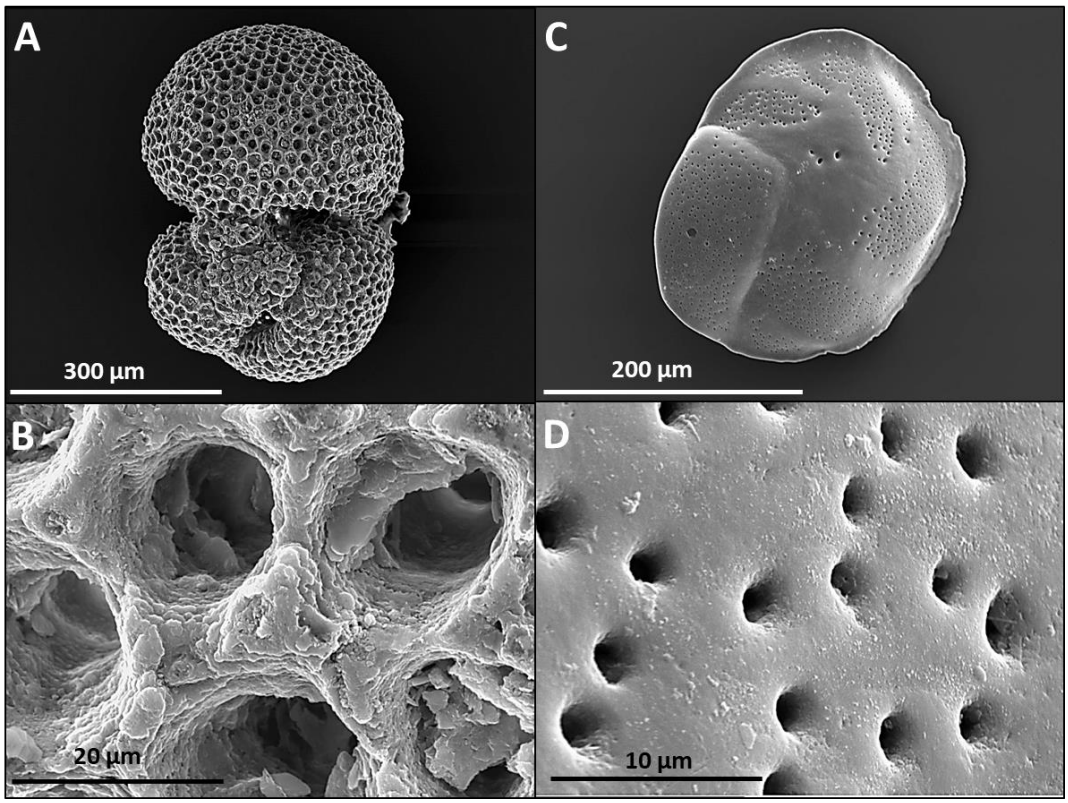

Plate 3-1: SEM images taken at the University of Liverpool highlight that foraminifera within core MD03-2708 are devoid of secondary calcification and diagenesis. Plates comprise: (A) *G. ruber* (white variety), whole specimen; (B) *G. ruber,* close up on pore spaces; (C) *C. wuellerstorfi,* whole specimen; and (D) *C. wuellerstorfi,* close up of pore spaces.

3.4.4 Coccolithophores

Palaeoceanographic reconstructions of surface conditions have long relied on the isotopic analysis of the individual specimens of planktic foraminifera due to their reduced range of habitat (Stoll, 2005). However, in sediments where planktonic foraminifera are smaller in number, or do not occur or are not preserved, an alternative is to use the bulk or fine fraction carbonate. Bulk carbonate isotope analysis is sometimes used as an alternative, depending on the age and setting of the sediments. Coccolithophores (coccoliths) can account for the majority (> 90 %) of the carbonate within carbonate rich marine sediments (Stoll, 2005). Coccoliths are unicellular phytoplankton with a global distribution that is determined by light intensity, nutrient availability and ocean currents (Boeckel *et al.*, 2006). Coccoliths additionally occupy the same depth habitats as *G. ruber,* allowing for a more comprehensive picture of past palaeoceanographic conditions to be determined.

Caution needs to be employed when utilising bulk carbonate stable isotopic analysis. Coccoliths grown in culture exhibit up to 5 ‰ array of interspecific vital effects in both oxygen and carbon isotopes (Dudley and Goodney, 1979; Ziveri *et al.*, 2003), meaning that changes in coccolith species assemblages could introduce significant artefacts into bulk carbonate isotopic records (Stoll, 2005).

3.4.5 Fine Fraction Carbonate Sample Preparation

Where horizons were bereft of either or both planktonic and benthic foraminifera [51 horizons], samples were prepared for fine fraction carbonate isotopic analysis. Freeze dried sediment samples (~ 10 g) were passed through a dry 63 μm sieve to obtain the fine fraction (<63 μm). To remove the organic component, once weighed, each sample was rehydrated with 50 ml of 5 % sodium hypochlorite (NaClO) and left for a maximum of 24 hours. Each sample was then diluted with 500 ml of DD H_2O, centrifuged at 3500 rpm for four minutes and the supernatant decanted. An additional 500 ml of DD H_2O was added until the supernatant reached a neutral pH (typically three washes). Once neutralised, the supernatant was discarded and samples were left to dry on filter paper in a drying cabinet (40 °C) overnight. Once dried, the samples were gently ground to a powder using a pestle and mortar and transferred to a glass vial before being weighed.

3.5. Stable Isotope Analyses

Stable isotope analyses were undertaken at the NERC Isotope Geosciences Laboratory (NIGL) at the British Geological Survey, Nottingham, UK. The analyses were funded through a NERC facility grant (IP-1557-051).

3.5.1 Foraminifera

Approximately 50-100 mg of carbonate foraminiferal tests (~20 tests per sample) were used for isotope analysis using an IsoPrime dual inlet mass spectrometer plus Multiprep device. The analysis was undertaken by Hilary Sloane at the NIGL. Samples were loaded into glass vials and sealed with septa. The automated system evacuated vials and delivered anhydrous phosphoric acid (H_3PO_4) to the carbonate at 90 °C. The evolved CO_2 was collected for 15 minutes, cryogenically cleaned and passed to the mass spectrometer. Isotope values ($\delta^{13}C$ & $\delta^{18}O$) are reported as per mil (‰) deviations of the isotopic ratios ($^{13}C/^{12}C$ & $^{18}O/^{16}O$) from integrated standards and calibrated to the Vienna Pee Dee Belemnite (VPDB) scale using a within-run laboratory standard calibrated against NBS-19. The calcite-acid fractionation factor applied to the gas values

was 1.00798. Due to the long run time of 21 hours, a drift correction was applied across the run, calculated using the standards that bracket the samples (beginning and end points and after every fifth sample). The Craig correction was also applied to account for $\delta^{17}O$ (Craig, 1957). The average analytical reproducibility of the standard calcite (KCM) is 0.05 ‰ for $\delta^{13}C$ and $\delta^{18}O$ (1σ).

3.5.2 Fine Fraction Carbonate

For stable isotope analysis of the fine fraction carbonate (<63 μm), an aliquot of the powder (equivalent to 10 mg of pure calcite) was reacted with anhydrous phosphoric acid *in vacuo* at 25.2 °C for 16 hours at the NIGL. The CO_2 liberated was cryogenically cleaned (to remove H_2O and Nitrogen (N)) and collected for analysis. Measurements were made on a VG Optima dual inlet mass spectrometer - operated by Chris Kendrick at the NIGL. Isotope values ($\delta^{13}C$, $\delta^{18}O$) are reported as per mil (‰) deviations of the isotopic ratios ($^{13}C/^{12}C$, $^{18}O/^{16}O$) calculated to the VPDB scale using a within-run laboratory standard calibrated against NBS-19. The calcite-acid fractionation factor applied to the gas values was 1.01025. The Craig correction was also applied to account for $\delta^{17}O$. Overall analytical reproducibility for isotopic data obtained from these samples is on average better than 0.1‰ for $\delta^{13}C$ and $\delta^{18}O$ (1σ) (Craig, 1957).

3.6. Trace Element Analysis

G. ruber foraminifera shells were gently crushed between two glass plates to open the chambers and then cleaned following the 'Cambridge Method' procedure of Elderfield and Ganssen (2000). Fine clays were removed through five washes where each time 500 μl of ultra-high quality (UHQ) water was added to each tube, the samples were sonicated for 30 seconds and then the water was siphoned off. This was followed with two washes with 250 μl of methanol (CH_3OH) before a final rinse with UHQ. Oxidisation was then undertaken to remove the organic matter from the samples. For this, 250 μl solution of 50 μl hydrogen peroxide (30 %) and 15 ml 0.1 M of sodium hydroxide (NaOH) was added to each sample before placing the tubes in a boiling water bath for two, five minute intervals, sonicating after each emersion. UHQ water was added to the samples, allowed to settle and then siphoned off. A weak acid leach was performed by adding 250 μl 0.001 M nitric acid (HNO_3) to each sample, ultrasonicating for 30 seconds, allowed to settle for one minute, before siphoning the solution away. Finally, sample dissolution was implemented by adding 400 μl of 0.001 M HNO_3, ultrasonicated, and transferred to new vials. Samples were run by Dr Leon

Clarke, using a Thermo Scientific iCAP6300 ICP-OES within the School of Science and the Environment at Manchester Metropolitan University, UK.

Foraminiferal Mg/Ca were calibrated using an established ICP-OES intensity ratio calibration method (de Villiers *et al.*, 2002). Calibration standards were made up from high-purity single element standard solutions, initially at a Ca concentration of 1000 mg/g. These were diluted to Ca concentrations of 5 - 40 mg/g and the calibration line closest to the concentration of Ca in the foraminiferal sample solutions was used to convert ICP-OES signal intensity ratios into molar ratios.

Mg and Ca were measured at 279.5 nm and 317.9 nm, respectively. Foraminiferal Mg/Ca molar ratios were calibrated using an established ICP-OES intensity ratio calibration method (de Villiers *et al.,* 2002). Calibration standards were made up from high-purity single element standard solutions, initially at a Ca concentration of 1000 mg/g. These were then diluted to Ca concentrations of 5 to 25 mg/g, in 5 mg/g increments. The gradients of the ICP-OES signal ratio (279.5 nm/317.9 nm) to molar ratio (mmol/mol) calibration lines were constant between 5 and 15 mg/g Ca concentration, the range of Ca concentrations recorded within the foraminiferal solutions introduced to the ICP-OES, indicating no matrix effect, and a single calibration line correction was applied to all foraminiferal samples. Sample integrity was additionally assessed using Aluminium (Al) and Titanium (Ti) signals, as well Mn signals; samples that suggested high clay contaminates (indicated by high Al and Ti signals) and/ or oxide coatings (high Mn signals) were removed from the dataset.

3.7. The Palynological Method

Palynology is the study of organic particles, termed palynomophs, found in sedimentary records. Palynomorphs comprise pollen grains (mircogametophytes) and non-pollen palynomorphs (NPPs) including spores, algae and dinoflagellate cysts amongst others. Most pollen grains are spherical in shape and their size varies between ~ 6 and 100 µm, whilst NPPs can measure up to 500 µm. Marine palynology was developed as a stratigraphic tool for use in the oil industry (e.g. Muller, 1959). Through the identification and analysis of pollen and spores, it is now utilised to reconstruct past vegetation and environmental conditions on the adjacent continent (e.g. Dupont *et al.,* 1999; Behling, 2002), whilst palaeoceaographic conditions can be reconstructed using dinoflagellate cysts (e.g. Marret *et al.*, 2001).

Pollen grains are present within marine sediments extending from deltaic to deep sea environments, and from the tropics to high latitudes. Their wide occurrence attributes them as valuable climatic markers, in particular along the coast of arid environments where terrestrial records are often discontinuous and difficult to date (Dupont and Behling, 2006). Marine sediment sequences, within the chronological framework of an isotope stratigraphy, permit continuous climate reconstructions on much longer time scales and often span glacial-interglacial time cycles (Dupont *et al.*,1999; Zabel *et al.*, 2001). The correct interpretation of marine pollen records, however, relies on sufficient data about pollen transport, either by wind or water (Hooghiemstra *et al.*, 2006) from the adjacent continent and the distribution of the pollen in modern marine sediments (Dupont and Behling, 2006). Aeolian transport of pollen grains is dominant in deep-sea sediments and in arid environments, whilst fluvial transport predominates in humid areas and sites proximal to river mouths (Hooghiemstra and Agwu, 1986).

Palaeovegetation records provide vital information for understanding atmospheric fluxes (e.g. Hooghiemstra and Agwu, 1988; Dupont and Behling, 2006), fresh water input (e.g. Marret *et al.*, 2001; Lézine *et al.,* 2005), and continental data (Lezine *et al.,* 2005). Marine pollen records are an advantageous archive in the study of west equatorial African vegetation cover change over several climate cycles. However, caution should be taken as these pollen records only show a portion of the flora of the adjacent continent, in contrast to the pollen from terrestrial deposits, which provide a more detailed local vegetation history, albeit, in most cases over a relatively short time period (Dupont, 2011).

3.7.1 Palynological Preparation and Analysis

Samples for palynological investigation were prepared at the University of Liverpool according to the standard laboratory protocol in accordance with Scourse *et al.* (2005). In order to avoid damage to dinocysts, the oxidative stage of acetolysis was omitted.

A known volume of wet sediment (~ 5 cm^3) was oven-dried at 60 °C overnight and then subsequently weighed. The dried sediment was rehydrated in DD H_2O and then washed through a 100 µm mesh sieve. One tablet of the exotic spore *Lycopodium clavatum* (batch number 10680 or 20848) was added to each sample before adding cold 10 % HCl to remove the calcium carbonate content. Silicates were removed by treating the samples with 40 % hydrofluoric acid (HF) for a minimum of 24 hours. The

remaining sample was then treated again with 10 % HCl to remove any fluorosilicates that may have formed, before being decanted and diluted with DD H_2O. The substrate was then washed over a five µm mesh sieve using DD H_2O and, where necessary, with sodium pyrophosphate ($Na_4P_2O_7$), to deflocculate the clays. Lastly, samples were re-suspended in sodium polytungstate ($Na_6[H_2W_{12}O_{40}]$), with a specific gravity of 2.1; the floating organic residue was transferred into a new vial and the heavier substrate was discarded. The residue was concentrated by centrifuging for four minutes at 3500 rpm and then decanted into 5 ml tubes for storage. Between one and two drops of (10 %) phenol (C_6H_5OH) were added for preservation.

For the identification of pollen and non-pollen palynomorphs a subsample of homogenized residue was mounted onto a microscope slide in safranin jelly and a covering slip was placed over the remaining material and fixed with paraffin wax. Sample slides were microscopically examined at 400 times magnification under a light-transmitted microscope. Where possible, pollen grains were counted until a sum of 300 pollen specimens was reached. Where total pollen counts (≥ 300 pollen grains) contained less than 200 grains of non *Rhizophora* pollen, counts were increased to avoid overrepresentation of the dominant mangrove taxa. For a small number of samples, less than 150 pollen specimens were counted per sample, due to a low concentration of pollen grains in the sediment. NPPs were additionally counted alongside the pollen and comprised other microfossils such as spores, plant cuticles, fresh water algae, organic-walled dinoflagellate cysts, copepod eggs, organic-walled linings of foraminifera, and scolecodont jaws.

Pollen grains were identified using images in the 'African Pollen Database' (Vincens *et al.*, 2007) and the 'Atlas of the tropical West African pollen flora' (Gosling *et al.,* 2013). Identification of non-pollen palynomorphs was achieved using reference images in Gelorini *et al.* (2011) and van Geel *et al.* (2011).

Palynological results are presented as: percentages of the total palynomorph sum (%); as concentrations (specimens/cm^3); and as accumulation/ flux rates (specimens/cm^2/year). It should be noted that the pollen and non-pollen counts and equations are formulated independently of one another.

4 Sedimentology & Provenance of Core MD03-2708

Provenance studies of marine sediment cores aim to interpret and reconstruct the history of the sediment from the initial erosion of parent rock, through to the final burial of detrital material (Weltje and von Eynatten, 2004; Alizai *et al.*, 2011). Sediment properties are reflective of parent lithology, and modification by weathering, transport, deposition and diagenesis. Terrigenous sediments are composed of both detrital grains - the residues of weathered parent rocks, and clay minerals - formed through the weathering of unstable minerals (Weltje and von Eynatten, 2004). Source area climate and topography, in combination with principal regional vegetation, are the main factors controlling weathering and erosion and the consequent detrital spectrum delivered into first-order tributaries of river systems (Weltje *et al.,* 1998), and ultimately the marine sediment record.

The bedrock geology of Gabon ranges in age from the lower Precambrian to the Tertiary Period and is overlain by unconsolidated Quaternary sediments [Figure 4-1-a] (Upton and O' Dochartaigh, 2016). The geological formation of the bedrock varies along a southwest to northeast gradient. Alluvial and marine deposits are located at the coast in the southwest and trend through felsic igneous and sedimentary rocks north and east of the country. The pattern of soil types presented in Figure 4-1-b reflects the continuous and intensive weathering of Western Africa and attributes Gabon as one of the highest soil unit diversities in Africa (Jones *et al.*, 2013).

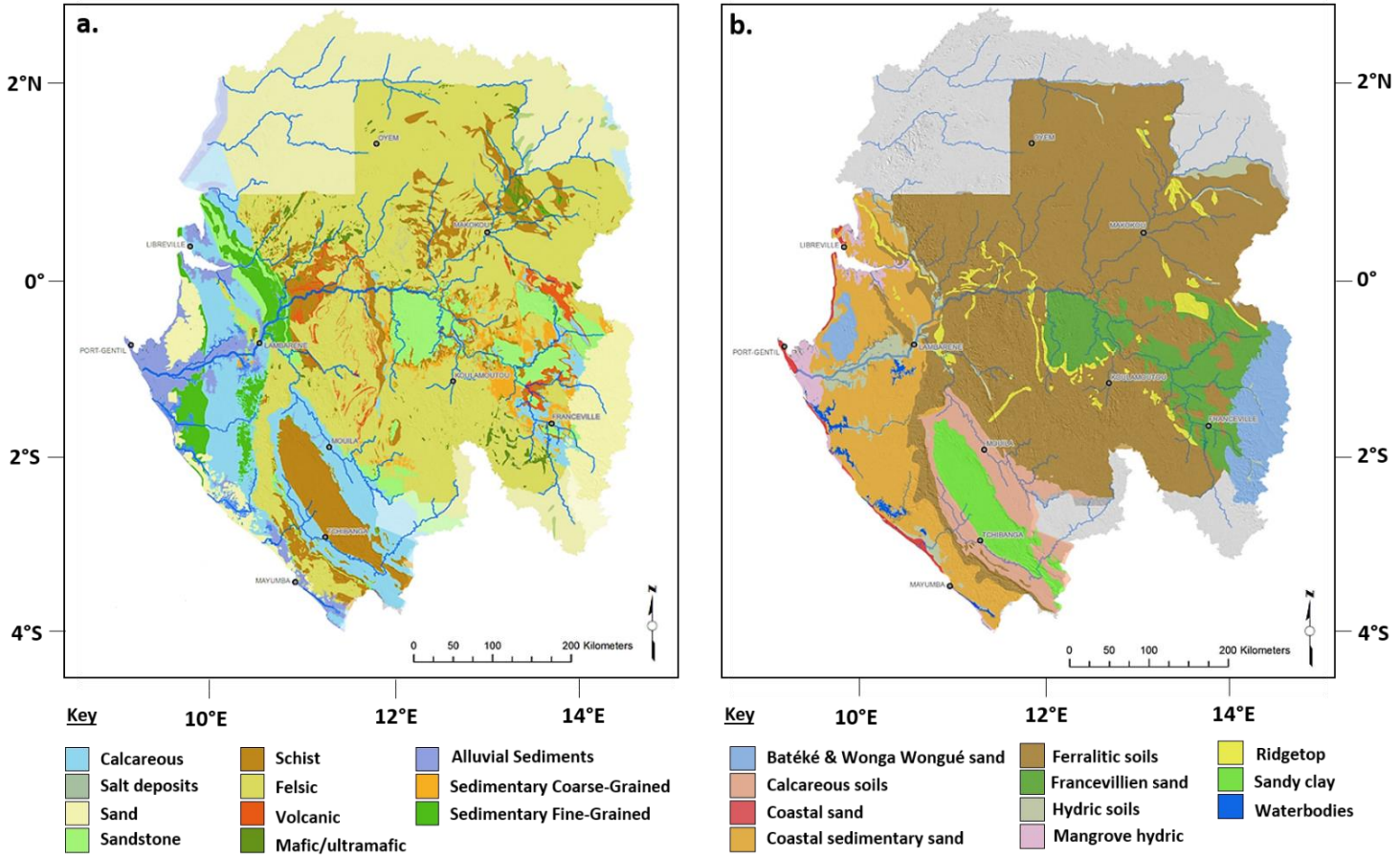

Figure 4-1: Geologic map of Gabon comprising: (a) 11 geologic bedrock classes based on chemistry and groundwater potential; (b) surface soil types of Gabon subdivided into 10 classes [modified after Thiéblemont et al., 2009].

4.1 Previous Sedimentological Analysis of core MD03-2708

An understanding of sediment stratigraphy prior to analysis is essential for identifying event layers within sediment core material (Schillereff *et al.*, 2016). A sediment description produced for core MD03-2708 on-board the 2003 PICABIA cruise [Appendix]. The original sediment description details broad intervals of clay and silty-clay horizons based on colour, however, by 2013 these differences were no longer visible by eye.

The initial sediment properties of the core, recorded on-board using a Geotek MSCL 6.2, comprise sediment density (g/cm^3), magnetic susceptibility (10^{-5} SL) and fractional porosity (%) [Figure 4-2] and provide preliminary evidence that there are stratigraphic changes over the length of the core sequence. A notable hiatus is present at 30 m, evidenced by a decrease in sediment density and a concomitant increase in fractional porosity, which suggests compaction of sediment material below 30 m. The magnetic susceptibility record is more variable than the density and fractional porosity and is most likely reflective of the terrigenous input into the core. There is potentially another smaller hiatus recorded at 7 m, which is succeeded by an increase in terrigenous input until the top of the sediment sequence.

Whilst providing preliminary information on the sedimentological history of core MD03-2708 these properties cannot be used independently to construct a coherent sedimentological record. Lithostratigraphy (the geological concept that divides sedimentary facies into horizons depending upon their physical features) and chemostratigraphy analyses (the technique of sediment characterisation and correlation using variations in the elemental/isotope composition of the sediments) are used together to develop an accurate sedimentological history for core MD03-2708.

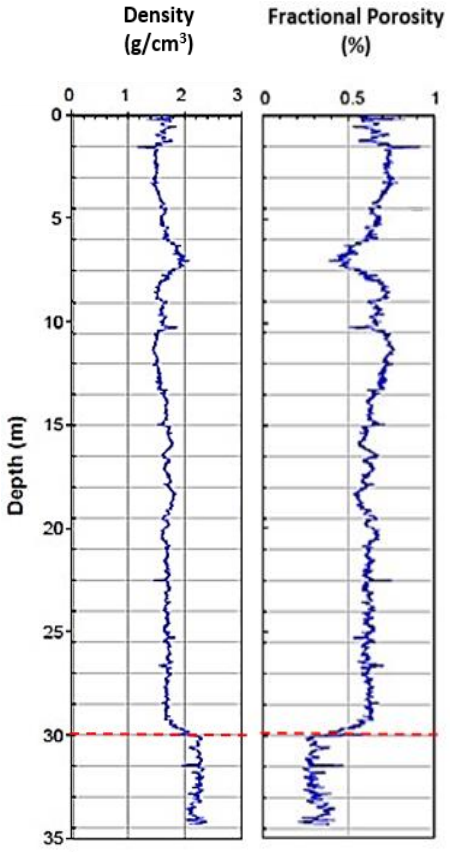

Figure 4-2: Physical properties of core MD03-2708: sediment density (g/cm³) and fractional porosity (%) obtained from the original core scanning by Beard (2004). A hiatus in sedimentation is highlighted at 30 m [horizontal red dashed line].

4.2 Lithostratigraphical Analysis

Lithostratigraphic units are generally defined on the basis of observable rock or sediment characteristics. Here, particle size analysis was mainly used to define the lithostratigraphy of core MD03-2708.

4.2.1 Particle Size Analysis

Particle size analysis (PSA) is a fundamental tool for classifying sedimentary environments (Blott and Pye, 2001). In a marine setting with high terrigenous input, PSA can be used in the determination of sediment provenance, transport history and depositional environment. PSA is a key proxy in its own right, but is also instrumental in not only supporting, but testing the grain size hypotheses inferred from the chemostratigraphic elemental ratios of core MD03-2708.

In order to establish the sedimentological history of core MD03-2708, a suite of 58 grain size distributions was obtained. Particle size parameters were calculated using the geometric formulae of Folk and Ward (1957) within the GRADISTAT 8.0 software (Blott and Pye, 2001). Figure 4-3 [sample 410 cm from core MD03-2708] is an example of a particle size distribution curve produced in GRADISTAT, and is presented on a logarithmic scale.

4.2.2 Particle Size Analysis Parameters

The parameters used to describe a particle size distribution fall within four principal groups: average particle size; spread of the sizes around the average (sorting); preferential spread to one side of the average (skewness); and the degree of concentration of the grains relative to the average (kurtosis) (Blott and Pye, 2001). Here, the focus is on the first three categories. The average size of the particles can be categorized into sediment type: clays (<2 μm), silts (2 – 63 μm) and sands (63 μm – 1 mm), represented respectively by the light, medium, and dark grey shaded units under the graph on Figure 4-3. Cumulative percentile values are used to determine the median grain size (D50), and the coarsest component of the sediment fraction (D90) (Clarke *et al.*, 2014), and are indicated on the Gaussian grain size distribution shown in Figure 4-3.

The D50 and D90 downcore variability of core MD03-2708, in addition to the particle sorting and skewness, is depicted on Figure 4-4. The D50 ranges between 17 μm (medium silt) at 2900 cm and 159 μm (fine sand) at 2700 cm. The D90 varies from 78 μm (very fine sand) at 150 cm to 1309 μm (very coarse sand) at 2220 cm. The D90 drives the particle size sorting with the 'most well sorted' fraction occurring in tandem with the lowest D90 at 150 cm, and the 'least well sorted' fraction occurring alongside the highest D90 at 2220 cm. Overall, the sorting for core MD03-2708 is very poor, extending from very poorly sorted (1309 0′) at 2220 cm to poorly sorted (2 0′) at 150 cm. The skewness follows the trend of the D50, D90 and sorting, and ranges between -0.3 Sk_1 at 3240 cm and 0.25 Sk_1 at 251 cm, and extends from very fine skewed to symmetrical throughout.

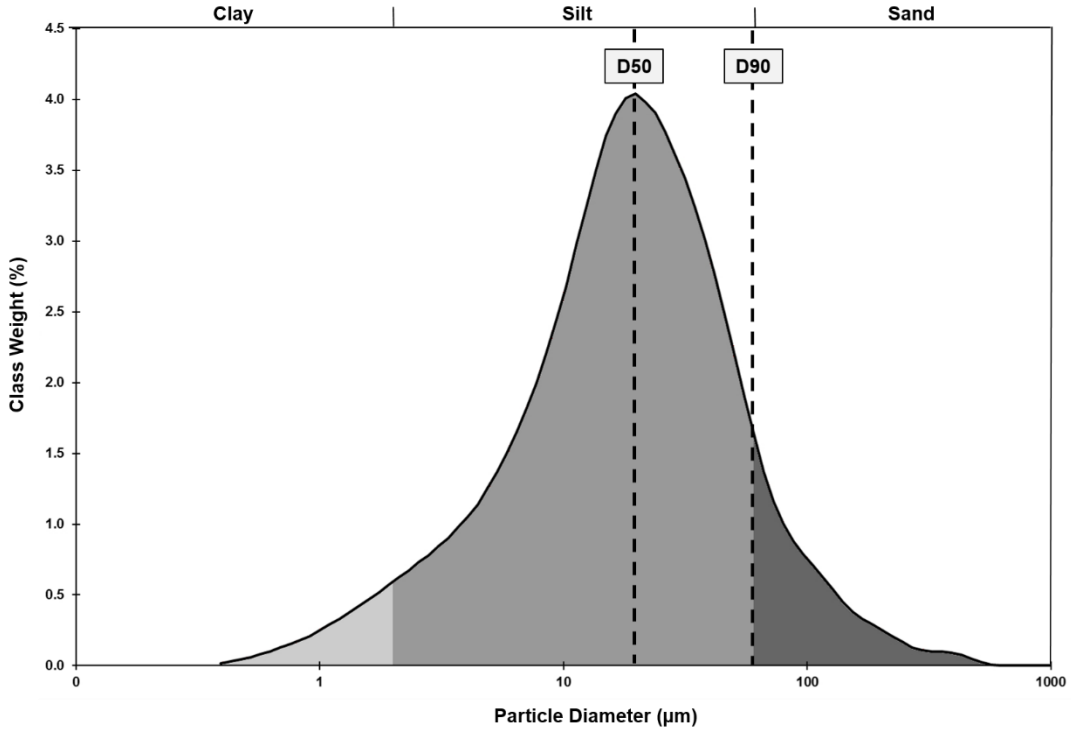

Figure 4-3: Particle size frequency histogram for core MD03-2708 sample 410 cm, highlighting: sediment size classification of clay (<2 µm - light grey), silt (2 – 63 µm – medium grey) and sand (63 µm – 1 mm) sediments; median grain size (D50 – dashed line) and the 90th percentile of the grain size distribution representing the coarse sediment fraction (D90 – dashed line).

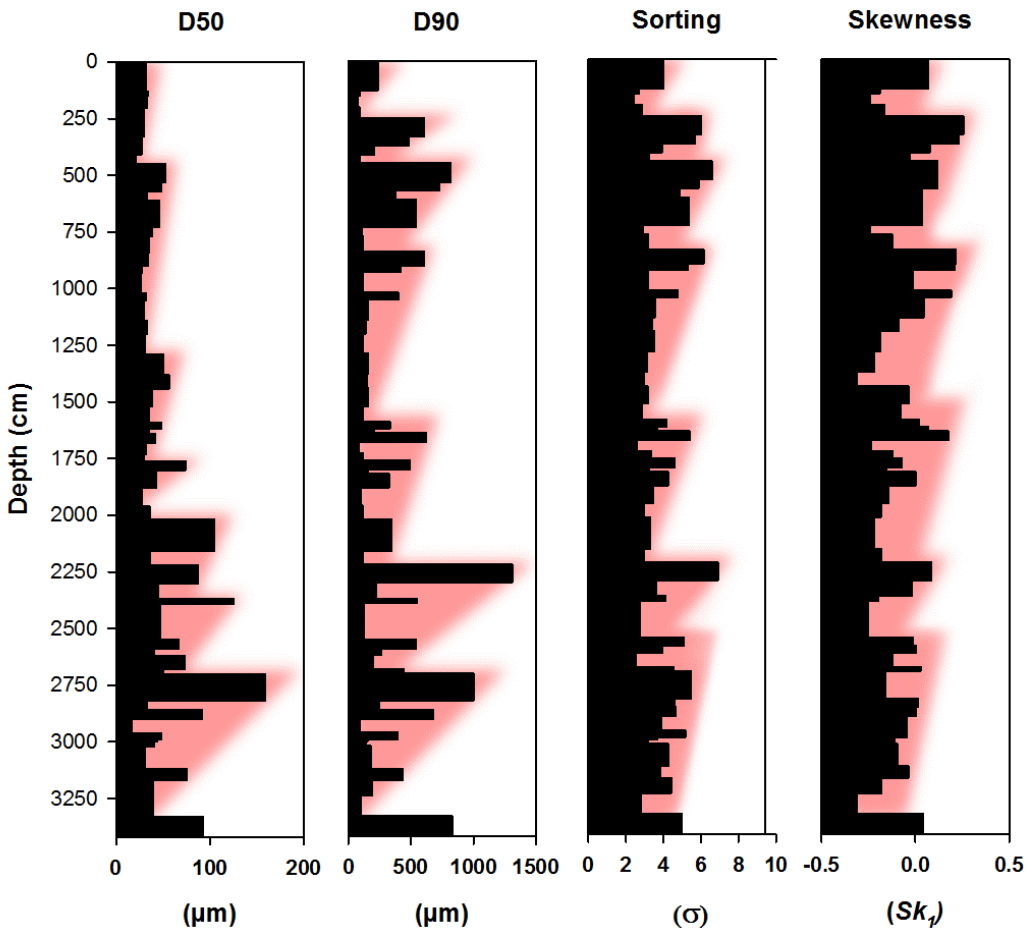

Figure 4-4: Downcore variability of core MD03-2708 particle size variability comprising the median value (µm) [D50], 90th percentile (µm) [D90], particle sorting (σ) and particle skewness (Sk_1). Deltaic prograding sequences are highlighted behind the data in red.

The variables in Figure 4-4 present a saw tooth pattern, exemplified between 3250 and 2600 cm by gradual increases in grain size, sorting and skewness, followed by a rapid return to lower values for all variables. This pattern occurs seven times throughout the sediment sequence and is most notable in the D90 size fraction. It can be seen that an increase in D90 not only drives a concomitant increase in the D50, but also reduces the level of sediment sorting and results in a more symmetrical skew.

This saw tooth pattern most likely indicates cycles of deltaic progradation, or rather the growth of the Ogooué River delta farther out into the Atlantic Ocean over time. This process occurs when the mass balance of sediment coming into the delta is higher than the volume lost through erosion, sea level rise and subsidence. Progradation can be caused by periods of relative sea level low stands, when sediment which would normally be deposited on the continental shelf is transported across the exposed shelf

by fluvial and subaerial processes and deposited in the marine environment (Burgess and Hovius, 1998). Consideration of grain size populations, and particularly the D90, is also important since the proportion of sand sized sediment transferred to the shelf can be reflective of intervals of extremely high sediment input, assuming the sediment has not been trapped within coastal plains (Burgess and Hovius, 1998).

4.2.3 Particle Size Distribution

The sediment coarsening upwards trends in Figure 4-5 can be further examined by inspecting the particle size distribution curves (PDSCs) of each MD03-2708 sample horizon. Visual analysis and categorisation of PDSCs provides an effective foundation for the identification of recurring modal sizes and subpopulations (Clarke *et al.*, 2014). Each particle size grouping probably reflects different modes of transport and sediment deposition as well as variation in sediment provenance. Examination of the individual PDSCs may also offer insight into mesoscale system behaviour of the Ogooué delta at a sub-centennial resolution.

Four key PDSC groupings are presented, two unimodal and two bi-modal. The unimodal distributions are depicted in Figure 4-6: distribution type 'a' largely comprises moderately sorted coarse silt; distribution type 'b' is composed of well sorted coarse silt. The two bimodal distributions include a poorly sorted distribution comprising silts and fine sands (distribution type 'c') and a very poorly sorted distribution composed of medium silts and coarse sands (distribution type 'd'). Since different particle deposition and transport processes affect grain size distributions, it is important to identify the individual components of multi-modal grain size distributions (Holz *et al.,* 2004; Briceno-Zuluaga *et al.*, 2016).

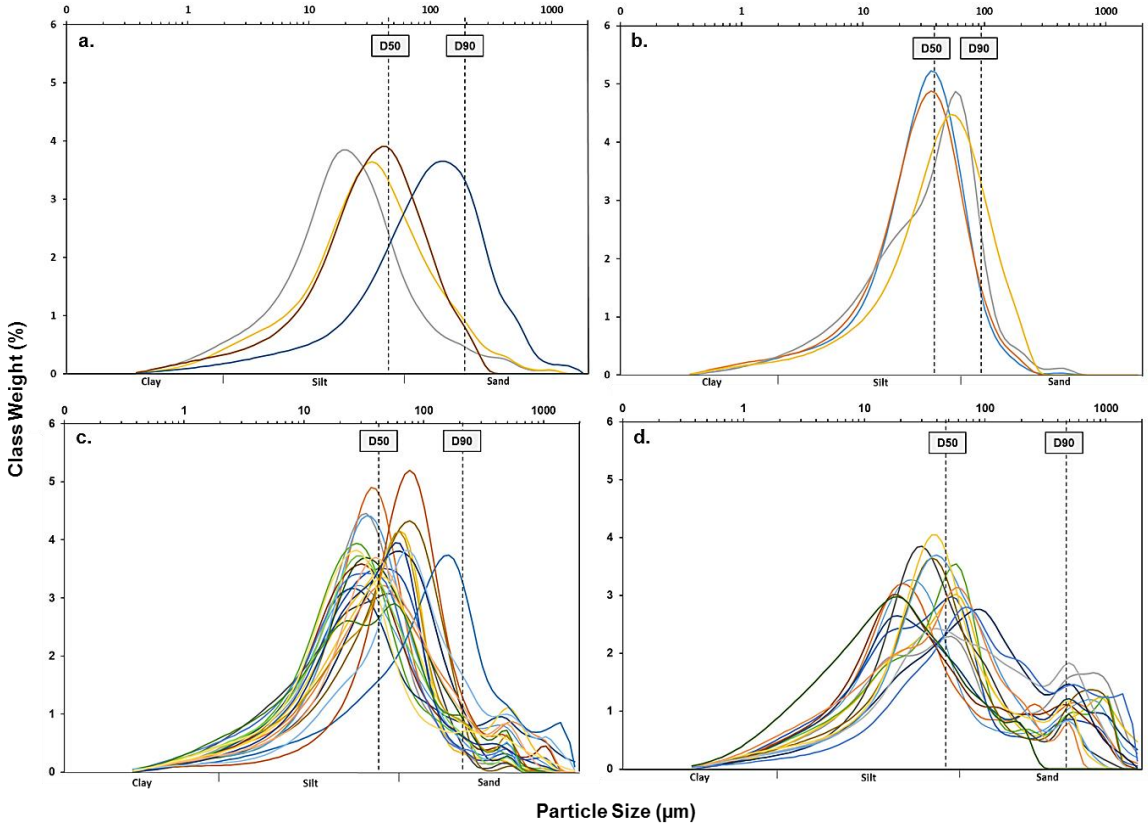

Figure 4-5: The four key particle size distribution curve groupings of core MD03-2708. Two unimodal distributions are presented: 'a' – moderately sorted coarse silt (D50: 46.34 µm; D90: 198.63 µm); and 'b' – a well sorted coarse silt (D50: 38.23 µm; D90: 95.84 µm). Two bimodal distributions are presented: 'c' – poorly sorted distribution comprising silts & fine sands (D50: 44.98 µm; D90: 214.86 µm); and 'd' – very poorly sorted composed on medium silts & coarse sands (D50: 48.61 µm; D90: 476.51 µm).

4.2.4 End Member Modelling Analysis

End-member modelling analysis (EMMA) of particle size data unmixes distributions and partitions datasets into statistically meaningful end members that can potentially correspond to sediment delivery processes (Dietze *et al.*, 2012). An end member modelling algorithm was applied to the 58 MD03-2708 grain size distributions using the R package EMMAgeo (Dietze and Dietze, 2013) (v.3.0.1, R Core Team, 2014). In-programme statistical testing confirmed that the optimum number of end-members (EMs) was four (r^2_{mean} = 0.85) [Figure 4-6]. The four end members account for 33 % (EM1), 24 % (EM2), 15 % (EM3) and 27 % (EM4) of the variance respectively.

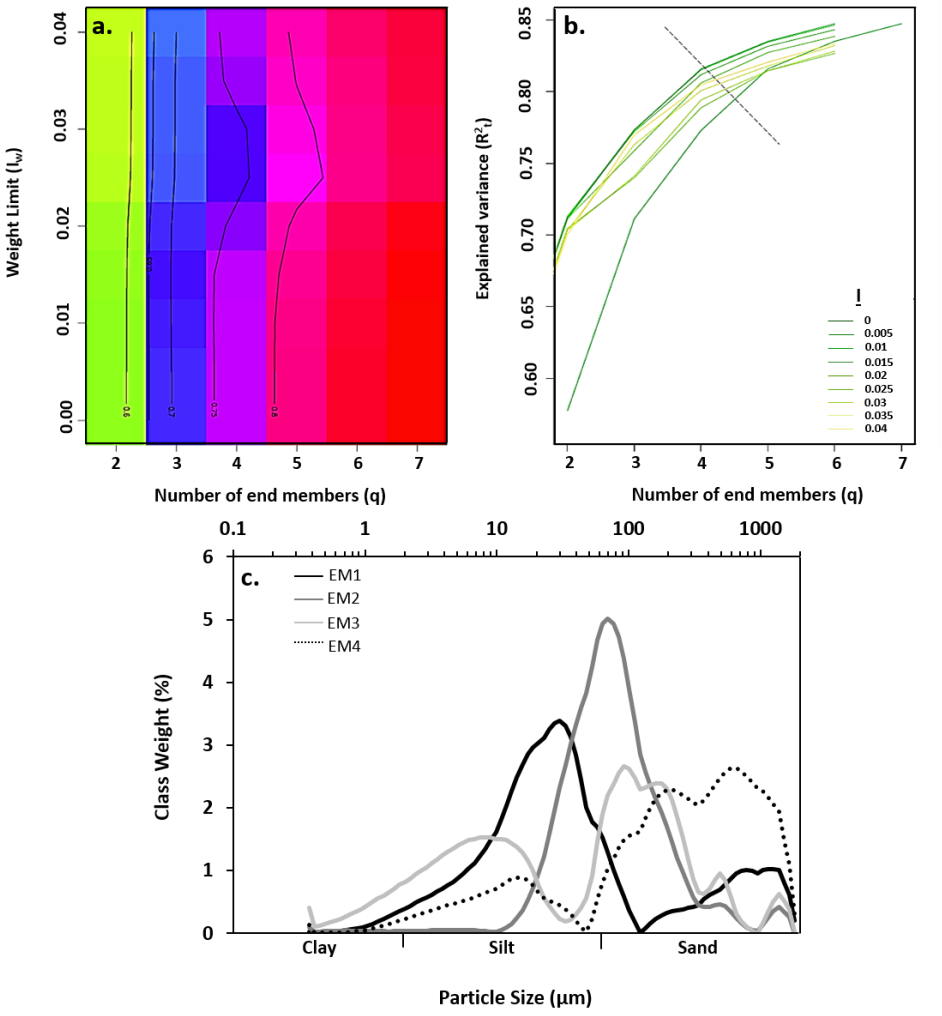

Figure 4-6: MD03-2708 End Member Modelling Output: 'a' Weight limit (l_w) of the number of end members; 'b' Variance explained [r^2_{mean} = 0.85] by the four end members created through the end member modelling analysis; and 'c' the four end member distributions plotted as particle size (µm) against class weight (%).

Distinct groupings are notable within the four end member histograms with preferential modality located within the coarser silt and sand fractions. EM2 presents the only unimodal distribution with a dominant mode within the fine sand fraction (73.02 μm). The other three end members are bimodal (EM1: dominant modalities at 50.28 μm [very coarse silt] and 1199 μm [very coarse sand]) and polymodal (EM3: 8.54 μm [medium silt], 96.60 μm [very fine sand] and 169.10 μm [fine sand]; EM4: 14.96 μm [medium silt], 203.70 μm [fine sand] and 684.90 μm [coarse sand]) deeming them more difficult to interpret in terms of sediment transport processes.

Pearson's correlation was undertaken in Minitab to assess the relationship between particle size, end member proportion and sediment composition data. The largest Pearson correlation coefficient value of 0.941 ($p = <0.001$) is between the D90 and sand percentage variables, supporting the notion that an increase in the sand fraction is driving an enhancement of the D90 value. Sand is most represented by EM4 with a moderate correlation of 0.502 ($p = <0.001$). The saw tooth pattern presented in the sand fraction is most likely representative of deltaic progradation events [navy arrows on Figure 4-7].

These progradation events alternate with an increase in the silt fraction (white arrows), as represented by an increased presence of EM1 [coefficient of 0.936 ($p = <0.001$)] and reflect an alternation between terrigenous sediment sources, most likely between episodes of deltaic progradation and changes in vegetation coverage and stability on the hinterland (Holz *et al.* 2004). In addition to the cyclical alternation of sediment provenance, abrupt shifts are documented in the sediment sequence at 2750 cm, 2300 cm, 1750 cm and 400 cm and are accompanied by a dominance of EM4, and due to the coarse nature of the sediment, resemble rapid discharge events of the Ogooué River (Holz *et al.*, 2007) driven by an intensification of the monsoon system. A potential hiatus in the sedimentation rate of the core is presented at 3000 cm, indicated by a uniform representation of EM4. In order to validate the working hypotheses regarding sediment delivery transport processes to core MD03-2708, the sediment chemostratigraphy also needs to be considered.

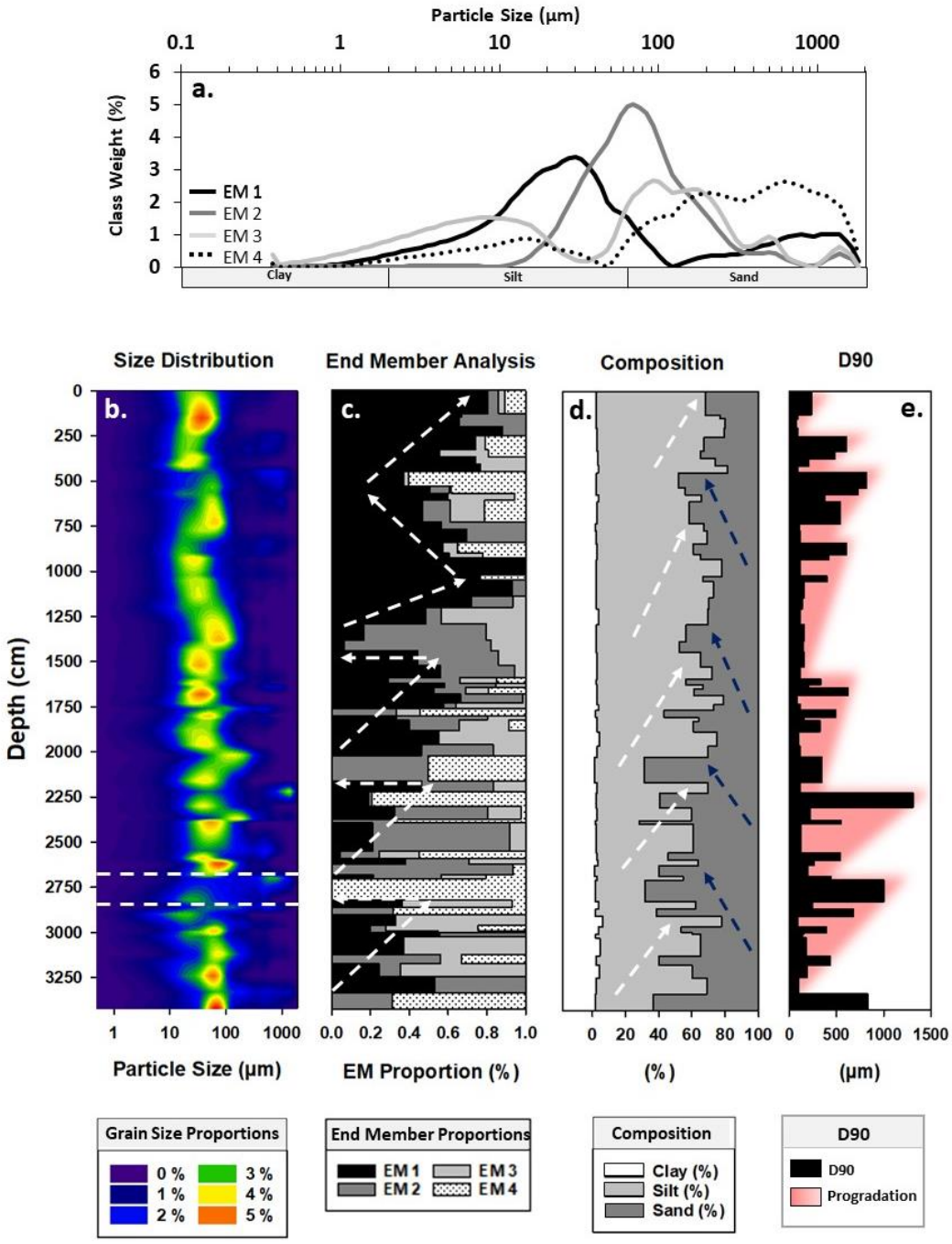

Figure 4-7: Lithostratigraphic summary of core MD03-2708 comprising: 'a' the four EMMA end members; 'b' distribution of grainsizes throughout the core [uniform horizon at 2750 cm highlighted with white dashed lines]; 'c' four end members plotted proportionally [silt influx pattern in EM1 highlighted with white dashed arrows]; 'd' core sediment composition [silt influx -highlighted with white dashed arrows and sand progradation events with navy blue arrows]; and 'e' D90 grain size component [progradation pattern shown in red].

4.3 Chemostratigraphy

4.3.1 Mineralogy

The mineralogical composition of marine sediments is dependent upon multiple factors including the type and weathering of source rocks, sediment transport, depositional conditions and diagenesis (Li and Schoonmaker, 2003; Weltje and von Eynatten, 2004). The content of a given mineral within a marine sediment sample is dependent upon the relative proportions of its constituent phases which are derived from the continent (crystalline and non-crystalline lithogenous components), sea floor (diagenetic and authigenic components) and the water column (endogenic and biogenic material) (Calvert and Pedersen, 2007). The composition of marine inorganic sediments therefore reflects this mixture of components since almost all marine sediments have multiple sediment source inputs.

4.3.1.1 Mineralogical Analysis of core MD03-2708

Mineralogical analysis was undertaken to determine the bulk sediment composition and primary lithology of core MD03-2708. Eleven exploratory samples were taken across the core sequence and were targeted to encompass notably different stratigraphic horizons, determined using preliminary bulk elemental data. Eleven minerals of varying proportions were identified using X-ray diffraction across the sediment sequence [Figure 4-8]. The mineralogy is dominated by silicates throughout (>80 %), with more carbonate rich horizons present towards the middle of the stratigraphic sequence. The mineralogy comprises detrital silt and sand sized grains (quartz and feldspars), clay (illite, kaolinite and chlorite) and calcite, which is most likely biogenic.

4.3.2 Elemental Composition

Elemental data have been used to interpret past climate regimes, oceanic circulation and post-depositional sediment processes (Calvert and Pedersen, 2007). High resolution element measurements of marine sediments allow for both small-scale local climate variation and larger global changes to be detected (Adegbie *et al.*, 2003). In the context of western equatorial Africa, elemental data have been used to understand changing terrestrial climates and more specifically, identify glacial and interglacial periods through disentangling the source provenance of coarse grained – zirconium

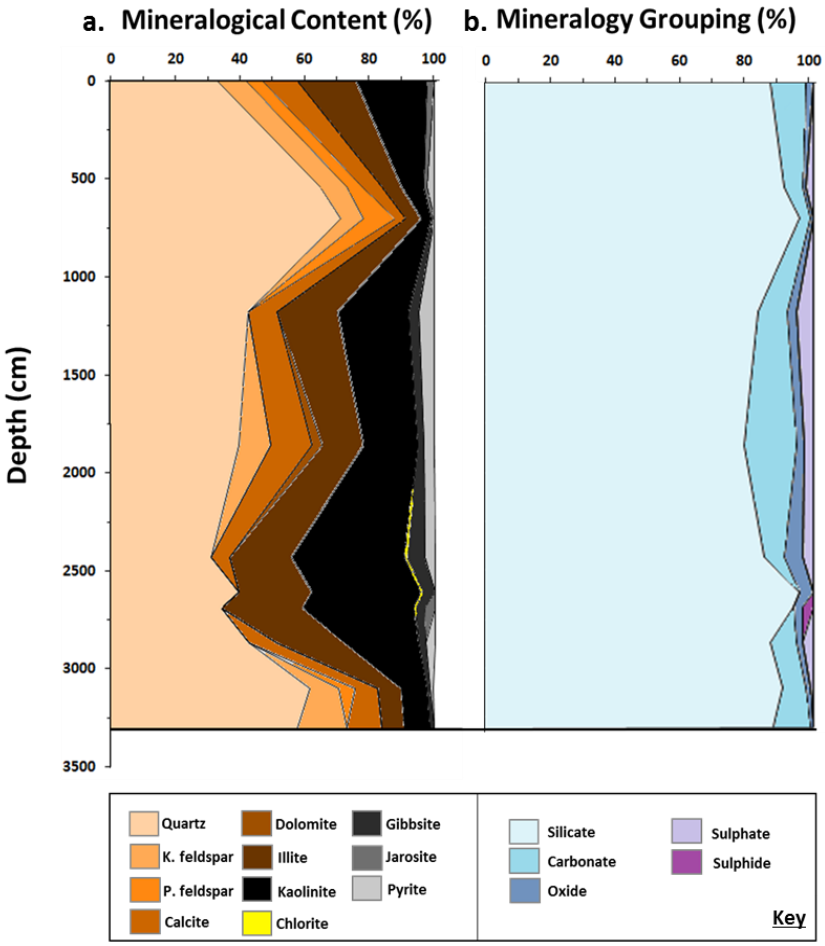

Figure 4-8: Mineralogical component of core MD03-2708 acquired from preliminary XRD analysis from 11 targeted horizons across the core sequence.

rich (indicating glacial periods) and finer grained - iron rich (interglacial periods) sediment input (Holz *et al.*, 2004; Tjallingii *et al.*, 2008; Mulitza *et al.*, 2010; Skonieczny *et al.*, 2015). Similarly, the biogenic carbonate fraction can be utilised to interpret past climate variations, with intervals of higher Ca (i.e. indicative of enhanced carbonate productivity due to sea level fall, documented in higher proportions of $CaCO_3$ shells deposited on the sea floor) reflecting the occurrence of glacial periods (Farrell and Prell, 1989). The XRF elemental data for core MD03-2708 is given here in Figure 4-9.

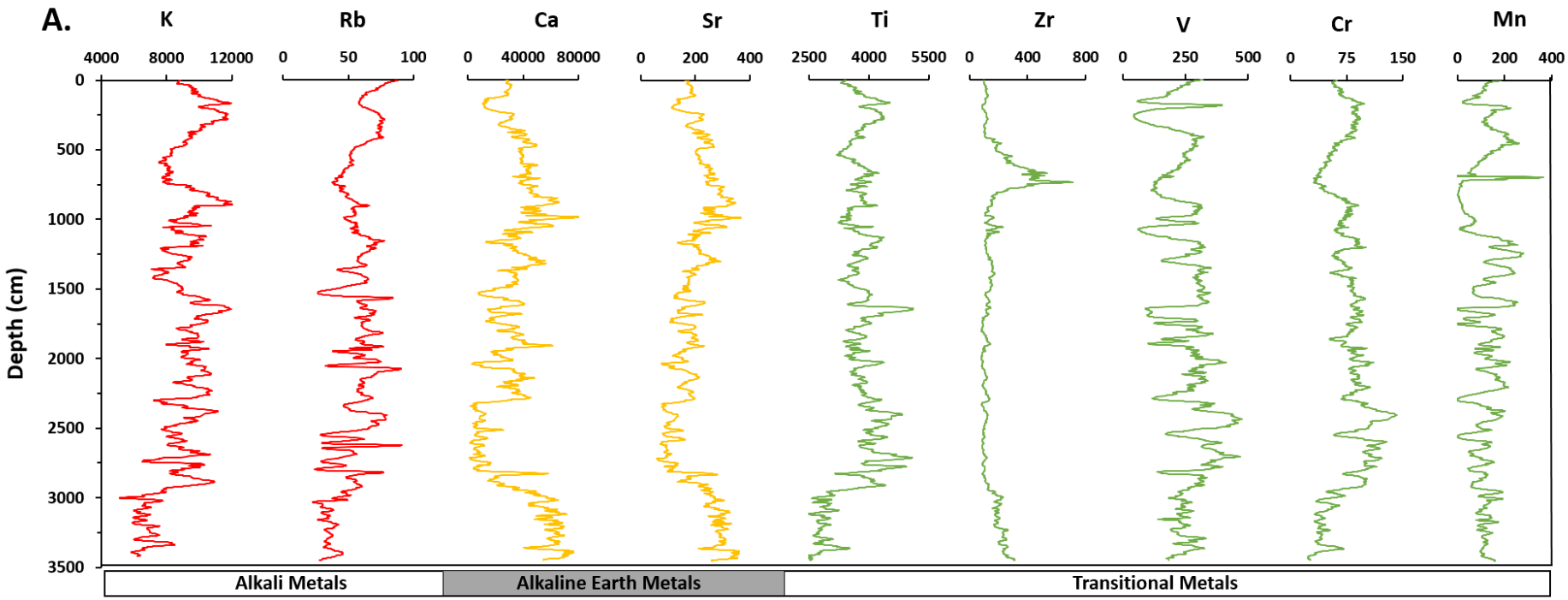

Figure 4-9: (A) Single elements obtained from XRF scanning, grouped into alkali, alkaline earth, and transitional metals.

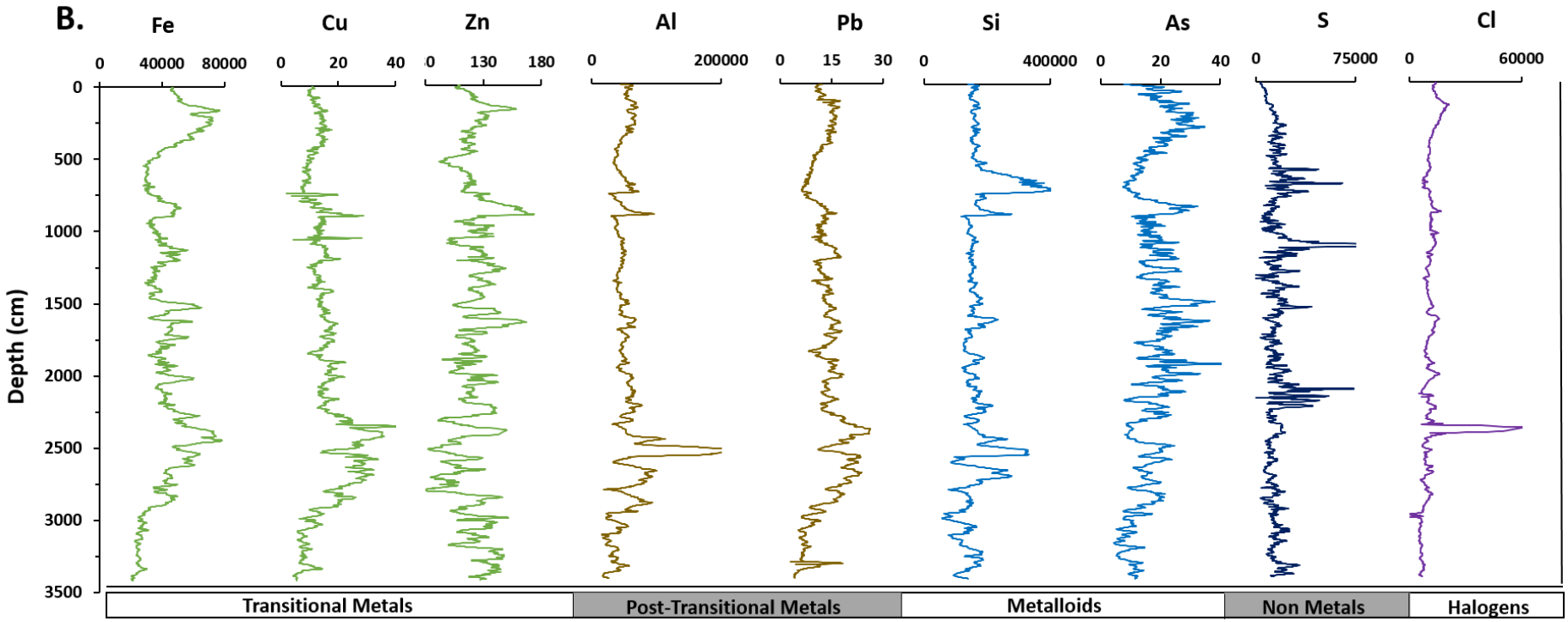

Figure 4-9: (B) Single elements obtained from XRF scanning, grouped into alkali, alkaline earth, and transitional metals.

4.3.3 Chemostratigraphic Approach

Numerous studies use major element concentrations measured on continental margin sediment to reconstruct terrestrial climate variations (e.g. Govin *et al.*, 2012; Mulitza *et al.,* 2008; Collins *et al.,* 2013). The choice and interpretation of major elements varies from site to site and the rationale behind using specific elements or elemental ratios can at times be subjective. Elemental ratios used here followed those described in (Croudace and Rothwell, 2015) [Table 4-1].

Forty-one elemental ratios were selected for principal component analysis (with a correlation matrix) in Minitab version 17. The assimilated loading plot [Figure 4-10] was used to group ratios with similar component scores, in order to attribute certain ratios to particular processes (i.e. fine and coarse fraction terrigenous input, biogenic components, diagenetic processes, etc.). Elements were divided into six groups given in Table 4-1 and plotted in Figure 4-10.

Group one was further split into three subgroups, each with similar principal component scores, yet which detail different sedimentary types. Using the literature outlined in Table 4-1, each group has been attributed an initial sedimentary process or palaeoenvironmental interpretation.

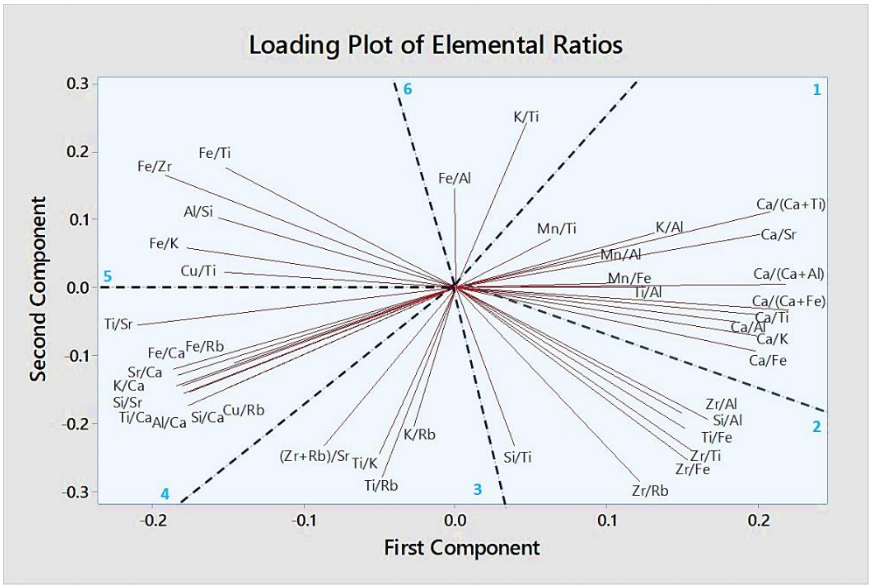

Figure 4-10: Loading plot of the 41 MD03-2708 elemental ratios inputted into a principal components analysis (using Minitab v. 17) in order to group the ratios into similar environmental categories.

Table 4-1: Grouping of 41 MD03-2708 elemental ratios according to the calculated principal component analysis loading scores. Reciprocal ratios are shaded in grey. References in italics are those used in addition to the references used from the (Rothwell and Croudace, 2015) compilation.

Group		Elemental Ratio	Proxy Indicator	References
1	a	Mn/Fe	Assessment of sediment redox conditions	Marsh *et al.* (2007)
		Mn/Ti	Identification of redox transitions	Thomson *et al.* (2006)
		Mn/Al	Assessment of sediment redox conditions	*Calvert and Pedersen (*2007); Spofforth *et al.* (2008)
	b	K/Al	Sediment provenance change	*Calvert and Pedersen (2007)*; Spofforth *et al.* (2008)
		Ti/Al	Sediment provenance or energy change	Spofforth *et al.* (2008)
	c	Ca/K	Biogenic carbonate presence	Hebbeln *et al.* (2006)
		Ca/Ti	Biogenic carbonate presence	Ingram *et al.* (2010)
		Ca/Al	Biogenic carbonate presence	Blanchet *et al.* (2009)
		Ca/Fe	Variation in sediment delivery	Nizou *et al.* (2010)
		Ca/(Ca+Fe)	Biogenic carbonate presence	*Boyle (2016) pers.comm.*
		Ca/Sr	High detrital carbonate	Hodell *et al.* (2008)
		Ca/(Ca+Al)	Biogenic carbonate presence	*Boyle (2016) pers.comm.*
		Ca/(Ca+Ti)	Biogenic carbonate presence	*Boyle (2016) pers.comm.*
2		Si/Ti	Biogenic silica content; terrestrial quartz	Marsh *et al.* (2007); *Boyle (2016) pers.comm.*
		Ti/Fe	Sediment provenance	Zarriess (2010)
		Si/Al	Sediment provenance - quartz indicator	Hoffman *et al.* (2005); *Calvert and Pedersen (*2007)
		Zr/Rb	Sediment provenance - riverine flooding	*Dypvik and Harris (2001); Calvert and Pedersen (2007);* Wang *et al.* (2011)
		Zr/Fe	Sediment provenance	Konfirst *et al.* (2011)
		Zr/Ti	Sediment provenance	*Boyle (2016) pers.comm.*
3	a	K/Rb	Grain size indicator	Croudace and Rothwell (2015)
		Ti/Rb	Sediment provenance indicator	Rothwell *et al. (2006)*
	b	Ti/K	Sediment provenance indicator	Siani *et al.* (2010)
		(Zr+Rb)/Sr	Siliciclastic vs carbonate contents	*Dypvik and Harris (2001)*
4		Si/Ca	Aeolian dust input	Haneburth & Lantzsch (2008)
		Sr/Ca	Terrigenous vs biogenic supply	Hodell *et al.* (2008)
		Al/Ca	Terrigenous vs biogenic supply	Nizou *et al.* (2010)
		Ti/Ca	Terrigenous vs biogenic supply	Tjallingii *et al.* (2011)
		K/Ca	Terrigenous vs biogenic supply	McGregor *et al.* (2009)
		Fe/Ca	Terrigenous vs biogenic supply	Adegbie *et al.* (2003); Lebreiro *et al.* (2009)
		Si/Sr	Terrigenous vs biogenic supply	Hodell *et al.* (2008)
		Ti/Sr	Terrigenous vs biogenic supply	Zaragosi *et al.* (2006)
		Cu/Rb	Diagenetic mobilisation of copper	Rothwell *et al.* (2006)
		Fe/Rb	Terrigenous vs biogenic supply	Rothwell *et al.* (2006)
5		Cu/Ti	Post-depositional oxidation of organic-rich layers	Thomson *et al.* (2006)
		Fe/K	Changes in terrigenous mineralogy	Kuijpers *et al.* (2003)
		Fe/Ti	Changes in terrigenous mineralogy	Blanchet *et al.* (2009); Itambi *et al.* (2010)
		Fe/Zr	Hinterland precipitation	Haneburth and Lantzsch (2008)
		Al/Si	Clay Content	Hoang *et al.* (2010)
6	a	K/Ti	Chemical Weathering	(Diekmann *et al.*, 2008; Hodell *et al.*, 2010)
	b	Fe/Al	Anoxic bottom waters	(Spofforth *et al.*, 2008)

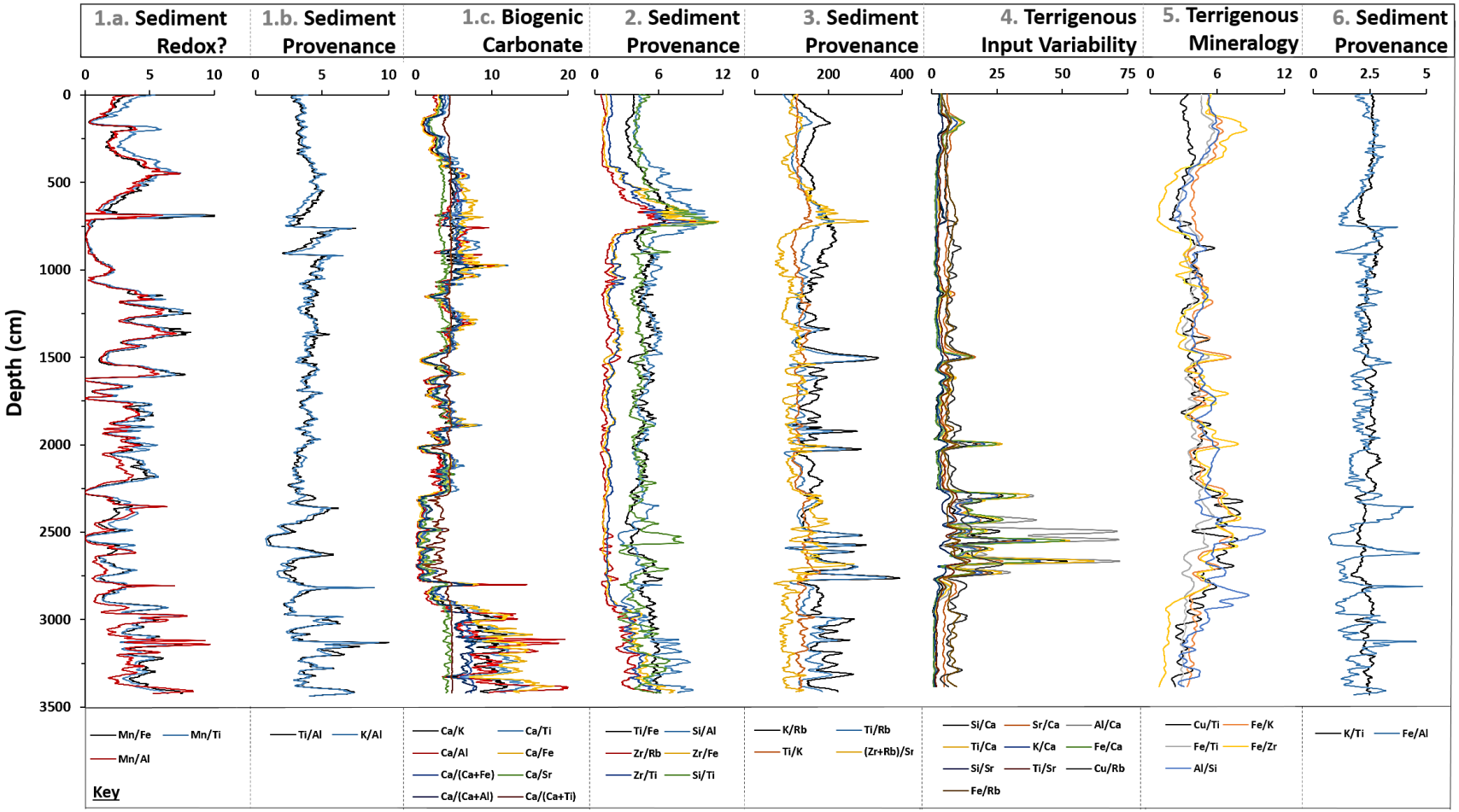

Figure 4-11: The 41 elemental ratios of core MD03-2708 plotted into the groups determined by the principal component analysis. Preliminary environmental interpretations have been attributed to each group according to the literature outlined in Table 4-1.

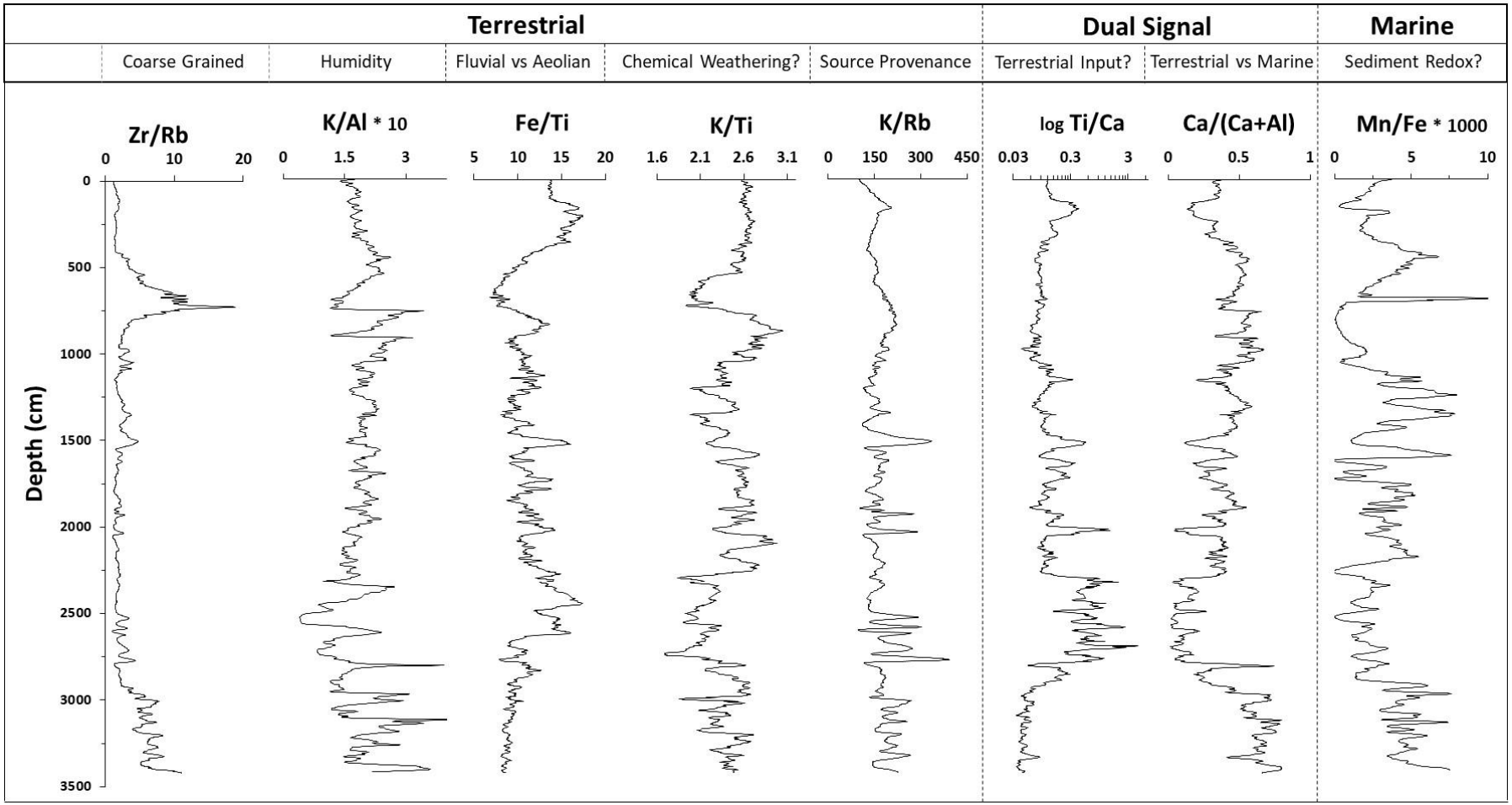

Figure 4-12: The key eight elemental ratios chosen to represent the terrestrial, marine and dual signal sediment provenance and palaeoenvironmental histories of core MD03-2708.

4.3.3.1 Key Elemental Ratio Selection

The elemental ratios plotted in Figure 4-12 are divided into those that reflect terrestrial, marine and dual (terrestrial and marine) signals. An elemental ratio was assigned to represent each of the eight sedimentary processes [Figure 4-12] yielding five ratios representative of the terrestrial signal (coarse grained sediment; humidity indicator; fluvial versus aeolian signal; chemical weathering indicator; and source provenance proxy), two dual signal ratios (terrestrial input and terrestrial versus marine signal) and one marine ratio (sediment redox).

4.4 Sediment Provenance

In order to fully reconstruct the provenance of sediments of core MD03-2708 it is necessary to examine the lithostratigraphic and chemostratigraphic data together. A Pearson's correlation was undertaken between the lithostratigraphic and chemostratigraphic variables, but no significant correlations were found. In light of this, the two data sets were plotted alongside each other and three noteworthy sediment provenance trends were observed. An elemental ratio has been assigned to represent each of these trends, yielding two terrigenous sediment provenance pathways, and one marine.

4.4.1 Terrigenous Sediment Provenance Pathways

The Fe/Ti, K/Ti and K/Al ratios presented very similar morphological outlines, as did the Zr/Rb and Si/Ti ratios. To ease interpretation, the Fe/Ti was chosen to represent the first grouping, and Zr/Rb the second.

4.4.1.1 Fe/Ti as a Fluvial Outwash Indicator

Iron and titanium have been used by authors as proxies for terrigenous input into marine environments (Haug *et al.*, 2001; Zabel *et al.*, 2001a; Govin *et al.*, 2012). Itambi *et al.* (2010) use the iron/ titanium (Fe/Ti) ratio as a proxy for fluvial versus aeolian terrigenous input in the Gulf of Guinea. In the eastern equatorial Atlantic, high precipitation facilitates the intense chemical weathering of bedrock resulting in highly weathered soils with a large Fe geochemical signature (Govin *et al.*, 2012). The iron is transported into the Gulf by the multiple river systems (e.g. Ogooué and Sanaga) and is thought to vary positively with hydrological changes (Itambi *et al.,* 2010). Titanium has been used as a Saharan dust tracer in marine sediments (Zabel *et al.*, 2001a; Itambi

et al., 2009). Itambi *et al.* (2010) infer that a high Fe/Ti ratio reflects enhanced fluvial input during warm periods when precipitation is higher, whilst an increase in aeolian dust is evidenced by a higher proportion of Ti.

As shown in Figure 4-13 there is a notable coincidence between the influx events of EM1 and the peaks in the Fe/Ti ratio. An increase of EM1 and silt [white arrows], and a decrease of the D90 [navy arrows] is accompanied by an intensification of iron [navy shaded horizons and white dashed arrows], which can be interpreted here as higher fluvial input, rather than a decrease in aeolian blown titanium, due to the equatorial positioning of the marine core. The Fe/Ti ratio dovetails the magnetic susceptibility trend with higher magnetism indicating increased terrigenous outwash, further strengthening the reliability of the elemental ratio as a fluvial outwash proxy.

4.4.1.2 Zr/Rb as an Aridity Marker

Changes in the zirconium/rubidium (Zr/Rb) ratio have been used by (Schneider *et al.*, 1997) to reflect the enrichment of zircon ($ZrSiO_4$) relative to feldspar in deeply weathered soils. The Zr/Rb ratio can be indicative of the proportion of heavy minerals present within sediment since Zr is commonly associated with the heavy mineral fraction (e.g. quartz and rutile), whilst Rb is attributed to the fine grained clay fraction and is a particular constituent of illite ($(K,H_3O)(Al,Mg,Fe)_2(Si,Al)_4O_{10}$) (Matthewson *et al.*, 1995). The Zr/Rb ratio can therefore be a useful proxy for the grain size of sediment (Dypvik and Harris, 2001).

Working on the Niger Fan, (Zabel *et al.*, 2001) accredited an increase of Zr, relative to Rb, during glacial periods to a combination of reduced precipitation and a subsequent reduction in vegetation cover. Despite particularly large freshwater inputs coinciding with periods of maximum wetness during the Holocene periods, they document a maximum terrigenous input of the Niger River during the arid last glacial maximum. During this period, low runoff and reduced vegetation cover, in combination with large amounts of river suspended matter, evidence that the degree of weathering, or rather the more exposed soil types, was the controlling factor of zirconium input to the Niger Fan during arid periods (Zabel *et al.*, 2001).

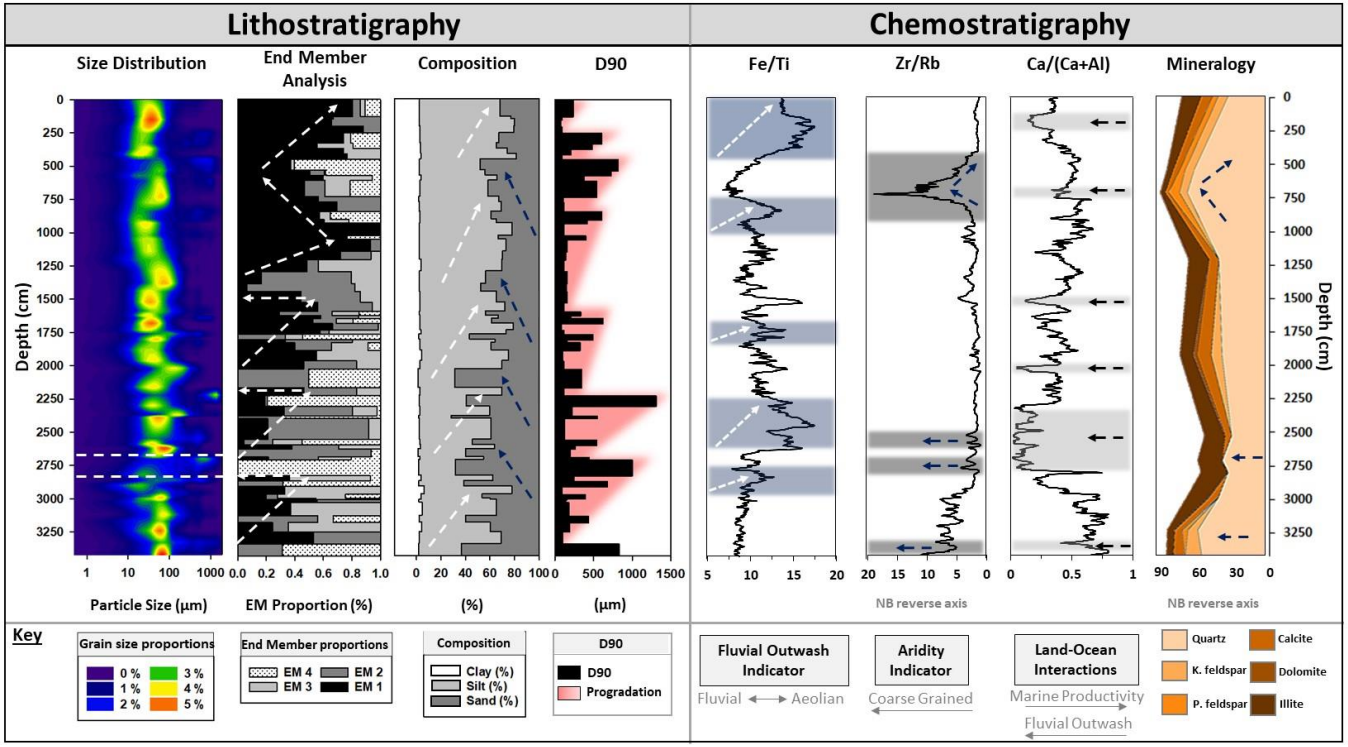

Figure 4-13: Key sedimentological proxies for core MD03-2708 comprising: Grain Size Distribution with a uniform distribution highlighted by white arrows at 2750 cm; End Member proportions – EM1 dominance and morphology highlighted by white arrows; Sediment composition – alternation between silt and sand dominances indicated with white and navy arrows respectively; D90 with progradation emphasised in red; Fe/Ti ratio as a fluvial outwash indicator – dominant horizons with grey shading and white arrows; Zr/Rb ratio as an index for aridity – coarse sections shown in dark grey with navy arrows; Ca/(Ca+Al) ratio as a proxy for land-ocean interactions – fluvial outwash shown by light grey shading and black arrows; and detrital siliciclastic and clay mineralogy – increases highlighted by navy arrows.

The MD03-2808 record shows a relationship between the Zr/Rb ratio, the mineralogical and sedimentological compositions of the core and the grain size distribution. Increases in the sand fraction [navy arrows], D90 and EM4 are concurrent with fluxes of zirconium [grey shading and navy arrows] paired with detrital quartz and feldspars [blue arrows]. Following on from the work undertaken in the Niger Fan (Zabel *et al.*, 2001) these coarse, zirconium rich horizons can be attributed as periods of aridity. The alternation between the two dominant terrigenous sediment provenances highlights an alternation between an arid and humid hinterland driven by changes in the strength and positioning of the West African monsoon system, and the consequent extent and coverage of the terrestrial vegetation.

4.4.2 Ca/(Ca+Al) as an Index for Land-Ocean Interactions

Terrestrial elemental concentrations in ratio to calcium (e.g. Ti/Ca, Fe/Ca, Al/Ca) have been widely used to trace changes in the terrigenous input of aeolian and fluvial components offshore Northeast Brazil (Arz *et al.,* 1998; Jaeschke *et al.*, 2007) and Western Africa (Adegbie *et al.*, 2003; Romero *et al.,* 2008; Govin *et al.*, 2012). In a West African context, aluminium has been used to reflect the siliciclastic component of terrigenous sediment (Jansen *et al.,* 2008), and calcium is used to represent the carbonate content of marine sediment (Peterson, 2000). An enhancement of aluminium is reflective of more humid periods, with higher Al relative to Ca reflecting increased precipitation producing enhanced terrestrial sediment inwash, whilst higher calcium reflects enhanced marine carbonate productivity during arid periods. The ratio between aluminium and calcium can therefore be used to not only support the two terrigenous elemental ratios, but it also details the response of the adjacent ocean to climatic shifts over the time frame.

Caution needs to be taken when interpreting elemental ratios including Ca (e.g. Ti/Ca, Fe/Ca) as they do not solely reflect the proportion of terrigenous material deposited onto the seafloor (Govin *et al.*, 2012). Concentrations of calcium within the sediment vary with changes in marine carbonate productivity and dissolution. Due to the caveats associated with using an elemental ratio comprising Ca to interpret terrestrial versus marine variations, it has been necessary to develop and alternative proxy to address this. Through dividing Ca by the elemental ratio in question (i.e. Ca/(Ca+Al), the potential error associated with marine carbonate productivity and dissolution (Boyle,

2017 pers. comm.) has been removed, thereby attempting to produce a more accurate terrestrial versus marine signal.

The Ca/(Ca+Al) record presented on Figure 4-13 presents an alternation between Ca dominated horizons and Al rich horizons (grey shading and black arrows). This alternation between Ca and Al is reflective of more arid periods with higher marine productivity and more humid periods with high terrestrial outwash and lower marine productivity respectively. Towards the top of the core the Al rich horizons considerably decrease in size and are most likely representative of rapid, fluvial outwash events. These Al rich horizons are accompanied by the presence of EM3, but EM2, indicating a dominant source provenance comprising clays and sands, but not coarse silts.

Exploration of the lithostratigraphic and chemostratigraphic components of marine core MD03-2708 provides a platform upon which to explore sediment source provenances, sediment transport dynamics, and land-ocean interactions driven by the variability of the West African Monsoon system in Western Equatorial Africa. A robust chronology allows the understanding of these sedimentological processes on a temporal scale and to disentangle the role that palaeoclimate change has played in determining the sediment make-up of the Ogooué Fan.

5 Geochronological Control of Core MD03 2708

5.1 Geochronology

Geochronology is the science of determining the age of fossils, sediments and rocks using the signature characteristics of the rocks themselves. A geochronological record can be absolute, achieved with radioactive isotopes (e.g. ^{14}C), and relative, developed with tools such as stable isotope ratios (e.g. $\delta^{18}O$).

5.2 Previous Age Determination of Marine Core MD03-2708

A preliminary age framework for the MD03-2708 core sequence was constructed by Kim *et al.* (2010) using radiocarbon dating of marine biogenic carbonate [Figure 5-1]. Accelerator mass spectrometry (AMS) ^{14}C dating was undertaken by Kim *et al.* (2010) on bivalve molluscs from 14 horizons (8 from the short 'casq' core and 6 from the long 'GPC' core) [Table 5-1] at the NERC Radiocarbon Laboratory AMS Facility [East Kilbride, Scotland, UK] (Allocation number: 1162.1005).

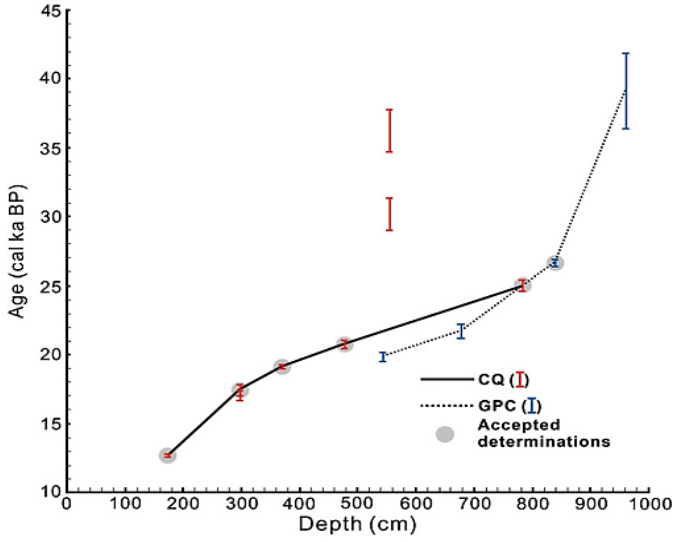

Figure 5-1: 'Calibrated age-depth curves for the GPC MD03-2708 (dotted line) and MD03-2708 CQ (solid line) cores based on AMS ^{14}C dating; CQ core samples (red bars), GPC samples (blue bars), and accepted ^{14}C dates (grey circles)' (Kim *et al.*, 2010).

Table 5-1: Radiocarbon data from the short MD03-2708 (CQ) and long MD03-2708 (GPC) marine sediment cores (after Kim *et al.,* 2010 and Jacobsen, 2012).

Publication Code	Sample Identifier	Depth (cm)	Materials	Conventional radiocarbon age (yr BP +/– 1σ)	Calib age (yr, BP)	2 σ range of cal. age (yr. BP)	Decision
AAH18136	MD03-2708 CQ	54-56	Foraminifera	6,233 +/– 35	6,682.50	6,636-6,729	–
SUERC-7752	MD03-2708CQ	173-174	Bivalve mollusc	10,984 +/– 33	12,675	12,567-12,782	Accepted
SUERC-7753	MD03-2708CQ	297-298	Bivalve mollusc	14,923 +/– 53	17,455	17,040-17,870	Accepted
SUERC-7754	MD03-2708CQ	297-298	Bivalve fragments	14,671 +/– 51	17,040	16,633-17,444	Rejected
SUERC-7756	MD03-2708CQ	371-372	Bivalve fragments	16,285 +/– 62	19,090	18,929-19,251	Accepted
SUERC-11719	MD03-2708CQ	476-477	Bivalve mollusc	17,944 +/– 47	20,740	20,455-21,039	Accepted
SUERC-10448	MD03-2708CQ	553-554	Bivalve fragments	31,316 +/– 779	36, 270	29,063-31,375	Rejected
SUERC-10451	MD03-2708CQ	553-554	Taxodont bivalve	25,143 +/– 356	30,219	29,641-30,797	Rejected
SUERC-7757	MD03-2708CQ	781-782	Bivalve fragments	21,202 +/– 113	25,020	24,606-25,434	Accepted
SUERC-10452	GPC MD03-2708	542-543	Bivalve fragments	17,151 +/– 127	19,860	19,551-20,164	Rejected
SUERC-10453	GPC MD03-2708	675-679	Bivalve fragments	18,679 +/– 155	21,680	21,174-22,189	Rejected
SUERC-11720	GPC MD03-2708	838-839	Bivalve fragments	22,196 +/– 35	26,670	26,428-26,904	Accepted
SUERC-10454	GPC MD03-2708	959-960	Bivalve fragments	33,985 +/– 1091	39,140	36,396-41,876	Rejected
SUERC-10455	GPC MD03-2708	1191-1192	Bivalve fragments	> 40,700	–	–	Rejected
SUERC-10456	GPC MD03-2708	2592-2593	Bivalve fragments	Indistinguishable from background	-	-	Rejected

A further ^{14}C date [Figure 5-1] was obtained from bulk foraminifera from a single horizon near the top of the casq core at the AMS Dating Centre, within the Department of Physics and Astronomy, Aarhus University, Denmark (Jacobsen, 2012). The ^{14}C ages were corrected to calibrated ages using CALIB version 5.01 (Stuiver and Reimer, 1993) and for ages over 26,000 years before present (BP), calibration was achieved using the Fairbanks 0107 calibration programme (Fairbanks *et al.*, 2005). The standard marine ^{14}C reservoir correction (ΔR) (i.e. 400 years) was also applied (Stuiver *et al.,* 1998). Of the 14 ^{14}C dates acquired by Kim *et al.* (2010), six dates extending between 12,675 and 26,670 cal ka BP were accepted to form the final age model.

5.2.1 $\delta^{18}O$ Stratigraphies as Chronological Frameworks

Ranging from sub annual, to hundreds of thousands of years, marine $\delta^{18}O$ stratigraphies afford a globally comparable tool of palaeoclimate reconstructions. Synchronicity with terrestrial records (e.g. the $\delta^{18}O$ recorded in ice cores, speleothems, and lake sediment sequences) allows correlations to be made between archives that are thousands of kilometres apart (Pisias *et al.* 1984; Prell *et al.* 1986). The consistent stable isotope signal preserved in marine sediments across the globe has enabled the production of commonly recognisable marine isotope stages (MIS) (Emiliani, 1955). MIS warm periods (interglacials) are defined by odd numbers and the colder (glacial) periods, even numbers [Figure 5-2].

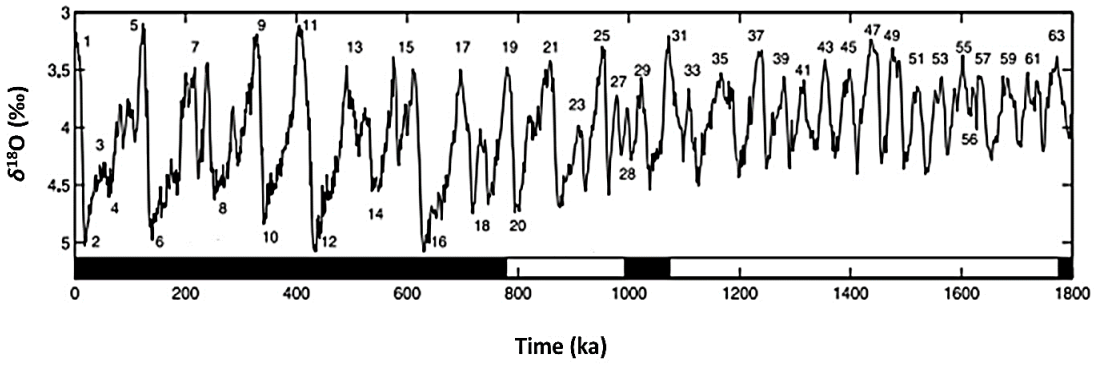

Figure 5-2: The upper third of the LR04 benthic $\delta^{18}O$ stack record constructed by the graphic correlation of 57 globally distributed benthic $\delta^{18}O$ records. Marine Isotopes Stages are numbered and denote interglacial (odd numbers) and glacial periods (even numbers) [Lisiecki and Raymo, 2005].

5.3. Building a New Age Model for MD03-2708

The primary objectives in the creation of a new age model were two fold. The first was to produce an age skeleton that would accurately encompass the entire core sequence and extend beyond the oldest previously generated radiocarbon date of > 40,700 cal ka BP at 1191.5 cm. The second was the production of a globally comparable age framework.

5.3.1 Data Comparisons

In order to establish a chronology for the MD03-2708 sequence, the benthic and planktic $\delta^{18}O$ oxygen isotopes were compared to regional records. However, the poor resolution of foraminifera between 2750 and 2250 cm in conjunction with a paucity of foraminifera between 250 cm and 0 cm, meant that an accurate comparison could not be made using the MD03-2708 isotope record alone. Additional geochemical, isotopic and palynological MD03-2708 proxies were employed in order to create a more comprehensive age framework for the core site.

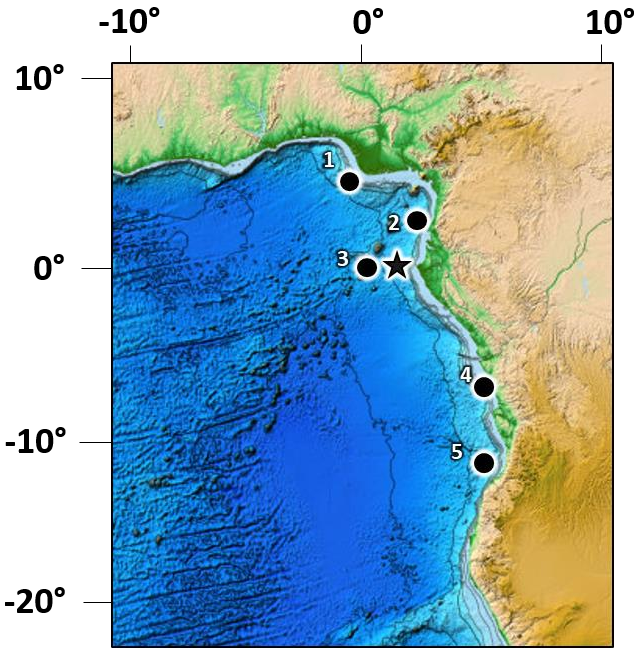

Figure 5-3: Comparison sites used in the construction of the new MD03-2708 age model: (1) GIK 16856 in the Niger Delta (Dupont and Weinelt, 1996); (2) MD03-708 in the Sanaga Basin (Weldeab *et al.,* 2007); (3) GIK 16867 offshore Gabon (Dupont *et al.,* 2000); (4) GeoB 1008-3 in the Congo Fan (Jahns *et al.,* 1996; Schneider *et al.,* 1997); (5) GeoB 1014-3 offshore Angola (Schneider *et al.,* 1994). The LR04 global benthic $\delta^{18}O$ stack record (Lisiecki and Raymo, 2005) and the Antarctic Vostok $\delta^{18}O$ H_2O ice core record (Johnsen *et al.,* 2001) were also used for the comparisons but are not included on this figure.

The following proxies were used in order to establish age control points for the MD03-2708 record: calcium and magnetic susceptibility were compared with a record from the Congo Fan (GeoB 1008-3) [Figure 5-3 (4) and Figure 5-4-A]; the MD03-2708 benthic $\delta^{18}O$ isotope record was compared to records from offshore Angola (GeoB 1014-3) [Figure 5-3 (5) and Figure 5-4-A], a global benthic $\delta^{18}O$ stack record (LR04) [Figure 5-4-A] [*NB not show on Figure* 5-2], a planktic $\delta^{18}O$ record from the Sanaga Basin (MD03-2707) [Figure 5-3 (2) and Figure 5-4-A], and a record further offshore Gabon (GIK 16867) [Figure 5-3 (3) and Figure 5-4-A]; the MD03-2708 benthic $\delta^{13}C$ record was compared with the Angolan and Congolese records [Figure 5-4-B]; the MD03-2708 benthic $\delta^{18}O$ record was compared with the $\delta^{18}O$ H_2O record in the Antarctic Vostok ice core [Figure 5-4-B] [*NB not show on Figure* 5-3]; MD03-2708 *Cyperaceae, Podocarpus* and *Rhizophora* pollen records were compared to the Congolese record [Figure 5-3-B]; the *Rhizophora* pollen was also compared with a record from the Niger Delta (GIK 16856) [Figure 5-3 (1) and Figure 5-4-B]. The corresponding ages for each proxy comparisons were compared against depth of the MD03-2708 record. This resulted in 31 comparable horizons which were then averaged to give a preliminary age-depth chronology [Table 2-A and Table 2-B].

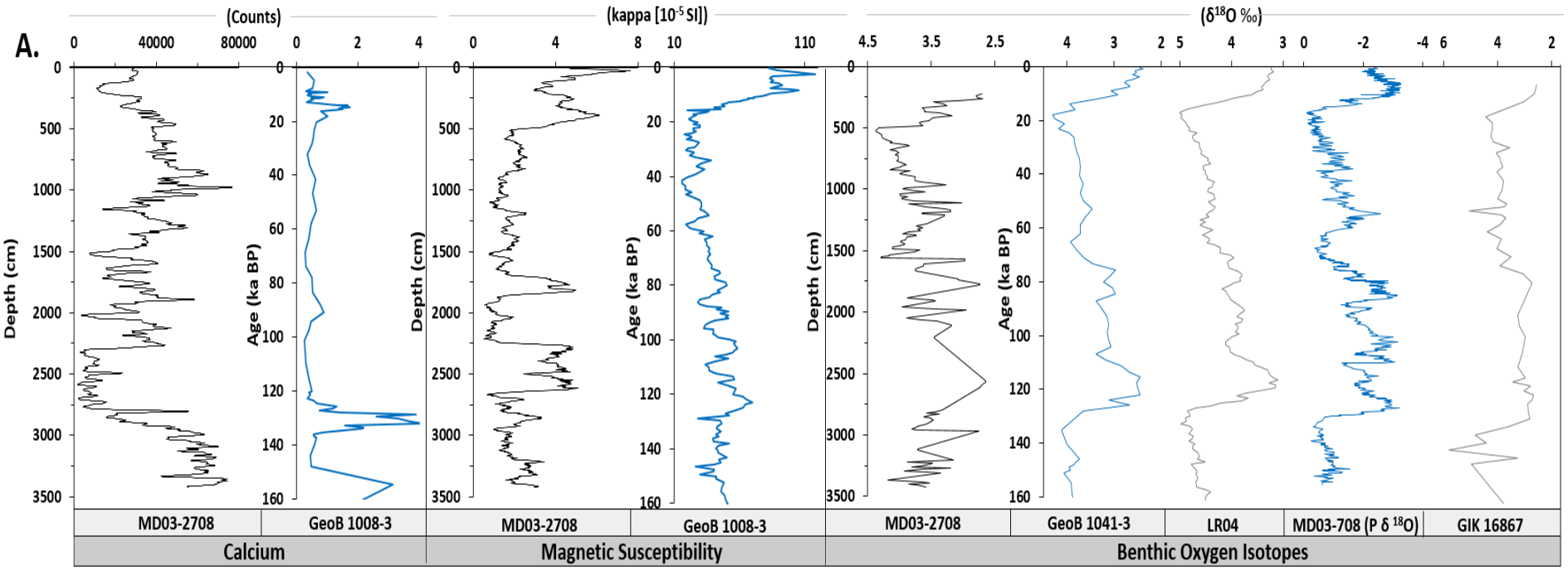

Figure 5-4-A: Proxies and core labels of cores used in core comparisons and determination of age-depth control points.

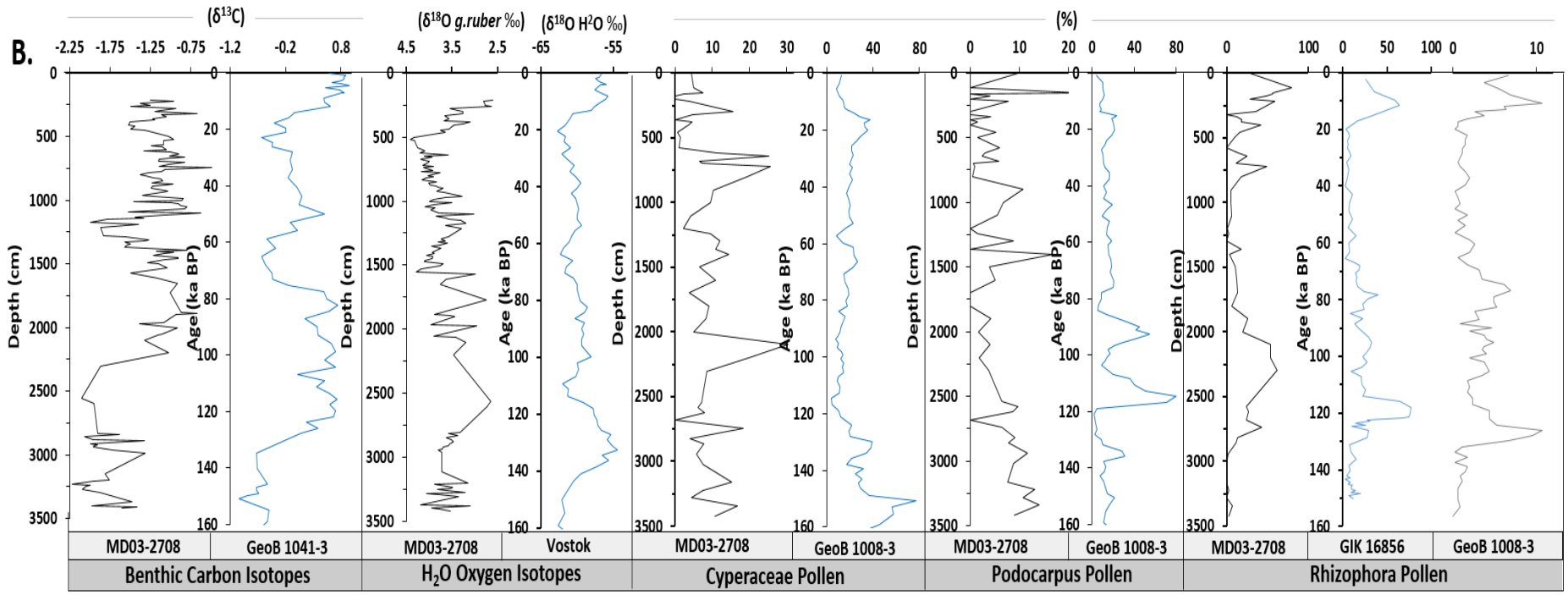

Figure 5-4-B: Proxies and core labels of cores used in core comparisons and determination of age-depth control points.

Table 5-2-A: Depth – age control points for the new MD03-2708 sequence (part A): original MD03-2708 14C dating is in included (Beard, 2004 & Jacobsen 2012).

Depth (cm)	^{14}C Dating	Ca	Mag Sus	Benthic ^{18}O				Benthic ^{13}C	^{18}O H_2O
	MD03-2708	GeoB1008-3	GeoB1008-3	GeoB1041-3	LR04	MD03-2707 P^{18}O	GIK67867	GeoB1041-3	Vostok
27			2.5						
55	6.68								
110									
173	12.68								
297	17.46								
371	19.09								
476	20.74								
781	25.02								
838	26.67								
960						37.29			
1040						38.28			
1101						54.12			
1201									
1550						66.74			60.34
1580				75.5					
1660				80					
1700									
1770						84.24			
1780				85	84				
2210				107	110				
2300									
2680									
2880					130				
2930									
2940						132.5			150.27
2950				135	140		140.75		
2970							143.58		
3120							145.84		
3190								149	
3220								151	
3370		154							

Table 5-2-B: Depth – age control points for the new MD03-2708 sequence (part B). Values averaged to produce preliminary age-depth sequence.

Depth (cm)	Cyperaceae	Podocarpus	Rhizophora		Average Values
	GeoB1008-3	GeoB1008-3	GIK16856-2	GeoB1008-3	
27					2.5
55					6.68
110			11.7	10.7	11.2
173					12.68
297					17.46
371					19.09
476					20.74
781					25.02
838					26.67
960					37.29
1040					38.28
1101					54.12
1201	57.32				57.32
1550					66.74
1580					75.5
1660					80
1700	80.4	80.4			80.4
1770					84.24
1780					84.5
2210					108.5
2300			120	128	124
2680	128	124	124	135	127.75
2880					130
2930					137
2940		135.91			139.56
2950					140
2970					143.58
3120					145.84
3190					149
3220					151
3370					154

5.3.2 Age Model Calibration

The age-depth values were inputted into *Clam* version 2.2 (Blaauw, 2010) in *R Studio* version 3.0.1. A smooth spline curve with the 'Marine13' calibration was fitted to the estimated tie point ages listed in Table 4-2 (Reimer *et al.*, 2013). Ages with 95 % confidence intervals were calculated for every 1 cm of the MD03-2708 sediment sequence, yielding a core base age of 155 579 cal ka BP [Figure 5-5-a]. Error age estimates were set at 1 %, in line with Lisiecki and Raymo (2005). Knowledge of the age of the MD03-2708 ages allowed for the sedimentation accumulation rate (SAR) (to be determined [Figure 5-5-b]. The SAR ranges between 3.42 cm yr^{-1000} (76 – 74 ka) and 101.11 cm yr^{-1000} (126 – 112 ka).

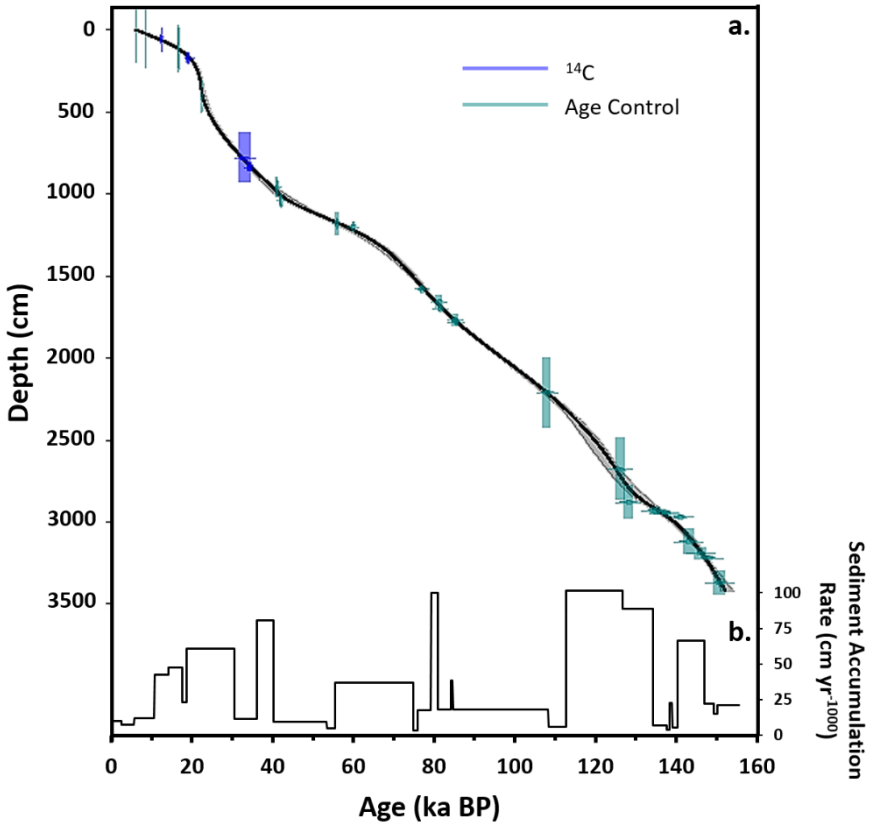

Figure 5-5: New MD03-2708 age-depth model fitted with a smooth spline curve fitted with Marine13 calibration. Purple symbols denote 14C control points and green symbols denote age controls points generated through proxy comparisons. The hiatus noted at 3000 m in Chapter 4 can be seen by the clumping of green symbols at 3000 m on the age-depth curve.

6 Eastern Equatorial Atlantic Response to Riverine Discharge Variability since MIS 6

6.1. Introduction

The Eastern Equatorial Atlantic (EEA) Ocean is a key area for Quaternary palaeoclimatic research due to the tight coupling between atmospheric and oceanic circulations in this region (e.g. Kallweit *et al.,* 2012). Previous studies of West African hydrology have unearthed alternating dry and humid conditions as reconstructed from lake-level fluctuations across the African continent (e.g. Gasse, 2000; Shanahan *et al.*, 2006; Miller and Gosling, 2014), and marine records from the West African continental margin (e.g. Schneider *et al.*, 1997; Lézine *et al.*, 2005; Weldeab *et al.*, 2007; Dupont *et al.,* 2008; Itambi *et al.*, 2009). This hydrological variability is thought to reflect the movement of the Intertropical Convergence Zone (ITCZ) in conjunction with high-latitude climate variability and tropical sea surface temperatures (SSTs) (Weldeab, *et al.*, 2007).

Prior research has explored the response of the EEA Ocean to the river discharge variability of large scale riverine catchments, for example the Congo (e.g. Schneider *et al.*, 1997; Marret *et al.*, 2001; Holtvoeth *et al.* 2003) and Niger Rivers (e.g. Zabel *et al.*, 2001; Weldeab *et al.*, 2007). Whilst these records provide further understanding of regional responses to orbitally forced climatic variability, the local sensitivity of smaller western African river catchments to such variability remains to be investigated. Here a high resolution planktic $\delta^{18}O$ record is used in combination with Mg-Ca derived sea surface temperatures and terrigenous geochemical sediment signals to resolve the response of the Ogooué River catchment to West African monsoon variability since the penultimate glacial period (156 – 0 ka BP).

6.2. Geographic and Oceanographic Setting

The study area is located in the EEA within the Gulf of Guinea [Figure 6-1]. Regional atmospheric circulation is controlled by the West African Monsoon, which affects

annual rainfall, temperature and wind (Leroux, 2001). The strength of the monsoon is related to changes in central and West African vegetation cover (Kutzbach *et al.,* 1996)

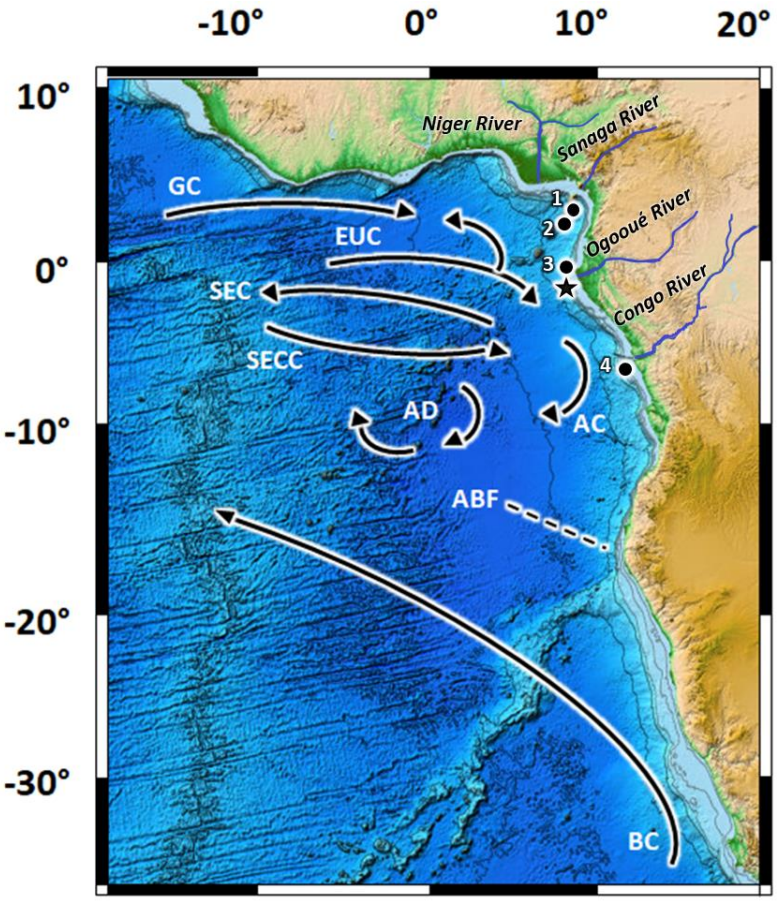

Figure 6-1 : General map of Western Africa and the Eastern Equatorial Atlantic Ocean (EEA). The Niger, Sanaga, Ogooué and Congo Rivers are shown in blue. EEA surface and subsurface currents depicted as: Warm currents - GC: Guinea Current; SEC: South Equatorial Current; SECC: South Equatorial Counter Current; AC: Angola Current; and AD: Angola Dome. Cold current – BC: Benguela Current. Under Current – EUC: Equatorial Under Current. Transient Angola-Benguela Front (ABF) depicted as a dashed black arrow. MD03-2708 core location highlighted as a star in conjunction with comparative cores: (1) MD03-2707 (Weldeab *et al.,* 2007); (2) GeoB 4905-4 (Adegbie *et al.,* 2003; Itambi *et al.,* 2010); (3) GeoB 4906-3 (Itambi *et al.,* 2010); and (4) GeoB 1008-3 (Schneider *et al.,* 1997).

and to periodic orbital changes in summer insolation (Kutzbach, 1981). Regional precipitation is further governed by seasonal variations in the strength and positioning of the ITCZ [Section 2.4]. The modern oceanography [Section 2.3] of the EEA is dominated by the outflow of four West African river systems (the Ogooué, Congo, Sanaga and Niger Rivers), and the interaction of a number of surface and sub-surface

currents [Figure 6-1]. The interplay between the Ogooué River discharge [Section 2.2] and the oceanic waters of the Ogooué Fan is the primary focus of this study.

6.3. Methodology

Marine core MD03-2708 [Figure 6-1] was extracted from the Ogooué Fan [Section 2.1], dated using $\delta^{18}O$ isotopes [Section 5] and an age model was produced [Section 5]. Bulk element abundances were obtained [Section 3.2.] and $\delta^{18}O$ planktic and benthic foraminifera and fine fraction carbonate isotopic stratigraphies were generated [Section 3.3] for the whole core sequence. In order to produce a sea surface temperature record, trace element (Mg/Ca) analysis was undertaken on planktic foraminifera from the top 8 m of the core [Section 3.6]. Mg/Ca values were converted into sea surface temperatures using the equation of Weldeab *et al.* (2007): 'SST (°C) = 0.09^–1*ln[Mg/Ca(mmol/mol)/0.38] + 0.78'.

6.4. Results

6.4.1 Fe/Ti

XRF elemental data was obtained at 1 cm intervals, resulting in an average temporal resolution of 45 years. As detailed in Chapter 4, the Fe/Ti ratio is used here as a fluvial outwash indicator, with higher Fe reflecting higher amount of terrigenous sediment input into the study site delivered by the Ogooué River. Fe/Ti ranges from 7 to 17.5 [Figure 6-2-A]. Minimum Fe/ maximum Ti is experienced during glacial MIS2 between 24 and 22 ka BP. Maximum Fe/ minimum Ti values occur during interglacial MIS 5 between 119,000 – 118,000 and at the glacial- interglacial MIS 2-1 transition between 15 and 13 ka BP.

6.4.2 Oxygen $\delta^{18}O$ Isotopes

Isotope values were yielded from 182 planktonic foraminifera, 142 benthic foraminifera and 65 bulk coccolith carbonate sample horizons, with mean sampling resolutions of 7.8, 10 and 23 ka respectively. Benthic $\delta^{18}O$ ranges from +2.60 ‰ and +4.41 ‰ [Figure 6-2-C]. The lowest positive $\delta^{18}O$ values occur in glacial MIS 2 (16 and 15 ka BP), with the highest positive $\delta^{18}O$ values also occurring MIS 2 (19 ka BP). Bulk coccolith carbonate ranges between -0.79 ‰ and +1.27 ‰ [Figure 6-2-D]. The most negative values $\delta^{18}O$ occur interglacial MIS 5 (120 – 106 ka BP) in and the most positive $\delta^{18}O$ values prevail glacial MIS 2 (15 – 14 ka BP). The Planktic $\delta^{18}O$ isotope signal extends between -2.11 ‰ and +0.64 ‰ [Figure 6-2-E]. The most negative δ 18 O values occur in interglacial MIS

5 (123 – 120 ka BP) and the least negative δ 18 O values prevail in glacial MIS 6 (155 – 149 ka BP).

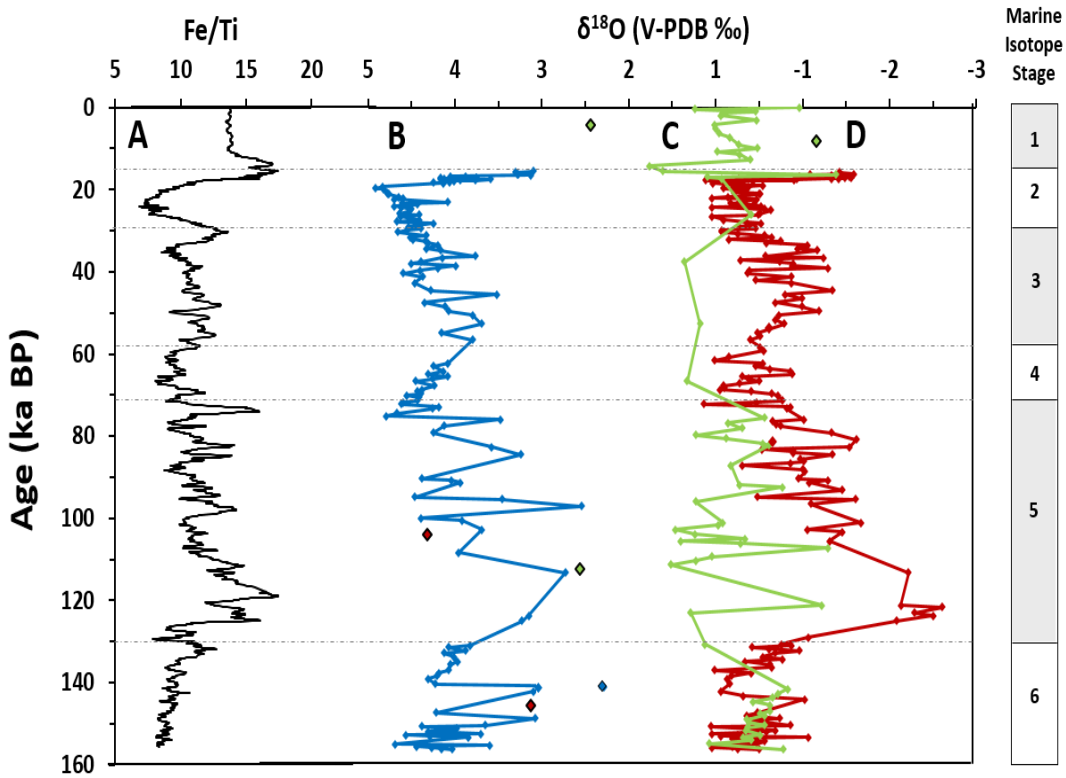

Figure 6-2: A: Fe/Ti ratio –; B: Benthic $\delta^{18}O$ (‰) derived from the benthic foraminifera *Cibicidoides wuellerstorfi* (blue line, outliers in blue diamonds); C: Bulk coccolith carbonate $\delta^{18}O$ (‰) denoted in green with green diamonds indicating outlier values; C: Planktic $\delta^{18}O$ (‰) derived from the planktic foraminifera *Globigerinoides ruber* (white variety) (red line, outliers in red diamonds).

6.4.3 Trace Element Analysis and Palaeothermometry

Thirty one horizons across the top 800 cm of core MD03-2708 were sampled for Mg/Ca analysis, yielding an average resolution of 6 ka. The Mg/Ca of the *G. ruber* (white variety) extends between 1.9 mmol/mol and 3.5 mmol/mol, which converts into SST values ranging between 18.5 °C and 25.3 °C using the calibration equation of Weldeab *et al.* (2007) [Section 6.3]. The lowest Mg/Ca and SST values prevail after the MIS 2-1 transition between 14 and 13 ka BP. The highest Mg/Ca and SST values occur during glacial MIS 2 and 25 ka BP.

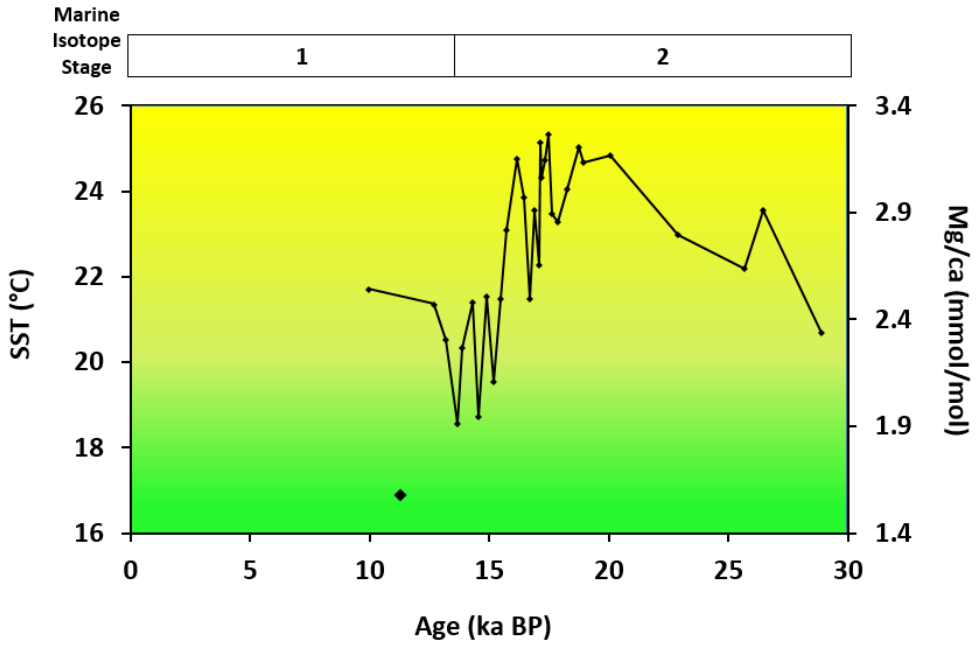

Figure 6-3: Right hand axis: Mg/Ca of *G. ruber* (white variety) in mmol/mol – outlier given as black diamond; Left hand axis: Mg/Ca SST of *G. ruber* (white variety) in °C, calibrated after Weldeab *et al.* (2007). Gradient shading mirrors EEA SST detailed in Figure 5-6.

6.5. Discussion

6.5.1 Terrigenous Sedimentology Composition as a Proxy for Riverine Discharge

The terrigenous input of sediment into the EEA Ocean via riverine discharge has been used as a proxy for monsoon strength and the positioning of the ITCZ by multiple authors (e.g. Zabel *et al.*, 2001; Govin *et al.*, 2012). The dual application of fluvial outwash episodes (from the Fe/Ti ratio of terrigenous sediments) in conjunction with the adjacent palaeoceanographic response (from the $\delta^{18}O$ of planktic foraminifera) has been used to produce high-resolution riverine discharge records of the Sanaga (Adegbie *et al.*, 2003; Itambi *et al.*, 2010) and Ogooué Rivers (Itambi *et al.*, 2010) covering the past 52,000 years. Further south, Schneider *et al.* produced high-resolution $\delta^{18}O$ (Schneider *et al.*, 1997) and SST (Schneider *et al.*, 1995) records from the Congo Fan spanning the last 200,000 years, however, a concomitant terrestrial record at such a resolution is lacking. Here, the MD03-2708 record bridges the temporal gap of these three published records.

With peaks in the Fe/Ti ratios interpreted as riverine outwash events, examination of the behaviour of the Sanaga, Ogooué and Congo rivers following the last glacial maximum highlights two riverine discharge patterns [Figure 6-4]. Indicated by sharp peaks in the Fe/Ti ratio, cores GeoB 4905-4 and GeoB 1008-3 detail an abrupt onset of rapid riverine freshening events at 16 and 18 ka BP respectively. Alternatively, cores GeoB 4906-3 and MD03-2708 indicate a gradual response of the Ogooué River to the termination of the Last Glacial Maximum (LGM), with freshening recorded in the cores from 20 to 12 ka BP and 26 to 20 ka BP respectively.

The discharge patterns of the three rivers can be attributed to their latitudinal positioning. Equatorially positioned, the Ogooué River catchment receives rainfall throughout the year, including during glacial periods, thus supporting the gradual increase in discharge intensity of the Ogooué River documented in the Ogooué River cores. The more marginal Sanaga and Congo cores act as more sensitive recorders of seasonal precipitation changes over Central Africa (Itambi *et al.,* 2010); the abrupt onset of both rivers evidences a sudden strengthening of the ITCZ and a northward migration of its mean positioning during the second half of MIS 2. A more uniform termination of the discharge events is documented in all four records, with rapid riverine discharge ceasing abruptly between approximately 7 and 5.5 ka BP, in line with other West African palaeoclimatological records (deMenocal *et al.*, 2000).

The different riverine discharge patterns identified here provides a platform for the examination of the local palaeoceanographic responses of the Eastern Equatorial Atlantic Ocean over the last 156 ka.

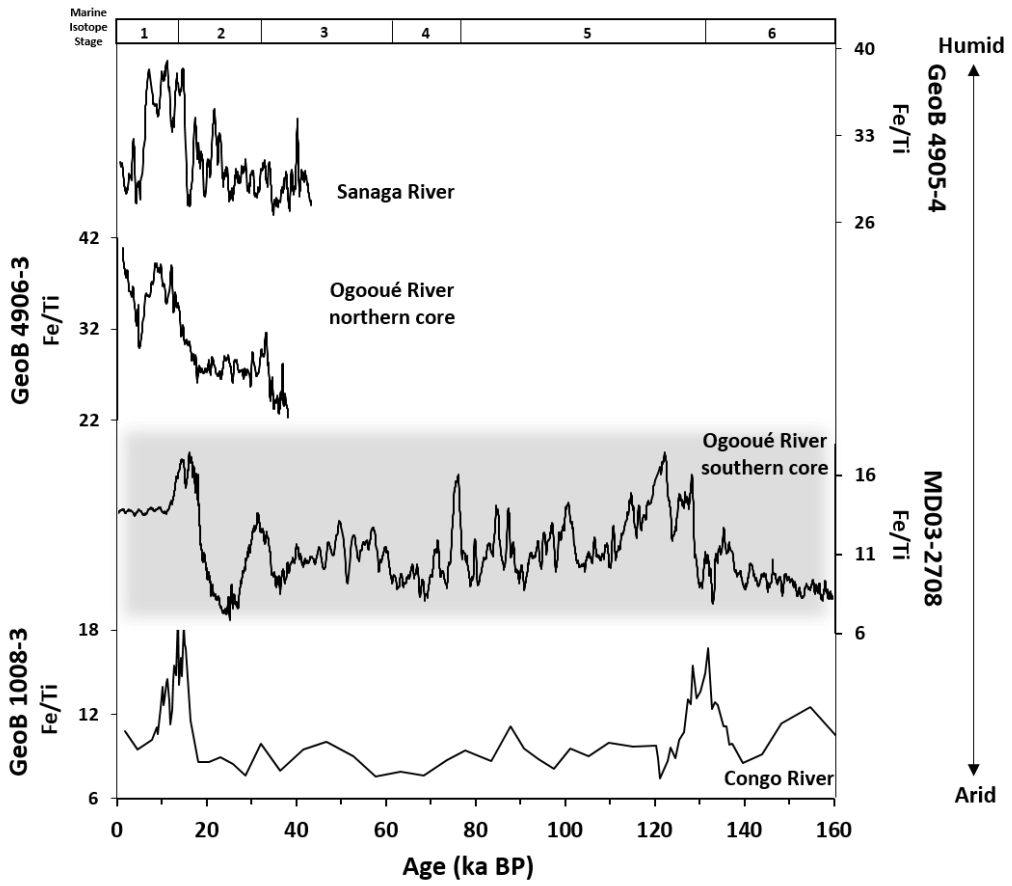

Figure 6-4: Riverine discharge variability in Western Africa over the past 156,000 years registered in the Fe/Ti ratio of the terrestrial fraction of marine sediments from the EEA. The figure is presented from north (top) to south and includes cores: GeoB 4905-4 (Adegbie et al. 2003; Itambi et al. 2010); GeoB 4906-3 (Itambi et al., 2010); MD03-2708 (this study); and GeoB 1008-3 (Schneider et al., 1997).

6.5.2 Riverine Palaeodischarge Events Recorded in Planktic $\delta^{18}O$

The $\delta^{18}O$ of planktic foraminifera has been used as an indicator of riverine freshening in the eastern equatorial Atlantic (e.g. Schneider *et al.*, 1997; Weldeab *et al.*, 2007). More negative (lower) values are indicative of warmer interglacial periods, due to the river water having lower $\delta^{18}O$ than marine water. This freshwater signature is then transferred to the $\delta^{18}O$ of planktic foraminifera during high riverine discharge events. Supported by a similarity to the MD03-2708 Fe/Ti ratio, the most negative planktic $\delta^{18}O$ values prevailing in interglacial MIS 5 suggests high riverine discharge, and the more positive occur during the three glacial periods of MIS 6, MIS 4 and MIS 2, and indicate significantly reduced Ogooué riverine discharge during colder episodes.

Comparison of the MD03-708 planktic $\delta^{18}O$ with neighbouring records allows for an assessment of the strength and timing of Ogooué River discharge events in contrast to those of the Sanaga [MD03-2707 -Weldeab *et al.* 2007) and Congo (GeoB 1008-3 - Schneider *et al.* 1997) rivers over the past 156,000 ka.

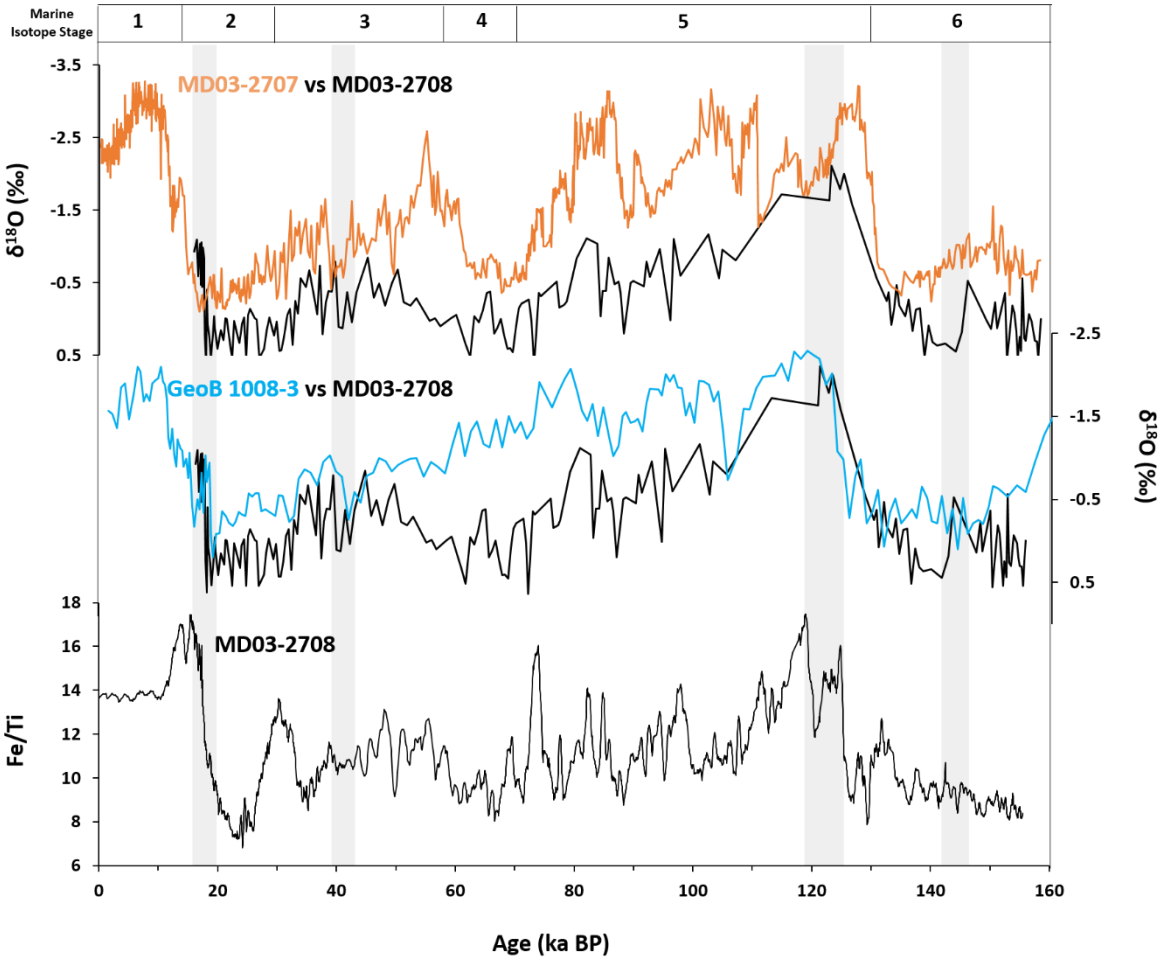

Figure 6-5: Eastern Equatorial Atlantic riverine discharge proxies, from bottom to top: Fe/Ti (Core MD03-2708); $\delta^{18}O$ (‰) black lines (Core MD03-2708), blue line (Core GeoB 1008-3 [Schneider *et al.* 1997]; and orange line (Core MD03-2707 [Weldeab *et al.* 2007]. Shading highlights where MD03-2708 $\delta^{18}O$ (‰) has concomitant values with comparative records.

As illustrated in Figure 6-5, the Sanaga and Congo $\delta^{18}O$ values generally record more negative values, and therefore stronger riverine discharge than the Ogooué River. There are, however, four time slices (two during interglacials: 124-122 and 16-13 ka BP; two during glacial: 146-142 and 43-41 ka BP) where the MD02-2708 planktic $\delta^{18}O$ values are concomitant with the neighbouring records.

The two horizons during interglacials MIS 5 and at the MIS 2-1 transition, are accompanied by high Fe/Ti, supporting the notion that higher equatorial rainfall is accompanied by enhanced riverine discharge. The two horizons during glacial MIS 6 and 2 are not coeval with a peak in Fe/Ti, suggesting that there is an additional factor controlling Ogooué riverine discharge over the time frame.

6.5.3 Riverine Control on Sea Surface Temperature

The Gulf of Guinea is situated within the eastern extension of the equatorial Atlantic warm tongue (Weldeab *et al.,* 2007). Regional sea surface temperature varies annually depending upon the positioning of the ITCZ. Warmer water temperatures are experienced in the boreal winter months with the top 20 m of the water column ranging between 26 °C and 28 °C (Weldeab *et al.,* 2007). Summer riverine freshening results in lower ocean surface temperatures and a wider latitudinal temperature gradient extending from 28 °C in the northern part of the Gulf to 17 °C off Congo [Figure 6-6].

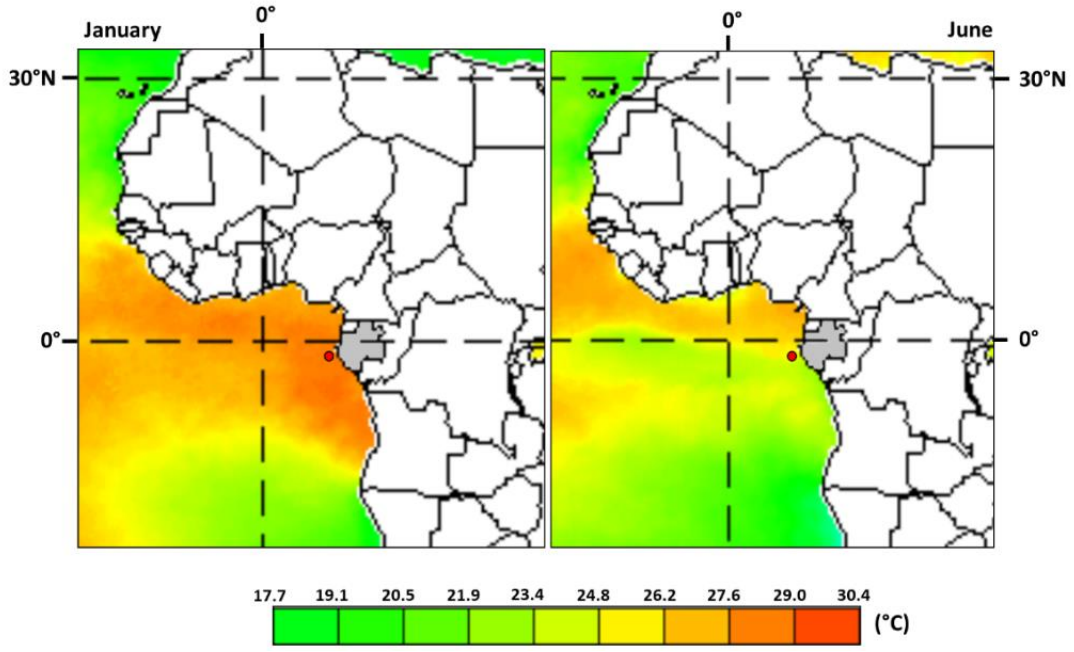

Figure 6-6: Monthly mean sea surface temperature for the Gulf of Guinea in January and June 1998. Images modified after NOAA (2015). [Gabon highlighted in light grey and positioning of core MD03-2708 denoted with a red circle].

6.5.3.1 The Ogooué River

On entering the Ogooué delta, the freshwater of the Ogooué River diffuses into a mixed layer. The riverine discharge induces a horizontal gradient of temperature, with a maximum value of around 30 °C at 8 °E longitude, and salinity, which is characterized by a 20 m thick mixed layer with a low salinity (29 psu), overlapping highly saline waters (36 psu) (Jourdin *et al.*, 2006) [Figure 2.4]. Jourdin *et al.*, (2006) found modern day water off the Ogooué delta to be depleted in nutrients at the surface, except for silica; this presence of silica confirmed that the surface waters of the Ogooué margin were fluvial in origin.

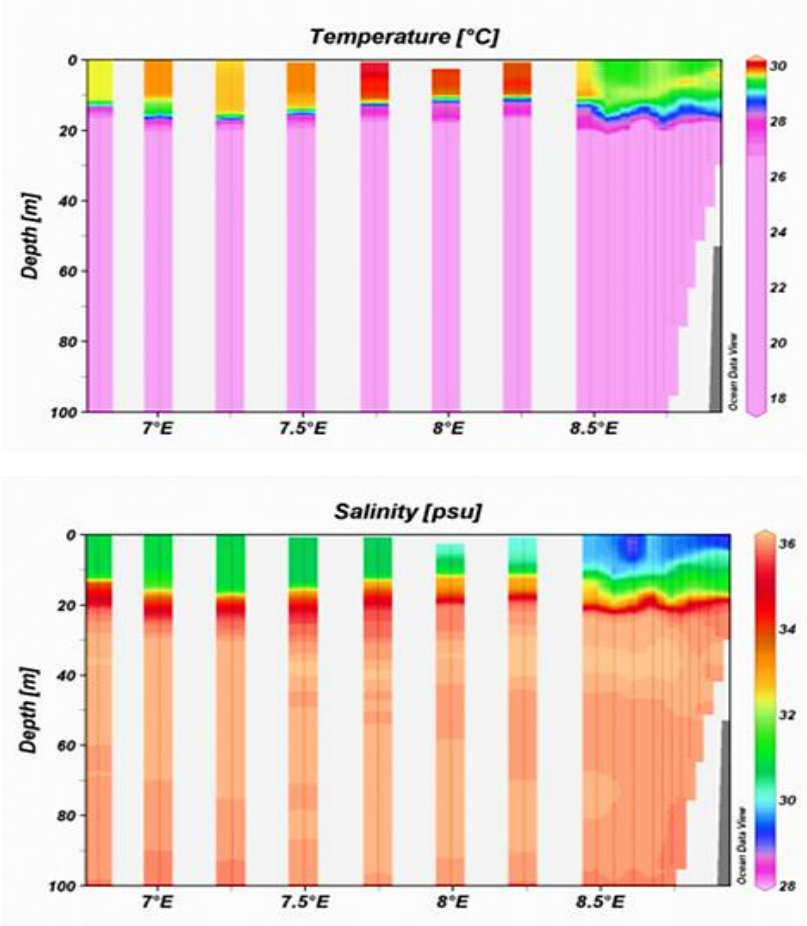

Figure 6-7: Vertical temperature and salinity profiles of the Ogooué delta surface water (0 – 100 m). Profiles extend between 6.5 °E and 9 °E and were obtained on March 4th and 5th 2005 using a CTD Sea Bird 911+ (Jourdin *et al.*, 2006).

6.5.3.2 Regional SST Comparison

The response of the tropical Atlantic SST over the last glacial-interglacial cycle is characterized by spatially heterogeneous patterns showing asymmetric SST changes (Jaeschke *et al.*, 2007; Weldeab, 2012). The spatial patterning may reflect regional imprints of wind strength, surface currents and riverine discharge (Weldeab *et al.,* 2007).

The MD03-2708 SST record was compared with neighbouring SST records [Figure 6-8] from off the Sanaga (Weldeab *et al.,* 2007) and Congo (Schneider *et al.,* 1997) rivers to better understand the regional SST gradient presented in Figure 6-6. Prior to the onset of the LGM, the three SST records reflected modern boreal winter SSTs with the values of 23° - 24°C (Schneider *et al.,* 1995). Temperatures diverge post 18 ka BP with the Ogooué SST record [MD03-2708)] varying in antiphase with the neighbouring Sanaga [MD03-2707 (Weldeab *et al.,* 2007] and Congo [GeoB 1008-3 (Schneider *et al.,* 1995)] SST records [Figure 6-6]. The SST of the comparative records increased during the deglaciation and into the Holocene, reaching maxima of 28.8 °C at 8.9 ka BP off the Sanaga and 25.7 °C at 8 ka BP off the Congo River, thereafter remaining relatively stable until present day. The opposite trend was manifested within the Ogooué SST record; SST increased from 21 °C at 29 ka to a maximum temperature of 25.5 °C at 17 ka BP, after which it decreased to a minima of 18 °C at 13.5 ka BP.

In conjunction with planktic $\delta^{18}O$, the Sanaga and Congo SST trends are reflective of the linkage between tropical and northern high latitude records, with SSTs increasing following the northward shift of the ITCZ during the deglaciation and the concomitant intensification of terrestrial precipitation and warm riverine discharge into the EEA (Schneider *et al.,* 1995). Despite the discrepancies between the SST trends, the MD03-2708 planktic $\delta^{18}O$ sequence does dovetail the comparative $\delta^{18}O$ and SST records, the notion that eastern equatorial Atlantic SST is governed by freshwater riverine discharge (Weldeab *et al.,* 2007). The opposite SST trend presented in the MD03-2708 record may be due to the low resolution and highly variable nature of the record. Enhanced discharge of cooler water from the Ogooué River, evidenced by an abrupt increase in the MD03-2708 Fe/Ti ratio [Figure 6-8], may explain the decrease of SST in the Ogooué Fan between 18 and 12 ka BP.

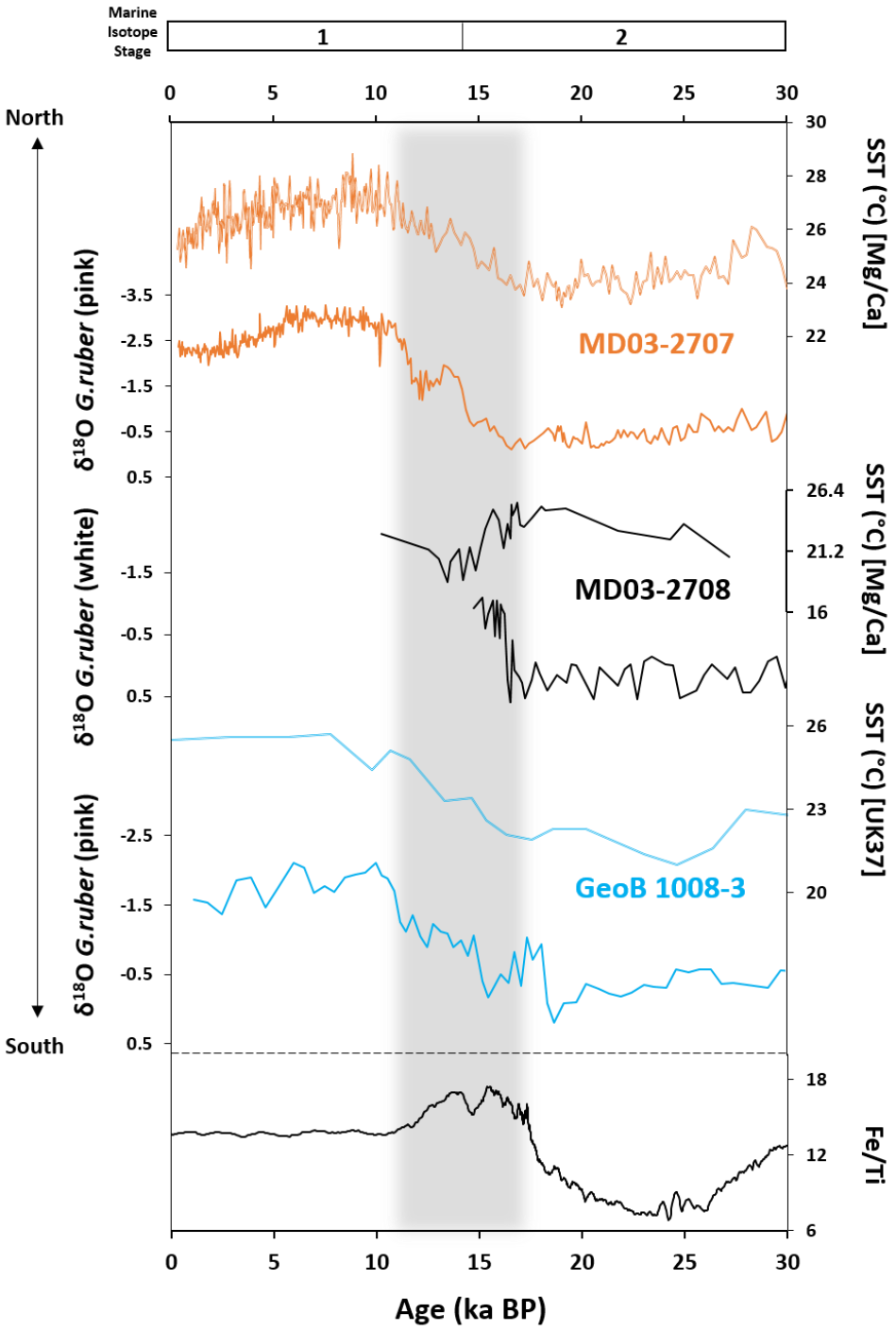

Figure 6-8: Latitudinal EEA SST and $\delta^{18}O$ variability over the past 30 ka. Data compiled from cores: MD03-2707 (Mg/Ca-based SST estimates and $\delta^{18}O$ of *G. ruber* (pink variety) [Weldeab *et al.* (2007)]; MD03-2708 (Mg/Ca-based SST estimates and $\delta^{18}O$ of *G. ruber* (white variety); and GeoB 1008-3 [Alkenone unsaturation index UK'37-based SST estimates and $\delta^{18}O$ of *G. ruber* (pink variety) [Schneider *et al.* (1995); Schneider *et al.* (1997)]. Fe/Ti of MD03-2708 is given; grey shading highlights sudden peak in Fe/Ti at 18 ka until 12 ka BP.

6.5.3.3 The Ogooué SST record

Exploration of additional MD03-2708 proxy variables illustrates trends coeval with the SST record [Figure 6-9]. As already discussed there is strong correspondence between riverine discharge indicated by the Fe/Ti and a concomitant decrease in the adjacent SST. From 12 ka there were not enough *G. ruber* tests (< 20) present within the MD03-2708 sediment to reconstruct the $\delta^{18}O$ and SST records. This is supported by a decrease in the percentage of *G. ruber* within the total foraminiferal assemblage to 3 % at 6.4 ka BP, after which no *G. ruber* is present between 5.2 and 2 ka BP (Davies *et al.* 2015). It is evident that from 7 ka BP onwards, riverine freshening altered the surface ocean to such an extent that *G. ruber* could no longer survive. What is not clear, is why this occurs only at this particular time interval, and not early in the record when equally high freshening was experienced.

Examination of the MD03-2708 dinoflagellate cyst record published by Kim *et al.* (2010) highlights a notable increase in the taxa *Operculodinium centrocarpum* from 8 ka onwards. In the Western Atlantic, adjacent to the Amazon River, *O. centrocarpum* has been found to increase in low saline environments with high riverine outflow (Marret and Zonneveld, 2003). In the Eastern Atlantic Ocean, high representation of this taxon is found where unstable conditions occur such as upwelling, including river-induced upsurges (e.g. Marret et al., 2013). This therefore suggests that despite *G. ruber* being able to prevail in laboratory cultures of salinities between 22 and 49 psu (%) (Davies *et al.,* 2015), the rapid freshening of the Ogooué River had such an intense impact on the salinity of the adjacent ocean, that *G. ruber* was not able to adapt and survive. Once again, this raises the question as to why the riverine freshening experienced in the Holocene had a more notable impact on the sea surface than the riverine discharge events of MIS 5.

6.6. The Role of Orbital Forcing in Regulating Equatorial Precipitation

Long-term humidity variations in tropical regions influenced by the West African monsoon are related to external orbital variability (e.g. McIntyre *et al.*, 1989). The primary orbitals that control low-latitude insolation are precession and eccentricity (McIntrye and Molfino, 1996). Eccentricity (the measure of the shape of the Earth's orbit around the sun) varies on a 100 ka time frame and causes variation in the total annual insolation received. It also modulates precessional insolation (the seasonal

configuration of the distance between the Earth and the Sun) (Berger and Loutre, 1991), which has a 23 ka cycle.

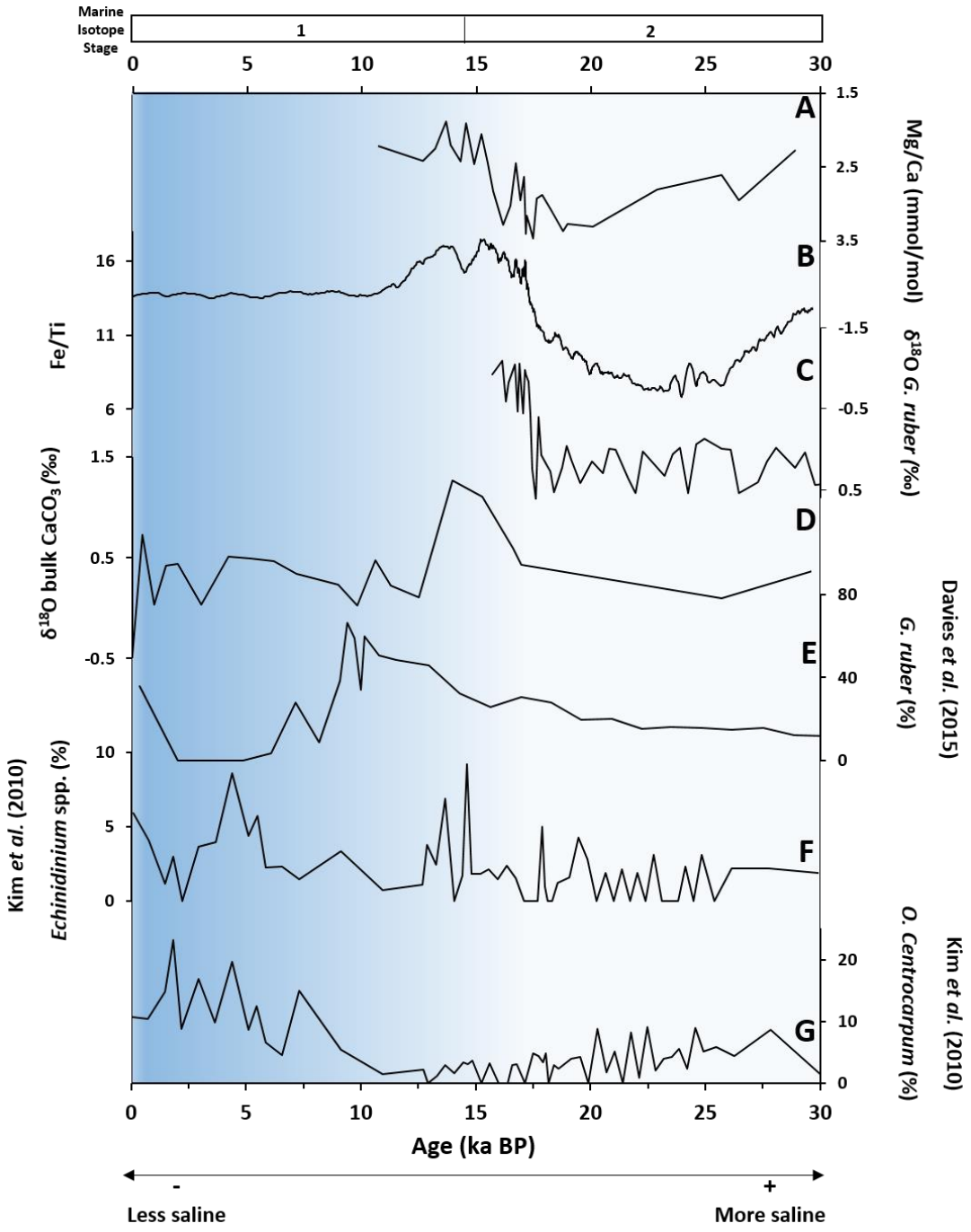

Figure 6-9: Desalinisation of the Ogooué Margin through riverine discharge intensification since the LGM. Evidenced by (from top to bottom): SST (°C) [temperature estimates from Mg-Ca analysis of *G. ruber* (white)] *(NB reversed axis)*; Fe/Ti ratio; $\delta^{18}O$ (‰) *G. ruber*; $\delta^{18}O$ (‰) bulk coccolith carbonate; *G. ruber (%)* [Davies *et al.* 2015]; *Echinidinium* spp. (%) [Kim *et al.* 2010]; and *O. centrocarpum (%)* [Kim *et al.* 2010].

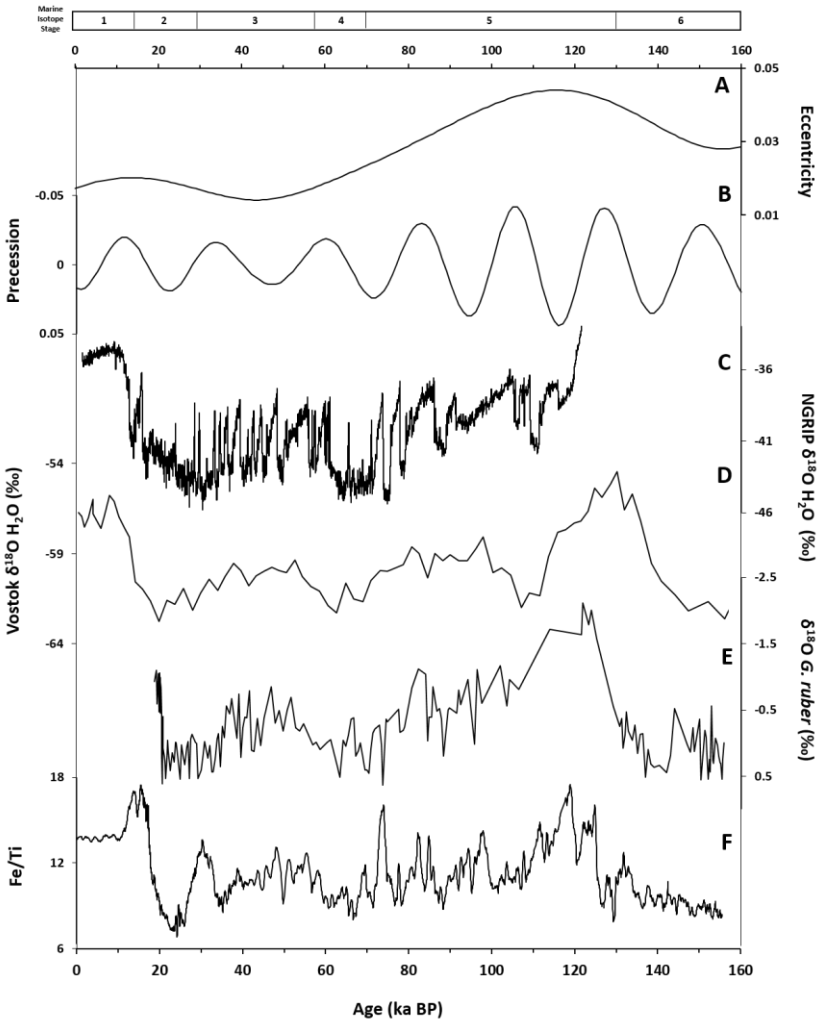

Figure 6-10: Timing and proxy evidence of riverine outwash into the Gulf of Guinea over the past 156 years. A: Eccentricity [Berger and Loutre, 1999]; B: Precession [Berger and Loutre, 1999] *(NB reversed axis)*; C: NGRIP δ18O H2O (‰) [Johnsen et al. 2001]; D: Vostok δ18O H2O (‰) [Lorius *et al.,* 1985]; E: MD03-2708 δ18O (‰) G. ruber (white variety); F: MD03-2708 Fe/Ti ratio.

Not only is there a concurrence between the MD03-2708 $\delta^{18}O$ record and the northern hemisphere NGRIP (Johnsen *et al.,* 2004) and southern hemisphere Vostok $\delta^{18}O$ (Lorius *et al.,* 1985) records, Figure 6-10 demonstrates that Ogooué riverine discharge events evidenced in the negative value excursions of the MD03-2708 planktic record are reflected in the minima of the precessional component of orbital variation, modulated by eccentricity maxima. Maximum riverine discharge is experienced during interglacial MIS 5 between 128 and 105 ka BP when precession minima and eccentricity maxima are coincident. Minimum discharge occurs during glacials MIS 6 (145 – 140 ka BP) and 3/2 (30 -20 ka BP), during precession maxima.

6.7. Conclusions

In summary, high resolution sedimentological and geochemical investigations demonstrated the potential of the Fe/Ti ratio as an indicator of Ogooué River discharge variability. A planktic $\delta^{18}O$ isotope stratigraphy was produced, using the foraminifera *G. ruber,* which dovetailed the Fe/Ti record, strongly suggesting that the $\delta^{18}O$ of the adjacent EEA was influenced by the discharge of the Ogooué River. The proxies evidence higher riverine discharge during interglacial MIS 5, with reduced discharge occurring in glacial periods MIS 6, 4 and 2. The $\delta^{18}O$ record is largely synchronous with the planktic $\delta^{18}O$ records of marine core records adjacent to the Sanaga and Congo Rivers. Maximum riverine discharge is concomitant with precessional minima and is modulated over the time frame by eccentricity variability. Preliminary Mg/Ca analysis undertaken on *G. ruber*, facilitated the production of a SST record for the last 30 ka. Supported by dinoflagellate cyst data, the SST pattern diverges from the $\delta^{18}O$ record, suggesting that Ogooué River discharge is a dominant control on salinity in the Ogooué Fan.

7 Orbitally-Driven Riverine Control of Surface and Bottom Water $\delta^{13}C$ in the Eastern Equatorial Atlantic

7.1. Introduction

Late Quaternary glacial-interglacial climatic fluctuations are believed to have altered deep ocean circulation patterns and subsequently the global oceanic distribution of nutrients (Boyle and Keigwin, 1985; Mix and Fairbanks, 1985). The intermediate-depth North Atlantic was nutrient-depleted during glacial periods relative to today, whilst deeper waters were much more nutrient-enriched (Duplessy *et al.*, 1988). Oceanic models developed in the 1990s suggested that the late Quaternary variations of atmospheric CO_2 concentrations recorded in ice cores could be driven by marine biological productivity changes (Berger *et al.,* 1989; Schneider *et al.,* 1994; Mulitza *et al.*, 1998). In light of this theory, a wealth of attention was given to the reconstruction of past nutrient dynamics in highly productive areas of the surface ocean (Schneider *et al.,* 1994). In the low latitudes of the Atlantic Ocean, these studies focused on the Western Equatorial Atlantic (e.g. Ruhlemann *et al.*, 1996) and the upwelling areas of the Eastern Atlantic (Müller *et al.,* 1983; Sarnthein *et al.*, 1988; Abrantes, 1991; Schneider *et al.,* 1994; Mulitza *et al.*, 1998).

Foraminiferal shell $\delta^{13}C$ values have been widely used as a proxy for reconstructing the distributions of past ocean water masses, particularly in the Atlantic Ocean (e.g. (Sarnthein *et al.,* 1984; Curry and Crowley, 1987; Mackensen *et al.,* 1999). The application of these records in furthering understanding of $\delta^{13}C$ ocean dynamics over glacial-interglacial timescales is harboured due to short core age lengths (< 60 ka) (Arz *et al.,* 1998; Mulitza *et al.*, 1998; Adegbie *et al.*, 2003; Kiefer *et al.,* 2006; Zarriess and MacKensen, 2011; Burckel *et al.*, 2016) and/or low temporal resolutions (Bird and Cali, 1998; Jonkers *et al.*, 2015). The Northwest African continental margin is one of the most intensively investigated areas of coastal upwelling (e.g. Mulitza *et al.*, 1998; Abrantes, 2003; Subramaniam *et al.*, 2013), however, focus has not been given to the waters that lie in between these upwelling regions [Figure 7-1]. Study of the intermediate waters

between upwelling regions allows for the primary drivers (riverine discharge, surface, subsurface and bottom water currents) of $\delta^{13}C$ in these quasi-nutrient rich water masses to be determined. Until now, continental shelf reconstructions of the $\delta^{13}C$ in the Gulf of Guinea have been limited to two records offshore Cameroon: a 20 ka benthic study [MD03-2707] (Weldeab *et al.*, 2016) and a 30 ka planktic record [GeoB 4905-4] (Adegbie *et al.*, 2003). This chapter employs high resolution planktic and benthic foraminiferal $\delta^{13}C$ isotopes, in conjunction with lower resolution bulk fine fraction carbonate $\delta^{13}C$ in the first palaeo-reconstruction of the $\delta^{13}C$ of the Ogooué Fan, Gabon. Glacial-interglacial changes in vertical $\delta^{13}C$ gradients will be reconstructed and compared with $\delta^{13}C$ records from Western Africa and the South Atlantic over the past 160 ka.

7.2. Geographic and Oceanic Setting

The study area is located in the Eastern Equatorial Atlantic (EEA) within the Gulf of Guinea [Figure 7-1]. Regional atmospheric circulation is controlled by the West African Monsoon, which effects annual rainfall, moisture, temperature and wind (Leroux, 2001). The strength of the monsoon has been related to Central and West African vegetation cover (Kutzbach *et al.*, 1996) and to periodic orbital changes in summer insolation (Kutzbach, 1981). Regional precipitation is further governed by seasonal variations in the strength and positioning of the ITCZ [Section 2.4]

The modern oceanography [Section 2.3] of the Eastern Equatorial Atlantic is modulated by the outflow of four West African river systems (the Ogooué, Congo, Sanaga and Niger Rivers), and the interaction of a number of surface and sub-surface currents. Three primary upwelling regions occur in the EEA adjacent to the Nigerian, Congolese Angolan and Namibian coastlines [Figure 7-1].

7.3. Methodology

7.3.1 Material and Age Model

Marine core MD03-2708 [Figure 6-1] was extracted from the Ogooué Fan [Section 2.1], dated using $\delta^{13}C$ isotopes [Section 5] and an age model was produced [Section 5]. Bulk element abundances were obtained [Section 3.2.] and $\delta^{13}C$ planktic and benthic foraminifera and fine fraction carbonate isotopic stratigraphies were generated [Section 3.3] for the whole core sequence.

7.3.2 Analytical Approach

Carbon $\delta^{13}C$ stratigraphies were produced to explore nutrient dynamics and surface, sub-surface and bottom water mixing. The $\delta^{13}C$ of foraminiferal shells and coccolithphores reflects the carbon isotopic composition of the dissolved inorganic carbon (DIC) in the seawater in which the shell calcified. The $\delta^{13}C$ DIC of seawater is influenced locally by changes in: the balance between photosynthesis and respiration; the mixture of water masses; and the original $\delta^{13}C$ DIC of water masses reaching the location (Ravelo and Hillaire-Marcel, 2007).

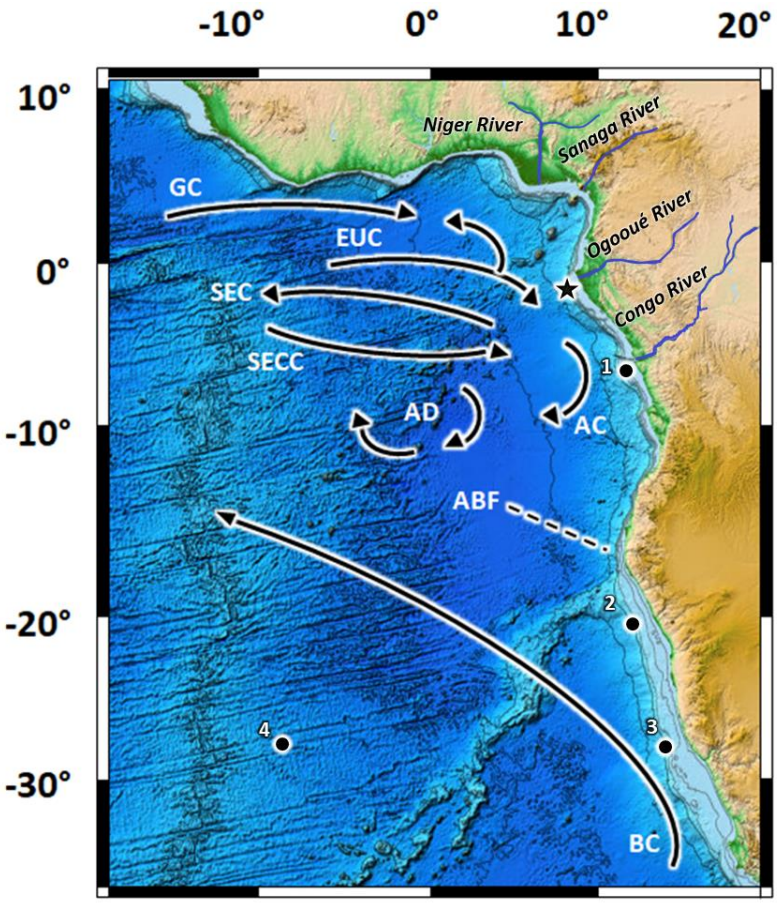

Figure 7-1: (A) Location map of marine sediment core MD03-2708 [star] used in this study along with comparative core locations: (1) GeoB 1106-3 [Müller *et al.,* 1994]; (2) GeoB 1710-3 (Schmiedl *et al.,* 1997); (3) ODP 175-1087A [Pierre *et al.,* 2001]; (4) GeoB 3808-6 (Jonkers *et al.,* 2015). The Niger, Sanaga, Ogooué and Congo Rivers are shown in blue. EEA surface and subsurface currents depicted as: Warm currents - GC: Guinea Current; SEC: South Equatorial Current; SECC: South Equatorial Counter Current; AC: Angola Current; and AD: Angola Dome. Cold current – BC: Benguela Current. Under Current – EUC: Equatorial Under Current. Transient Angola-Benguela Front (ABF) depicted as a dashed black arrow.

For the generation of the $\delta^{13}C$ isotope stratigraphies, indicator species of the planktic (*Globigerinoides ruber,* white variety) and benthic (*Cibicidoides wuellerstorfi*) foraminifera were picked at a minimum 10 cm resolution [Section 3.4]. For horizons devoid of tests, bulk coccolith (surface dwelling) carbonate analysis was employed to fill in the stratigraphic gaps and to verify the isotopic data generated from the foraminifera specimens. Samples were run for $\delta^{13}C$ stable isotope analysis at the NERC Stable Isotope Geosciences Laboratory, Keyworth [Section 3.5]. Isotopic values were yielded from 182 planktonic foraminifera, 142 benthic foraminifera and 65 bulk coccolith carbonate samples, with mean resolutions of 7.8, 10 and 3 ka respectively.

7.4. Results

7.4.1 Oxygen $\delta^{13}C$ Isotopes

The MD03-2708 planktic $\delta^{13}C$ isotope signal extends between -0.40 ‰ and 1.90 ‰ [Figure 7-2]. The highest $\delta^{13}C$ values occur in glacial MIS 2 (17 - 16 ka BP) and the lowest values prevail in interglacial MIS 5 (120 ka BP). Benthic $\delta^{13}C$ ranges from -2.90 ‰ and -0.50 ‰. The highest values occur in interglacial MIS 2 (26 ka BP) and the lowest values are present during the glacial – interglacial (MIS 6/5) transition of Termination 2 (130 – 129 ka BP). The bulk coccolith carbonate $\delta^{13}C$ ranges between -4.00 ‰ and 0.30 ‰. The highest values occur in interglacial MIS 1 (8 - 4 ka BP) and the lowest values prevail in glacial MIS 6 (154-143 ka BP).

7.5. Discussion

The three $\delta^{13}C$ isotopic stratigraphies presented in Figure 7-2 follow the same rudimentary trend but with differing amplitudes within and between glacial and interglacial periods. Differing $\delta^{13}C$ values allude to varying positions of the foraminifera and coccolith tests within the water column. Separate examination of the planktic and benthic foraminiferal $\delta^{13}C$ values allows for a more detailed understanding of the surface and subsurface currents operating in the Eastern Atlantic Ocean over the past 156 ka.

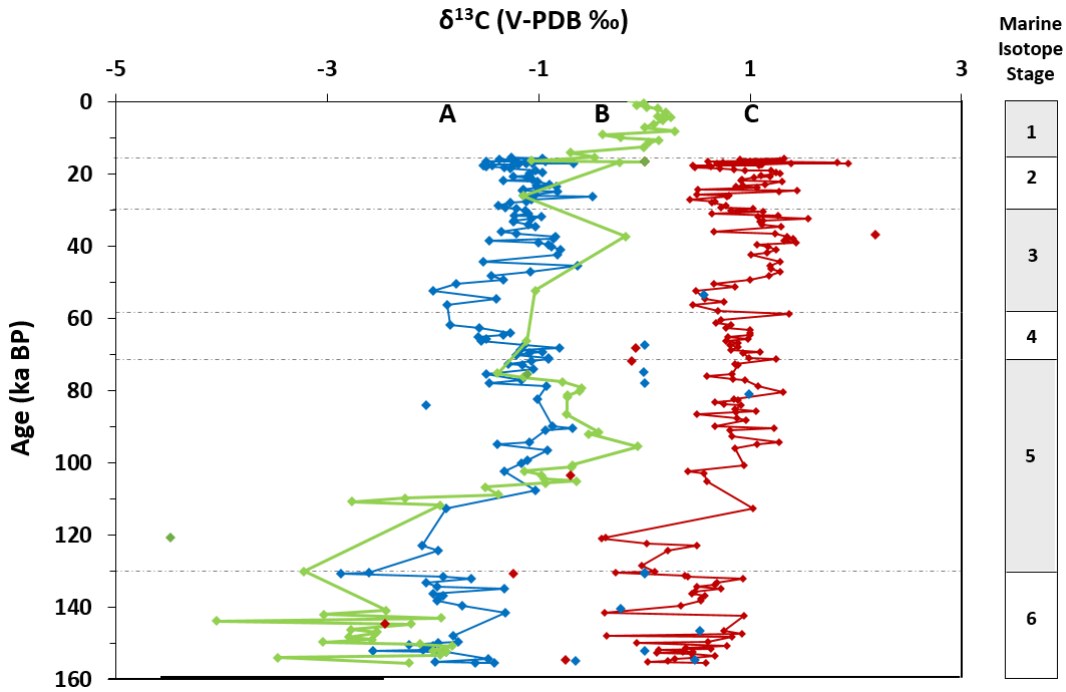

Figure 7-2: Marine Core MD03-2708 $\delta^{13}C$ isotope stratigraphies of the Ogooué Fan, covering the past 156 ka. Benthic $\delta^{13}C$ derived from the benthic foraminifera *Cibicidoides wuellerstorfi* (blue line, outliers in blue diamonds). Planktic $\delta^{13}C$ derived from the planktic foraminifera *Globigerinoides ruber* (white variety) (red line, outliers in red diamonds). Bulk coccolith carbonate $\delta^{13}C$ denoted in green with green diamonds indicating outlier values. Marine Isotope Stages depicted, with interglacial periods shaded in grey, and glacial periods in white.

7.5.1 Surface Water

Derived from the planktic foraminifera, *G. ruber*, the MD03-2708 $\delta^{13}C$ stratigraphy presents a highly variable record. Lower values [-0.5 to 0.8 ‰], representing low surface productivity (Schneider *et al.*, 1994) are present in glacial MIS 6, where after higher values [0.5 to 1.5 ‰], signifying increased surface productivity, are documented until the termination of the record at the end of MIS 2 [14 ka].

These higher values are comparable to modern seawater $\delta^{13}C_{\sum CO_2}$ values observed in the EAO for the vertical field temperature between 18 and 28 °C (Ravelo, 1991). In order to identify the drivers of surface $\delta^{13}C$ variability in the Eastern Equatorial Atlantic, the MD03-2708 $\delta^{13}C$ record was compared with the only two published $\delta^{13}C$ records of comparable length and resolution from the Eastern Atlantic Ocean (EAO) (Müller *et al.*, 1994; Pierre *et al.*, 2001) and with a EAO planktic $\delta^{13}C$ stack (Curry and Crowley, 1987) [Figure 7-3].

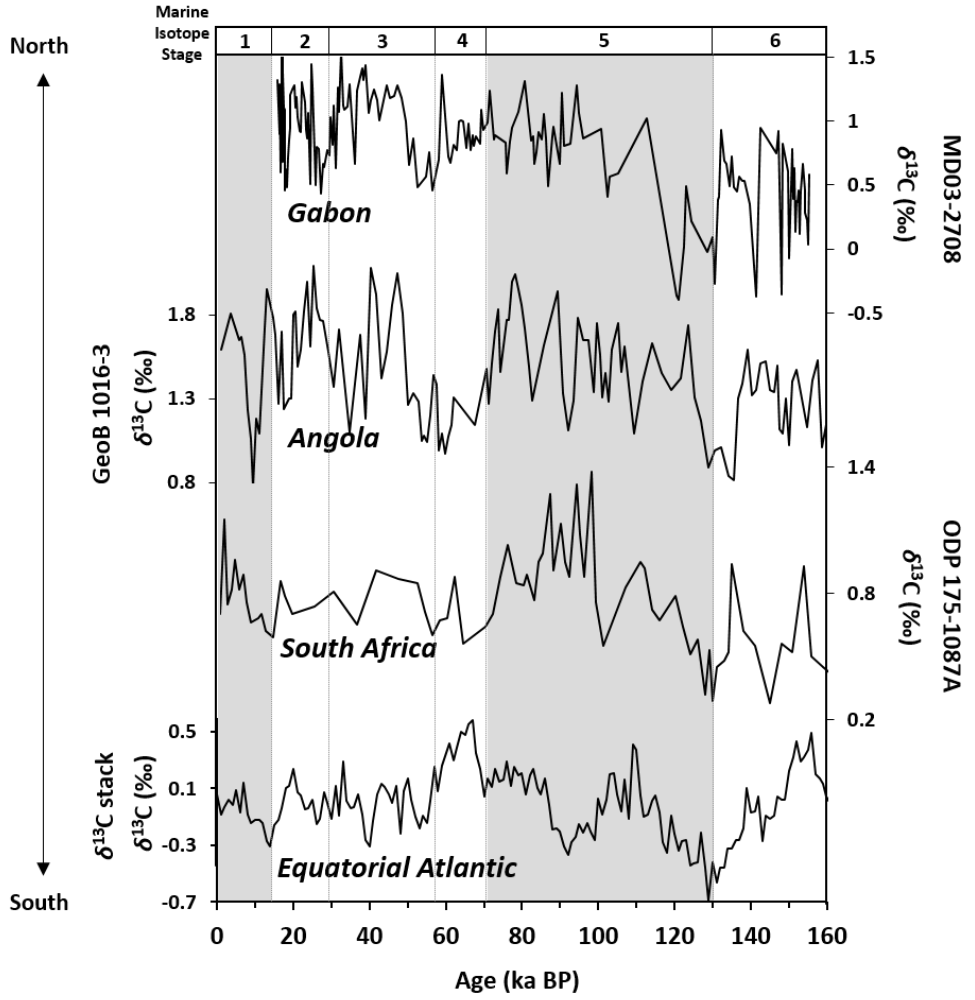

Figure 7-3: Palaeovariability of four planktic foraminifera-derived $\delta^{13}C$ isotope stratigraphies over the past 150 ka. From North to South: (Angola) core GeoB 1106-3 – *G. ruber* (pink variety) $\delta^{13}C$ (‰ PDB) (Müller *et al.,* 1994); (Gabon) this study core MD03-2708 - *G. ruber* (white variety) $\delta^{13}C$ (‰ PDB); and (South Africa) core ODP 175-1087A – *G. ruber* (variety not specified) $\delta^{13}C$ (‰ PDB) (Pierre *et al.,* 2001). Western African records compared with a stacked record of $\delta^{13}C$ (‰ PDB) derived from *Globigerinoides sacculifer* records from the Equatorial Atlantic (Curry and Crowley, 1987). Stacked $\delta^{13}C$ presented as difference from average Late Holocene (0 – 8 ka) isotopic composition; the record was linearly interpolated to 1000 year sample spacing (Curry and Crowley, 1987).

The high variability within and between each of the $\delta^{13}C$ records means overall synchronicity between the records cannot be easily determined. The $\delta^{13}C$ trends presented do not parallel the interglacial cyclicity presented in the $\delta^{18}O$ and geochemical records of Chapter 6 (Pierre *et al.*, 2001). However, concurrent with the EAO stack, all three comparative records show low $\delta^{13}C$ values at, or near to, the marine

isotope stage boundaries, with the exception of the MIS 3 – MIS 2 transition [Figure 7-3] (Curry and Crowley, 1987).

Isotopic $\delta^{13}C$ minima are experienced within all records between 135 and 127 ka. Maximum values vary between the locations [e.g. MIS 2 – Gabon; MIS 4 – Equatorial Atlantic stack; and MIS 5 – Angola and South Africa]. In conjunction with the highly variable nature of the records, this suggests that the localised $\delta^{13}C$ trends are most likely related to changes in surface water productivity, induced by vital effects due to different light levels or changes in the carbon chemistry of surface waters (Spero and Lea, 1993), or upwelling intensity (Jansen and Van Iperen, 1991). Examination of bottom waters is now necessary to further examine local versus regional variability of $\delta^{13}C$ in the Eastern Equatorial Atlantic during the Late Quaternary Period.

7.5.2 Bottom Water

The $\delta^{13}C$ values recorded in benthic foraminifera reflect the $\delta^{13}C$ of the dissolved inorganic carbon of ambient bottom and deep ocean water masses and as such, are widely used as a nutrient proxy to reconstruct deep ocean palaeocirculation (Mackensen and Bickert, 1999). Derived from the foraminifera *Cibicidoides wuellerstorfi,* the MD03-2708 benthic $\delta^{13}C$ record shows a trend which is more structured than its planktic counterpart. Low values [-2.1 to -1.4 ‰] signifying high nutrient concentrations (Mackensen and Bickert, 1999) prevail in MIS 6, the first half of MIS 5 (160 – 120 ka) and the start of MIS 3 (62 – 50 ka) [Figure 7-4]. Higher values [-1.3 to -0.6 ‰] occur during the remainder of the record.

Located to the south of Gabon, the benthic $\delta^{13}C$ of the Namibian record ODP 175-1087A presents clear glacial – interglacial cyclicity with low $\delta^{13}C$ values prevailing during glacial periods, and higher $\delta^{13}C$ values during interglacials. The benthic $\delta^{13}C$ in this region is governed by a glacial enhancement of North Atlantic Deep Waters (NADW) during glacial periods, and an advection of Atlantic waters during interglacial stages MIS 5 and 1 (Schmiedl and Mackensen, 1997; Mulitza *et al.*, 1998).

On the continental shelf of South Africa, Pierre *et al.* (2001) found that $\delta^{13}C$ values decreased at interglacial-glacial transitions. They interpreted this decrease to an equatorward shift of the Polar Front Zone during glacial periods in association with a lower rate of Antarctic Intermediate Water (AAIW) ventilation. Consistent with the

planktic $\delta^{13}C$ values from the same site, the benthic $\delta^{13}C$ values presented a different pattern from the glacial-interglacial cyclicity present in the Namibian record (Schmiedl and Mackensen, 1997), which Pierre *et al.* (2001) attribute to large climatic oscillations higher than the 100 ka eccentricity period.

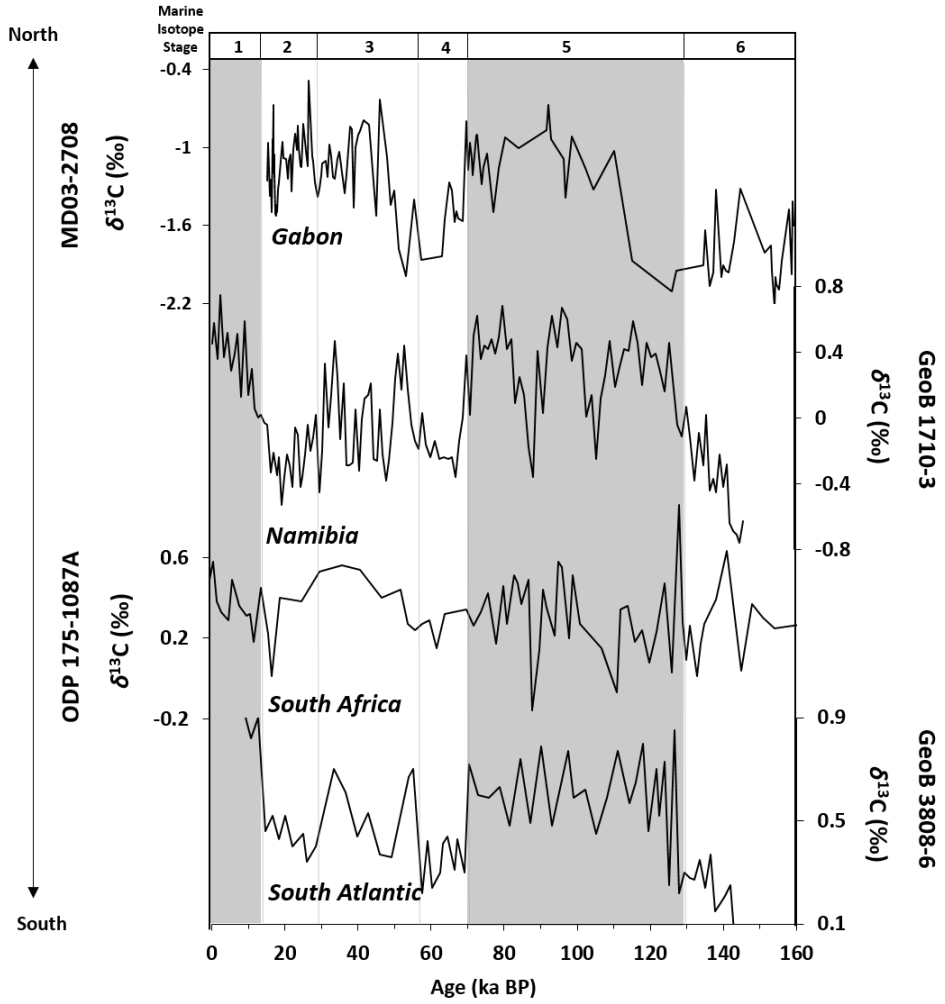

Figure 7-4: Asynchronous benthic foraminiferal $\delta^{13}C$ isotope stratigraphies from the Eastern Equatorial Atlantic and South Atlantic over the past 160 ka. From north to south the records comprise: (Gabon) *G. ruber* $\delta^{13}C$ [‰ PDB] of this study - MD03-2708; (Namibia) *Cibicidoides wuellerstorfi* $\delta^{13}C$ [‰ PDB] from core GeoB 1710-3 (Schmiedl and Mackensen, 1997); (South Africa) *Cibicidoides wuellerstorfi* $\delta^{13}C$ [‰ PDB] from core ODP 175-1087A (Pierre *et al.,* 2001); and *Cibicidoides wuellerstorfi* $\delta^{13}C$ [‰ PDB] from core GeoB 3808-6 (Jonkers *et al.,* 2015).

During glacial periods, two deep water sources prevailed in the Southern Atlantic Ocean: a dense Southern Component Water (SCW) and a less dense Northern Component Water (NCW) (Jonkers *et al.*, 2015). Lower benthic $\delta^{13}C$ values during glacial periods in the Southern Ocean are indicative of high-nutrient waters that are attributed to an increase in Southern Component Water (SCW) in the Atlantic Ocean (Jonkers *et al.*, 2015). Palaeohydrographic changes indicated by higher benthic $\delta^{13}C$ values at this locality reflect rapid transitions to a greater influence of the Northern Component Waters (NCW) of the Atlantic Ocean. The long-term increase in $\delta^{13}C$ documented in the Jonkers *et al.* (2015) records is consistent with deep ocean $\delta^{13}C$ global trends over the time frame (Bickert and Wefer, 1996).

7.6. Conclusions

High resolution planktic and benthic foraminiferal $\delta^{13}C$ stratigraphies were reconstructed from marine core MD03-2708 from the EEA and provide the first record of $\delta^{13}C$ gradients from a non-upwelling dominated area in the region during the Late Quaternary Period. Surface and bottom water $\delta^{13}C$ was compared with regional records over the past 156 ka and showed variable records not consistent with the glacial-interglacial trend presented in $\delta^{18}O$ data. Planktic $\delta^{18}O$ data were used as a proxy for riverine discharge and showed that precession driven discharge events of the Ogooué River played a dominant role in determining the $\delta^{13}C$ of both planktic and benthic foraminifera. Concomitant with other records from the South Atlantic Ocean, the $\delta^{13}C$ of the benthic foraminiferal tests was highly influenced by an influx of nutrient-poor North Atlantic Deep Water during glacial periods and more nutrient-rich Antarctic waters during interglacial periods (Mulitza *et al.*, 1998). The $\delta^{13}C$ trend of the planktic foraminifera is less pronounced.

8 Glacial – interglacial vegetation change in the Ogooué catchment over the past 156 ka

8.1. Introduction

Western Equatorial Africa (WEA) is composed of highly diverse tropical forests and grasslands (e.g. White, 1983), which play a key role in regulating global climate and carbon stocks (Gibbs *et al.*, 2007). The distribution of tropical African vegetation is principally governed by regional hydrology (White, 1983). Climate models suggest that temperature will increase in the coming decades (IPCC, 2014), altering the regional hydrological balance and precipitation regimes (IPCC, 2014). Current forecasting studies use vegetation models which do not accurately account for the complexity of the interactions that shape the distribution of WEA vegetation (Scheiter and Higgins, 2008). How the vegetation of WEA, especially the grassland-savannah-forest composite, will respond to these changes remains unclear (Scheiter and Higgins, 2008). Comprehension of the relationship between climate and vegetation can be advanced by exploring fossil vegetation records which span periods of global climate change of a comparable magnitude (e.g. Miller and Gosling, 2014).

Long term WEA climate variability has been documented through vegetation reconstructions from multiple terrestrial and marine records (e.g. Dupont, 2011; Marret *et al.,* 2013; Miller and Gosling, 2014). Evidence of increased monsoonal precipitation activity is demonstrated by the expansion of tropical rainforest into previously dominated savannah regions during interglacial periods (e.g. Elenga *et al.,* 1994) and by an extension of grassland and afromontane refugia during glacial periods (e.g. Dupont *et al.*, 2000). Many pollen studies have used indicator species to infer past changes in temperature and precipitation (e.g. Vincens *et al.*, 2007; Bouimetarhan *et al.*, 2015), however, at times these indicator species are not representative of whole vegetation assemblages (Jolly *et al.*, 1998). An alternative school of thought have demonstrated that past climate variations are most objectively documented through

vegetation biome reconstructions (Jolly *et al.*, 1998; Gasse *et al.*, 2008; Dupont, 2011; Dupont and Kuhlmann, 2017).

Marine cores adjacent to continental margins have been identified as key palaeoclimate archives due to their largely continuous sedimentation rates (Hooghiemstra and Agwu, 1988). Additionally, in opposition to terrestrial records which often have sporadic resolutions (e.g. Elenga *et al.,* 1994), WEA marine pollen records have high temporal resolutions which provide a regionally integrated signal of continental climate conditions through vegetation cover change (e.g. Dupont and Agwu, 1991; Lezine, 1991; Frédoux, 1994; Jahns *et al.,* 1998; Marret *et al.*, 2001; Dupont *et al.,* 2008; Kim *et al.*, 2010; Marret, *et al.,* 2013).

Located between the Congo and Sanaga basins, the past vegetation and climatic evolution of the Ogooué basin has been little explored due to a scarcity of long and continuous sedimentary records from the region. Preliminary work undertaken by Kim *et al.* (2010) demonstrated the potential of using palynological analysis to reconstruct vegetation change in the region since the LGM. The aim of this study is to extend this record, and to produce a millennial resolution palynological record for the last 156 ka, which through the identification of vegetation biome shifts, can be used to infer both regional and global climate change since the penultimate glacial period.

The Ogooué palynological record will be compared to other tropical West African records from the Niger, Congo and Angola basins, and also a record further offshore Gabon, in order to work towards developing a regional understanding of Western African vegetation change over the past 156 ka [Figure 8-1].

8.2. Geographic Setting

The study area is located in the EEA within the Gulf of Guinea [Figure 8-1]. Regional atmospheric circulation is controlled by the West African Monsoon, which affects annual rainfall, temperature and wind (Leroux, 2001). The strength of the monsoon is related to changes in central and West African vegetation cover (Kutzbach *et al.,* 1996) and to periodic orbital changes in summer insolation (Kutzbach, 1981). Regional precipitation is further governed by seasonal variations in the strength and positioning of the ITCZ [Section 2.4]. The modern oceanography [Section 2.3] of the EEA is dominated by the outflow of four West African river systems (the Ogooué, Congo,

Sanaga and Niger Rivers), and the interaction of a number of surface and sub-surface currents [Figure 6-1].

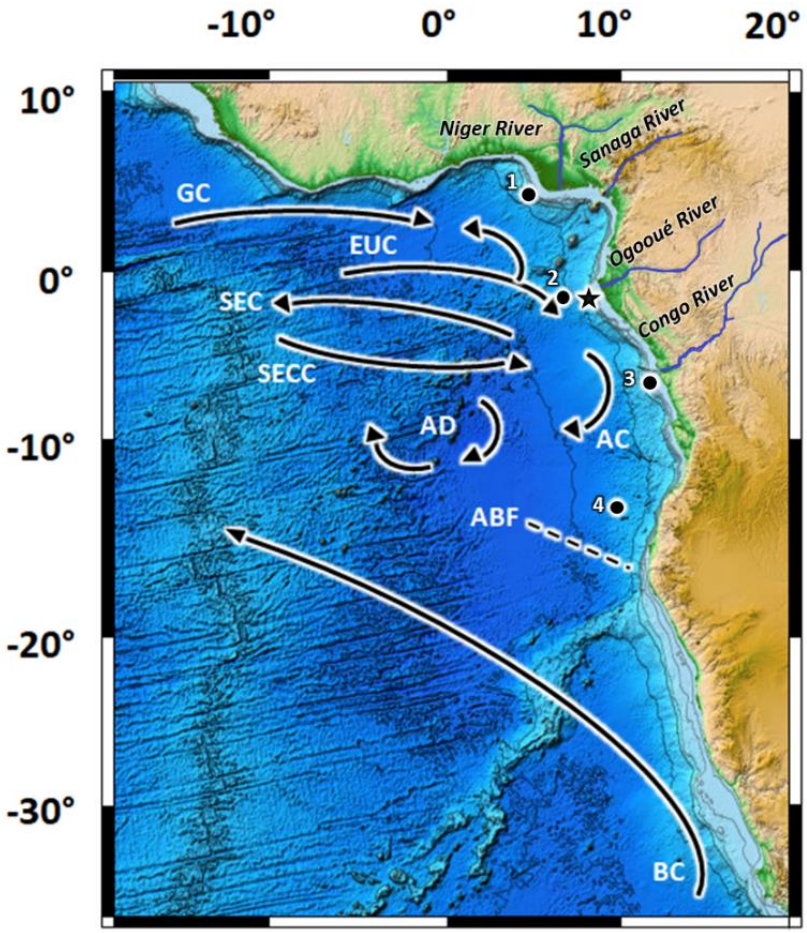

Figure 8-1: General map of Western Africa and the Eastern Equatorial Atlantic Ocean (EEA). The Niger, Sanaga, Ogooué and Congo Rivers are shown in blue. EEA surface and subsurface currents depicted as: Warm currents - GC: Guinea Current; SEC: South Equatorial Current; SECC: South Equatorial Counter Current; AC: Angola Current; and AD: Angola Dome. Cold current – BC: Benguela Current. Under Current – EUC: Equatorial Under Current. Transient Angola-Benguela Front (ABF) depicted as a dashed black arrow. MD03-2708 core location highlighted as a star in conjunction with comparative cores: (1) GIK 18656 – Niger Delta (Dupont and Weinelt, 1996); (2) GIK 16867 – offshore Gabon (Marret *et al.,* 1999; Dupont *et al.,* 2000); (3) GeoB 1008-3 (Jahns *et al.,* 1996); and (4) GeoB 1016 (Shi *et al.,* 2001).

8.3. Modern Vegetation and Pollen Source Areas

One of the most widely used classifications of African vegetation is the map of White (1983). Grouped according to floristic regions, White (1983) defined 16 phytogeographical zones for the African continent [Figure 8-2]. The phytogeographical distributions are largely determined by mean annual rainfall and dry season length, although local conditions such as water availability and soil type and structure can also contribute (White, 1983). The palynological representation of each of these vegetation types in marine sediments varies greatly depending on the floristic diversity and composition of the vegetation, the pollen productivity of the plants, and the transport mechanisms between the source area and the marine sediments (Dupont *et al.*, 2000).

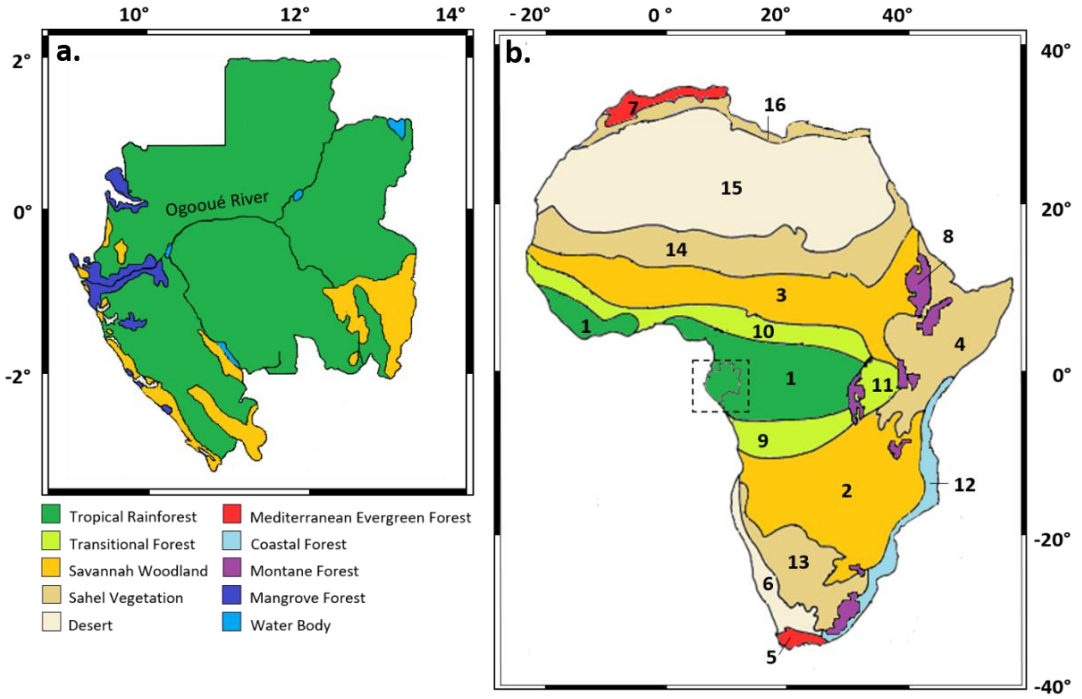

Figure 8-2: Simplified phytographic regions and vegetation biomes of Africa [after White 1983]. 1, Guinea-Congolian regional centre of endemism; 2, Zambezian regional centre of endemism; 3, Sudanian regional centre of endemism; 4, Somalia-Masai regional centre of endemism; 5, Cape regional centre of endemism; 6, Karoo-Namib regional centre of endemism; 7, Mediterranean regional centre of endemism; 8, Afromontane archipelago-like regional centre of endemism, including afro-alpine archipelago-like region of extreme floristic impoverishment; 9, Guinea Congolian/Zambezian regional transition zone; 10, Guinea-Congolian/Sudanian regional transition zone; 11, Lake Victoria regional mosaic; 12, Zanzibar-Inhambane regional mosaic; 13, Kalahari-Highveld regional transition zone; 14, Sahel regional transition zone; 15, Sahara regional transition zone; and 16, Mediterranean/Sahara regional transition zone.

The vegetation of Gabon is comparably uniform, consisting predominantly of tropical (Guinea-Congolian) rainforest [Figure 2-8-a]. Gabon is buffered by: transitional (Guinea-Congolian/ Sudanian) swamp and riparian forests to the north; transitional (Guinea-Congolian/ Zambezian) dry forest to the south; afromontane forest to the east; and mangrove swamps along the coastline and at the intertidal confluence of the Ogooué River (White, 1983). Comprehensive outlines of each of the Gabonese phytogeographical regions is given in Section 2.5.

The transportation of pollen and spores from their source areas into marine sediments involves numerous steps (Dupont *et al.,* 2000). Once pollen grains are released by plants, they are either dispersed by wind or carried into the ocean by fluvial processes. Once the pollen reaches the upper layers of the ocean, if it is caught on larger aggregates, it sinks to the sea floor.

8.4. Methodology

Marine core MD03-2708 [Figure 6-1] was extracted from the Ogooué Fan [Section 2.1], dated using $\delta^{18}O$ isotopes [Section 5] and an age model was produced [Section 5]. Bulk element abundances were obtained [Section 3.2.]Fifty three samples were prepared for palynological analysis following standard procedures [Section 3.7.1].

8.5. Results

8.5.1 Palynomorph Data

Pollen sums varied between 68 and 502 grains per sample and non-pollen palynomorph (NPP) sums between 29 and 287. Pollen and NPP percentages were calculated separately based on the total number in each category. Pollen and NPP taxa were grouped into biomes in line with (Dupont *et al.,* 2006; van Geel *et al.*, 2011; Miller and Gosling, 2014).

8.5.1.1 Pollen and Spores

The pollen data comprises 127 taxa, derived from 60 families, and is divided into seven biomes [Table 8-1 & Appendix 1]. Figure 8-2 shows percentages of the pollen groups with the exception of the mangrove (*Rhizophora*) data, which has been considered separately in Section 8.6.2 due to its over-representation and local origin (Marret *et al.,* 2006).

Glacial period MIS 6 is characterised by a dominance of grassland taxa (indicating cooler and drier conditions [e.g. (Gasse and Van Campo, 1994)] which accounts for up to 60 % of the total pollen percentage during this time period. Grassland taxa disappear from the record in MIS 5 between 112 and 80 ka and are replaced by the water rich biomes of lowland rainforest (LRF) and swampland. Rapid grassland fluctuations occur throughout MIS 2 and 1 (maxima of 73 % at 22 ka and minima of 1 % at 22.5 ka), alternating with pulses of rainforest and swamp taxa, suggesting a commencement of riverine discharge pulse events facilitated by a strengthening of the monsoon system [Dupont *et al.,* 2000].

Table 8-1: MD03-2708 pollen taxa were identified at species or family level and then further grouped into seven biomes. Mangrove taxa were omitted from the biome grouping and are considered separately.

Biome	Taxa	Families
Grassland	9	6
Dry Forest and Woodland	21	13
Lowland Rainforest	55	28
Swamp	6	3
Afromontane	6	6
Desert and Semi-Desert	16	9
Herbs and Shrubs	14	13

LRF minima occurs at 126 ka in tandem with maximum desert and semi-desert percentage (32 %) and, in conjunction with the most negative $\delta^{18}O$ values of the sequence, indicates a northward shift of the ITCZ facilitating the in-wash of taxa from northerly arid regions [Hooghiemstra, 1988]. Following a maximum (23 %) of dry forest and woodland at 112 ka, and in proportion to the composition of present day Gabonese vegetation, LRF becomes the dominant biome almost exclusively for the remainder of the sequence, with a peak abundance of 84 % at 96 ka. LRF is additionally the most diverse biome, concomitant with other regional studies (Marret *et al.*, 2008; Dupont *et al.,* 2000; Miller and Gosling, 2014). The presence of LRF during glacial periods, particularly MIS 4-2 suggests that a weak monsoonal circulation may have prevailed during boreal summer, permitting the survival of rainforest vegetation (Marret *et al.,* 2008).

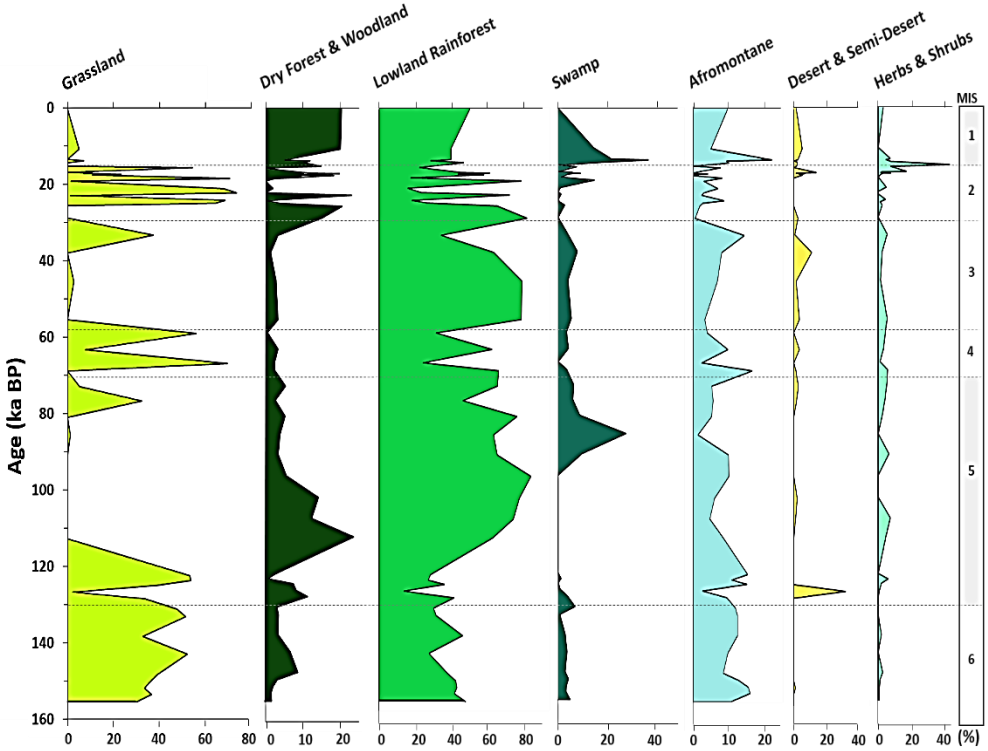

Figure 8-3: MD03-2708 pollen taxa were identified at species or family level and then further grouped into seven biomes. Mangrove taxa were omitted from the biome grouping due to their over-representation and are considered separately.

8.5.1.2 Non-Pollen Palynomorphs

The NPP data comprises 53 taxa that are divided into five biomes [Table 8-2]. Figure 8-3 shows percentages of the NPP groups, classified according to van Geel *et al.,* (2011).

Table 8-2: MD03-2708 pollen taxa were identified at species level and grouped into five biomes.

Biome	Taxa
Algal	6
Aquatic	1
Fern	4
Fungal	40
Terrestrial	2

The NPP assemblage comprises algal and fungal NPPs throughout the MD03-2708 record. Algal percentages, indicating an aquatic source provenance (Gelorini *et al.,* 2012) fluctuate between 20 and 40 % in MIS 6-3 and reach a maximum of 65 % during

the mid-Holocene (7.5 ka). Algal percentages largely co-vary with fungal percentages (in addition to a covariance with LRF), reflecting an alternation of NPP source provenance. The fungal group therefore, with a maximum of 99 % at 112 ka, could be interpreted as indicating a reduction in precipitation and therefore water body extent. Gelorini *et al.* (2012) also propose that due to the thin-wall of many fungal NPPs, an increase of the group could suggest a reduction in the monsoon and an enhancement of NE trade winds. Aquatic NPPS, representative of larger water bodies, do not appear in the record until 123 ka and in conjunction with LRF are most likely an indicator of increased precipitation.

Terrestrial NPPs, comprising poaceaous leaf cuticles prevail almost entirely in glacial periods and show a good correspondence with grassland abundance, therefore suggesting cooler and drier conditions. Ferns percentages increase in glacial MIS 4 and 3, presenting a maximum of 50 % at 38 ka, which Gelorini *et al.,* (2012) indicate as an additional terrestrial input.

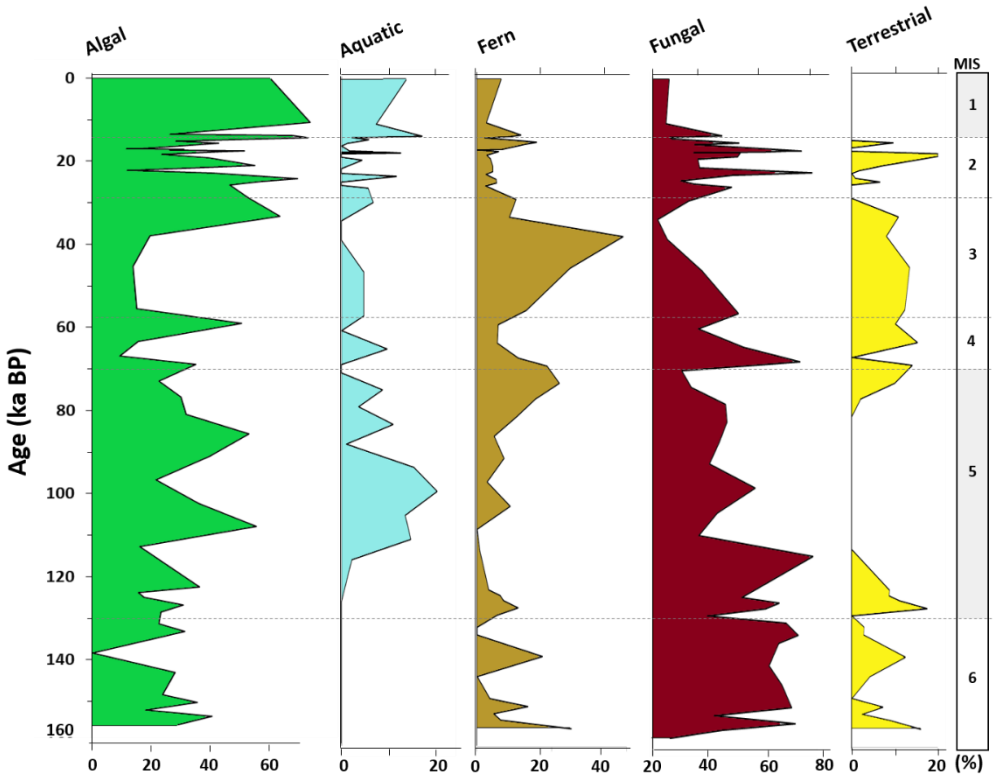

Figure 8-4: MD03-708 non-pollen palynomorph taxa were counted, identified and grouped into five biomes.

8.6. Discussion

8.6.1 Riverine Input of Palynomorphs

Marine pollen deposition is related to palynomorph source area and transport regime (Dupont and Agwu, 1991). The relative importance of transport mechanisms from the continent to the ocean, predominantly via aeolian or fluvial processes, varies from region to region (Dupont *et al.,* 1999). The fluvial transport of pollen and spores is particularly high in humid, tropical regions (Dupont *et al.,* 1999). The close proximity to multiple river mouths along the continental shelves of the Gulf of Guinea, further attributes this region as fluvially transported dominated (e.g. Muller, 1959; Dupont, et., 1999).

Within the MD03-2708 record, the Fe/Ti ratio and formaniferally-derived planktic $\delta^{18}O$ have been identified as indicators of riverine in-wash (Sections 6.5.1 and 6.5.2). Pollen influx varies quite considerably throughout the MD03-2708 record, ranging from 1.4 (cm yr^{-1000}) at 90 ka to 3.8 (cm yr^{-1000}) at 18 ka. The MD03-2708 pollen influx rate (here representing both the pollen and NPP assemblages) was compared with the Fe/Ti and planktic $\delta^{18}O$ proxies to further determine pollen source provenance and explore the climatic drivers of palynological influx over the last 156 ka [Figure 8-5].

The pollen influx rate is concurrent with the Fe/Ti and planktic $\delta^{18}O$ records during periods MIS 6, 4 and 2 [Figure 8-5] evidencing the mechanism of fluvially transported pollen into the Ogooué Fan during the last two glacial periods. Discrepancies between the pollen influx and the Fe/Ti and $\delta^{18}O$ records is manifested in the two interglacial periods, most notably during MIS 5 between 130 and 100 ka. The difference in MIS 5 may be explained by the high discharge of the Ogooué River, and its inability to effectively entrain pollen grains whilst moving so quickly (Chmura *et al.,* 1999; Piecuch *et al.,* 2018), and could also explain the low percentages of tropical rainforest taxa during the time frame. The record of sub-stage 5e is also diminished at site GIK 168867 (offshore Gabon) and is partly disturbed during in the GIK 16856 (Niger Delta) record (Dupont *et al.,* 2000). This An alternative explanation could be that pollen was being transported from a different source, but due to the proximity of the core to the land, this is not likely (Rossignol-Strick, 1983).

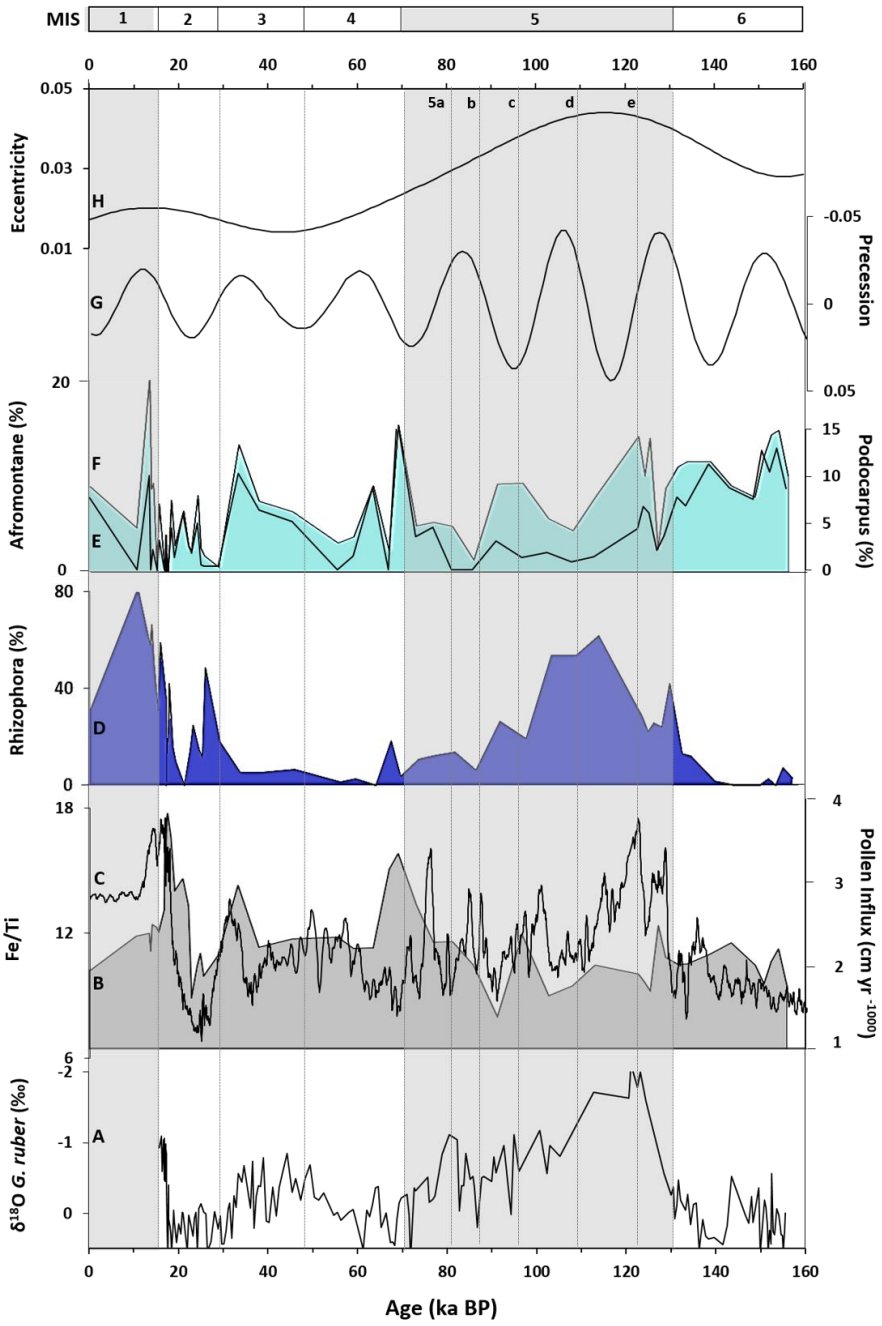

Figure 8-5: Glacial-interglacial change in the Ogooué catchment, Gabon and wider WEA over the past 156 ka. Grey bar shading denotes interglacial periods MIS 5 and 1. A: $\delta^{18}O$ *g. ruber* (‰); B: Pollen Influx (cm yr^{-1000}); C: Fe/Ti Ratio; D: *Rhizophora* (%); E: *Podocarpus* (%); F: Afromontane Vegetation (%); G: Precession *(NB reversed axis)*; and H: Eccentricity (Berger and Loutre, 1999).

8.6.2 Mangrove Vegetation

High abundances of mangrove pollen have been linked to marine transgressive cycles, or rather periods of sea level rise and shoreline encroachment, on tropical margins (Scourse *et al.*, 2005) during interglacial periods. Along the West African coastline, Holocene mangrove peat deposits comprising more than 50 % mangrove pollen evidence postglacial sea-level rise and its associated palaeogeographical modifications (Dupont *et al.,* 2000).

Mangrove stands [not depicted on Figure 8-2] prevail along the West African coastline between Senegal and Angola (White, 1983; Van Campo and Bengo, 2004). The largest swamps are found at the Niger Delta and at the Congo River mouth (White, 1983). Mangrove colonisation of the intertidal zone is largely governed by the input of freshwater and nutrients, sea level, and the stability and composition of the soil substrate (Blasco, 1982). *Rhizophora* [Red Mangrove] is dominant in most areas and largely comprises three species *R. mangle, R. harrisonii, R. racemosa* (Rhizophoraceae) (Van Campo and Bengo, 2004). The species *Avicennia germinans, A. africana, A. nitida,* (Avicenniaceae) and *Laguncularia racemosa* (Combretaceae) are also present, with the extent being governed by the local salinity gradient (Spalding *et al.,* 1997).

8.6.2.1 MD03-2708 Mangrove Record

Rhizophora pollen percentages range between 0 and 81 % [Figures 8-5 and 8-6]. Two pronounced peaks occur in interglacials MIS 5 (131 and 90) and over the glacial-interglacial MIS2-1 transition (17 -11 ka) *Rhizophora* minima (0 %) prevails during glacial MIS 6 (148 – 138 ka).

8.6.2.2 West Equatorial Mangrove Dynamics

In order to contextualise the MD03-2708 mangrove record, the *Rhizophora* pollen was compared to four *Rhizophora* records from Western Equatorial Africa: the Niger Delta (GIK 16856), offshore Gabon (GIK 16867), the Congo Delta (GeoB 1008-3), and offshore Angola (GeoB 1016) [Figures 8-1 and 8-6]. As can be seen from Figure 8-6, the MD03-2078 *Rhizophora* record show a concurrence in maxima with the GIK 16867 Niger Delta record (Dupont and Weinelt, 1996) during the glacial-interglacials transitions (MIS 6-5 and 2-1), and with the Congolese (GeoB 1008-3 (Jahns *et al.,* 1996)) and Angolan (GeoB 1016 (Shi *et al.,* 2001)) records during the last glacial-interglacial transition (MIS 2-1).

Minima within the MD03-708 record prevail during glacial MIS 6, 4, 3 and 2, coincident with the comparative WEA records.

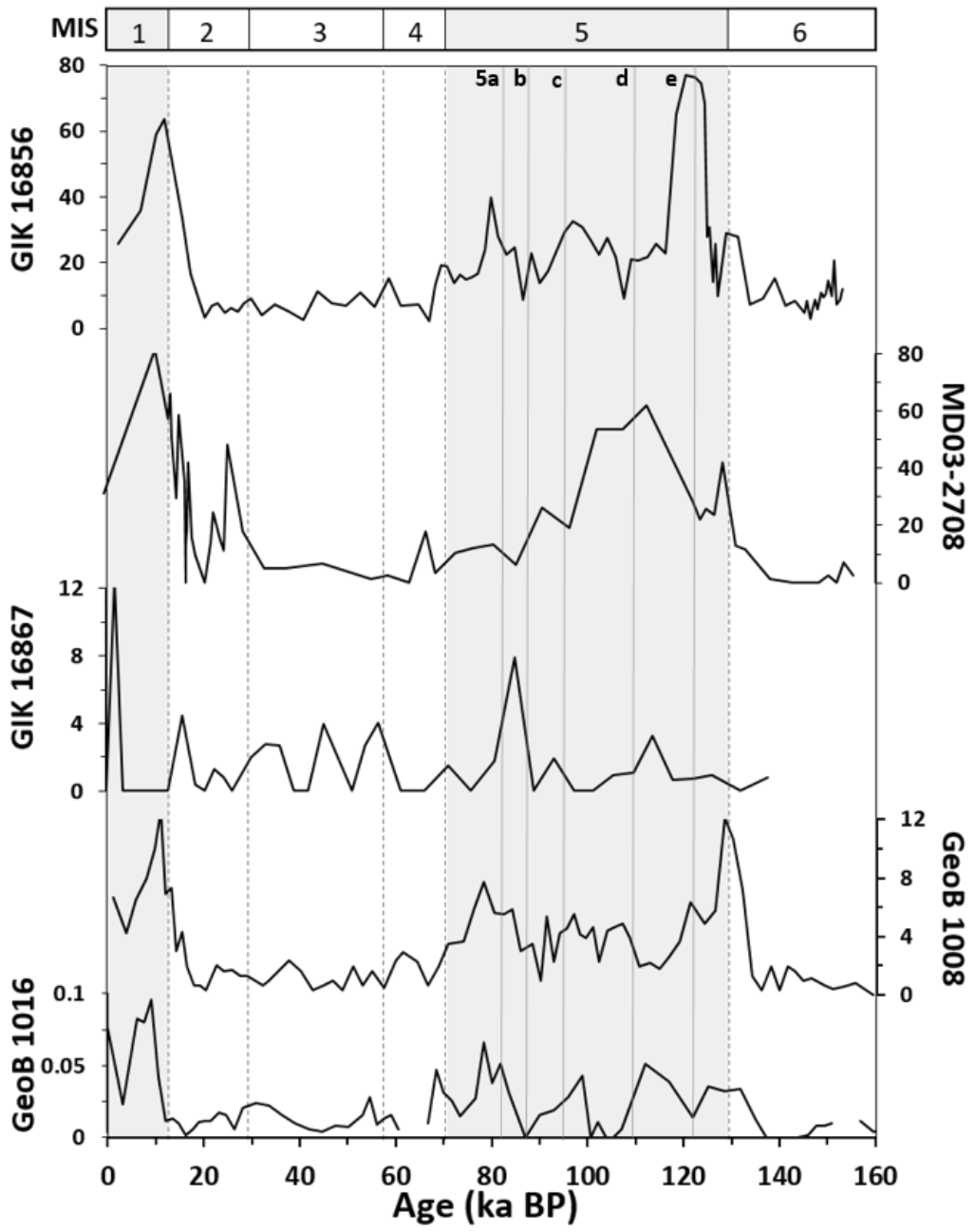

Figure 8-6: Percentages of *Rhizophora* pollen from five Western Equatorial African marine cores over the last 160 ka. Distributed latitudinally from north to south (top-bottom of figure): GIK 18656 – Niger Delta (Dupont and Weinelt, 1996); MD03-2708 – Gabon; GIK 16867 – offshore Gabon (Marret *et al.,* 1999; Dupont *et al.,* 2000); GeoB 1008-3 (Jahns *et al.,* 1996); and GeoB 1016 (Shi *et al.,* 2001).

As is exemplified in the Niger Record, the vicinity of the MD03-2708 core to the Ogooué Delta is reflected by the large amounts (< 81 %) of *Rhizophora* pollen during interglacial MIS sub-stage 5e (123 – 109 ka) and MIS 1 (14 – 0 ka) [Figure 8-7] (Dupont *et al.,* 2000). This increase in *Rhizophora* pollen at the beginning of the two interglacial periods is attributed as an indication of EEA sea-level rise (Dupont *et al.,* 2000). The onset of sea-level rise at the penultimate glacial-interglacial transition is documented by increases in *Rhizophora* pollen percentages at (First Rise (FR) at 135 ka, Maximum (M) at 130 ka), MD03-2708 (FR: 131 ka, M: 112 ka) and GIK 16856 (FR: 131 ka, M: 120 ka).

The spread of mangrove swamps after the Last Glacial Maximum is recorded by an early increase in *Rhizophora* pollen percentages at site MD03-2708 (FR: 21 ka, M: 10 ka) and is followed by sites GIK 16856 (FR: 20 ka, M: 11 ka), GeoB 1008-3 (FR: 20 ka, M: 10 ka), and GeoB 1016 (FR: 14 ka, M: 9 ka). All of the WEA records (with the exception of the further offshore GIK 16867 Gabonese record) indicate a reduction or a retreat of mangrove swamps towards present day, following maximal extensions at the beginning of the Holocene (Dupont *et al.,* 2000). The *Rhizophora* percentage maxima are most likely due to the erosion of mangrove peats by ocean transgressions (Versteegh *et al.*, 2004; Kim *et al.*, 2005), with the high *Rhizophora* abundances following Termination 1 (15 – 10 ka) facilitated by the rapid rise of sea level at this point in time (Dupont and Weinelt, 1996).

Concomitant with other West and East African studies (Dupont and Weinelt, 1996; Scourse *et al.*, 2005; Dupont, 2011; Dupont and Kuhlmann, 2017) the MD03-2708 *Rhizophora* pollen record comprises percentages of less than 10 % during glacial periods MIS 6, 4, and 3. This reduction in *Rhizophora* pollen is interpreted as a diminishment of the size of West African mangroves during glacial periods, and not an indication of lower glacial sea-levels (Peltier, 1994); if lower glacial sea-levels had caused the mangrove swamps of the Ogooué delta to migrate outwards, an increase in *Rhizophora* pollen at site MD03-2708 would have been expected (Dupont *et al.,* 2000). The low mangrove glacial pollen counts can be attributed to precluded mangrove expansion due to reduced river discharge in response to drier interior continental climates (Dupont and Weinelt, 1996) in conjunction with subaerial exposure of the continental shelf (Scourse *et al.,* 2005).

8.6.3 Afromontane Vegetation

Previous studies have documented a maxima of afromontane taxa (e.g. *Podocarpus* [evergreen tree]) in African palynological records during glacial periods MIS 6 and 2 (e.g. (Dupont *et al.*, 2000; Gasse *et al.*, 2008; Dalibard *et al.*, 2014; Dupont and Kuhlmann, 2017), indicative of lower temperatures under moderately arid to humid conditions (White, 1983; Dupont and Weinelt, 1996). In a West African context, the glacial expansion of afromontane taxa can also be attributed to a reduced latitudinal distribution of rainfall due to the strengthening of the trade wind system (Dalibard *et al.* 2014).

8.6.3.1 MD03-2708 Afromontane Record

Podocarpus pollen percentages range between 0 and 18 % [Figures 8-5 and 8-6]. *Podocarpus* maxima prevail in glacial stages MIS 6 (156 – 126 ka) and MIS 4-2 (72 -28 ka). Minimum values occur in interglacial MIS 5 (85 – 60 ka).

8.6.3.2 West African Afromontane Dynamics

So as to contextualise the MD03-2708 mangrove record, the *Rhizophora* pollen was compared to four *Rhizophora* records from Western Equatorial Africa: the Niger Delta (GIK 16856), offshore Gabon (GIK 16867), the Congo Delta (GeoB 1008-3), and offshore Angola (GeoB 1016) [Figures 8-1 and 8-6].

The comparative WEA records present *Podocarpus* peaks during MIS sub-stages 5e and 5c, highlighting an expansion of afromontane forest during these periods, under the assumption that lower temperatures allowed the forest to spread to lower altitudes (Dupont *et al.,* 2000). The MD03-2708 record does not dovetail the comparative records during Stage 5, and in conjunction with lower pollen influx, suggests that *Podocarpus* pollen did not reach the core site via fluvial input during the interglacial period.

Peaks in the MD03-2708 *Podocarpus* record during MIS 4 (10 % at 63 ka) and MIS 3 (10 % at 33 ka), correspond with peaks in the offshore Gabonese record of GIK 16867 with peaks of 65 % at 63 ka and 73 % at 38 ka. *Podocarpus* pollen is readily dispersed by wind (Bonnefille and Riollet, 1998), suggesting that higher relative abundances during this glacial period could reflect intensified wind regimes (Zhao *et al.*, 2003; Dupont *et al.*, 2007). In comparison to the MD03-2708 record, *Podocarpus* pollen is over-represented within the GIK 16867 core, which is a reflection of the aero dynamicity of the pollen

grain, meaning that it is able to travel longer distances before it enters the ocean (Dupont *et al.,* 2000).

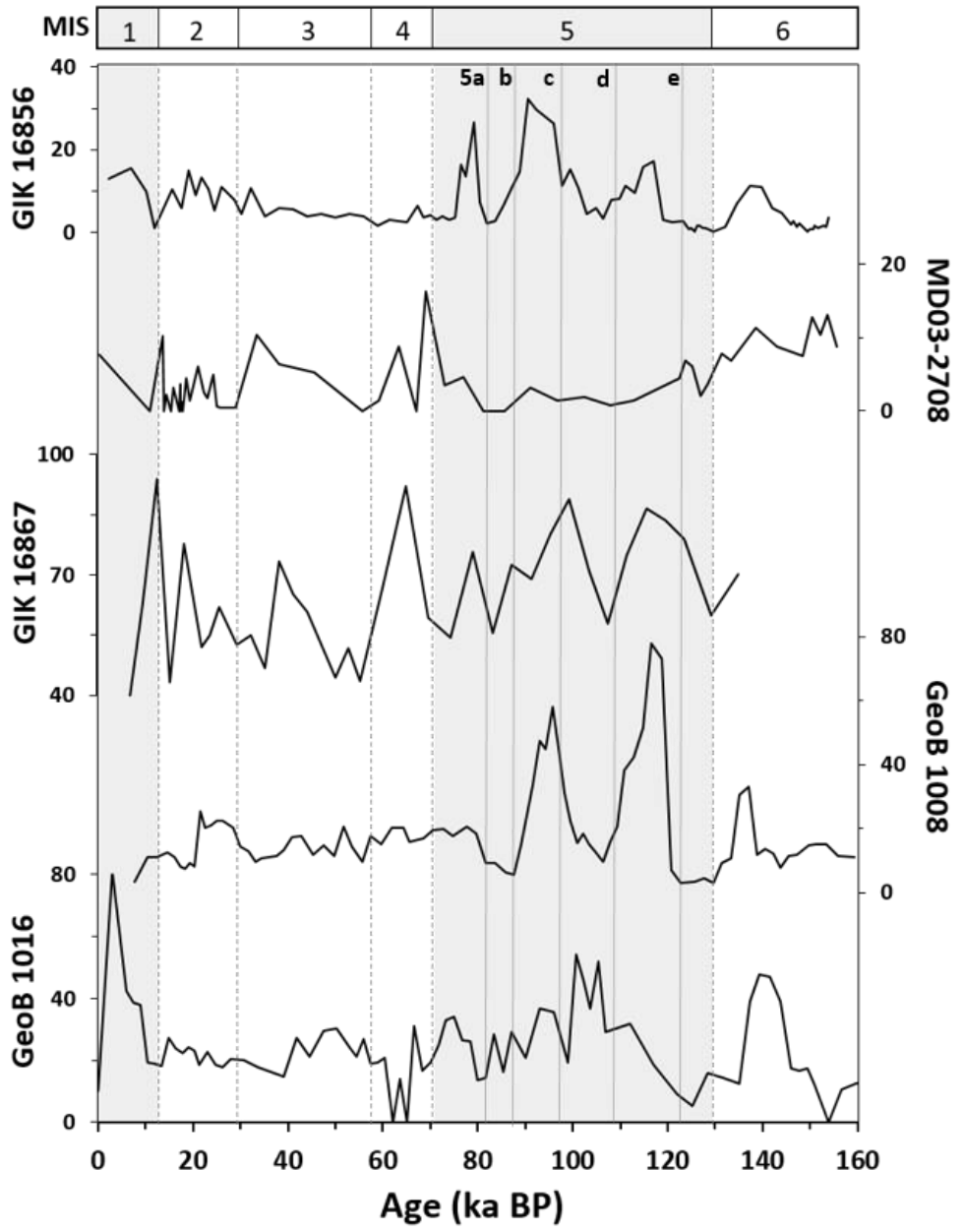

Figure 8-7: Percentages of *Podocarpus* pollen from five Western Equatorial African marine cores over the last 160 ka. Distributed latitudinally from north to south (top-bottom of figure): GIK 18656 – Niger Delta (Dupont and Weinelt, 1996); MD03-2708 – Gabon; GIK 16867 – offshore Gabon (Marret *et al.,* 1999; Dupont *et al.,* 2000); GeoB 1008-3 (Jahns *et al.,* 1996); and GeoB 1016 (Shi *et al.,* 2001).

As illustrated in Figure 8-7, the MD03-2708 *Podocarpus* record (0 – 5 %) dovetails the minima *Podocarpus* percentages of the Niger (0 – 20 %) record during glacial stage MIS

2 and during interglacial MIS 1. During Stage 2, the area of Podocarpus forest was very restricted north of the Equator, but such forest was well still well represented in Congo and Angola (Dupont *et al.,* 2000). In Equatorial West Africa, *Podocarpus* had a larger distribution than present during the early Holocene, but was most likely restricted to more elevated areas of Angola, Congo, Gabon, Cameroon, and possibly eastern Nigeria (Dupont *et al.,* 2000). Today, *Podocarpus* is a representative of the Afromontane forest of East and Southern Africa and is hardly represented in modern marine sediments of the Gulf of Guinea (Dupont *et al.,* 2000).

8.7. Conclusions

The MD03-2708 marine core documents vegetation change in the Ogooué River catchment, Gabon, and wider WEA over the past 150 ka. Pollen and NPPs were counted and identified and characterised into vegetation biomes in order to identify large-scale vegetation boundary shifts. The palynological dataset evidences a transition from cooler and drier grassland dominated vegetation in glacial MIS 6, through to more precipitation dependent LRF and swamp biomes in MIS 5. Facilitated by a mean equatorial positioning on the ITCZ from 100 ka onwards, LRF vegetation prevails throughout the remainder of the sequence and experiences rapid alternations with grassland abundances in MIS 2, which can be attributed to abrupt climate oscillations in response to northern hemisphere ice sheet retreat. The NPP record documents an alternation of algal and fungal taxa throughout the record, which is potentially due to the variable strength of the monsoon over the time frame. Terrestrial NPPs only occur in the record during glacial periods and support the presence of grassland taxa.

Examination of the MD03-2708 palynomorph influx data exhibits a correlation with the Fe/Ti ratio and planktic $\delta^{18}O$ record and supports the fluvial input of pollen into the study region. The *Rhizophora* pollen record can be used as a proxy for sea level change. Large *Rhizophora* abundances during interglacials MIS 5 and 1 propose raised sea levels and shoreline encroachment, particularly following Termination 1. Glacial periods are evidenced by very low percentages of *Rhizophora* and suggest contraction of mangroves areas. *Podocarpus* pollen peaks during glacial MIS 4 and 3 evidence an extension of afromontane forests into lower altitudes, facilitated by cooler climate. Podocarpus had a broader distribution during the early Holocene than it has now in equatorial West Africa, but it was still restricted to the more elevated areas of Angola, Congo, Gabon, and Cameroon.

9 Summary and Conclusions

The main objective of this thesis was to formulate a high resolution reconstruction of the climatic interactions of Western Equatorial Africa and the adjacent Eastern Equatorial Atlantic Ocean over the past 156 ka. Sedimentological, XRF, isotopic ($\delta^{18}O$ and $\delta^{13}C$), trace element and palynological analyses were performed on a marine sediment core from the Ogooué Fan, offshore Gabon, in order to explore the sensitivity of a small-scale river catchment in documenting glacial-interglacial hydrological variability since the penultimate glacial period.

9.1. Ogooué River Discharge Variability

Previous studies of West African hydrology have documented alternating dry and humid conditions from continental African lake level reconstructions (e.g. Gasse, 2000; Shanahan *et al.*, 2006; Miller and Gosling, 2014), and West African marine records (e.g. Schneider *et al.*, 1997; Lézine *et al.*, 2005; Weldeab *et al.*, 2007; Dupont *et al.,* 2008; Itambi *et al.*, 2009) during the Late Quaternary. Prior research has explored the response of the EEA Ocean to large scale riverine discharge variability (Schneider *et al.*, 1997; Marret *et al.*, 2001; Holtvoeth *et al.* 2003; Zabel *et al.*, 2001; Weldeab *et al.*, 2007), but the local sensitivity of the smaller Ogooué River Catchment remained to be investigated.

A 34 m marine core was extracted from the Ogooué Fan, offshore Gabon, which spanned the last 160 ka. High resolution sedimentological and geochemical investigations demonstrated the potential of the Fe/Ti ratio as an indicator of Ogooué River discharge variability. A planktic $\delta^{18}O$ isotope stratigraphy was produced, using the foraminifera *G. ruber,* which dovetailed the Fe/Ti record, strongly suggesting that the $\delta^{18}O$ of the adjacent EEA was influenced by the discharge of the Ogooué River. The proxies evidence higher riverine discharge during interglacial MIS 5, with reduced discharge occurring in glacial periods MIS 6, 4 and 2. The $\delta^{18}O$ record is largely synchronous with the planktic $\delta^{18}O$ records of marine core records adjacent to the Niger and Congo Rivers. Maximum riverine discharge is concomitant with precessional maxima and is modulated over the time frame by eccentricity variability. Preliminary Mg/Ca analysis undertaken on *G. ruber*, facilitated the production of a SST record for the last 30 ka. The SST pattern compliments the $\delta^{18}O$ record, further evidencing the

control of Ogooué River discharge on the EEA, although this is not evident in the neighbouring records that may be a function of both latitudinal positioning and catchment size.

9.2. Eastern Equatorial Atlantic $\delta^{13}C$

The $\delta^{13}C$ of planktic and benthic foraminifera has been widely used to reconstruct the past distribution of Atlantic Ocean water masses during the Late Quaternary Period (e.g. Sarnthein *et al.,* 1984; Curry and Crowley, 1987; Mackensen *et al.,* 1999). However, understanding of the glacial-interglacial variation of $\delta^{13}C$ has been harboured due to short cores and/or low temporal resolutions (Arz *et al.,* 1998; Mulitza *et al.*, 1998; Adegbie *et al.*, 2003; Zarriess and MacKensen, 2011; Burckel *et al.*, 2016). Until now, continental shelf reconstructions of $\delta^{13}C$ within the Gulf of Guinea have been limited to just two records: a 20 ka benthic record (Weldeab *et al.*, 2016) and a 30 ka planktic record (Adegbie *et al.*, 2003), both from offshore Cameroon.

High resolution planktic (*G. ruber*) and benthic foraminiferal (*C. wuellerstorfi*) $\delta^{13}C$ stratigraphies obtained from core MD03-2708 provide the first record of $\delta^{13}C$ from an EEA region not affected by upwelling. Changes in planktic and benthic $\delta^{13}C$ values are coeval with planktic $\delta^{18}O$, suggesting that Ogooué riverine discharge may have contributed to the $\delta^{13}C$ of the EEA indicator foraminiferal species.

9.3. West African Vegetation Change

The distribution of tropical African vegetation is principally governed by regional hydrology (White, 1983). Past evidence of increased monsoonal precipitation activity is demonstrated in the Late Quaternary by the expansion of tropical rainforest into previously dominated savannah regions during interglacial periods (e.g. Elenga, Schwartz and Vincens, 1994; Giresse, Maley and Brenac, 1994) and by an extension of grassland and afromontane refugia during glacial periods (e.g. Dupont *et al.*, 2000). Preliminary work undertaken by Kim *et al.* (2010) demonstrated the potential of using palynological analysis to reconstruct the vegetation change of the Ogooué River catchment, and wider WEA, from the LGM to present day. Extending the palynological record back to 150 ka will allow glacial-interglacial vegetation biome shifts since MIS 6 to be documented and the climatic drivers of these changes to be determined.

Vegetation change was documented through pollen and non-pollen palynomorph (NPP) biome reconstructions. The palynological dataset evidences a transition from cooler and drier grassland vegetation in glacial marine isotope stage (MIS) 6, through to more precipitation dependent lowland rainforest and swamp biomes from interglacial MIS 5 onwards. The high abundance of rainforest taxa through MIS 4-2 suggests the survival of rainforests as refugia during glacial periods facilitated by a weakening of the monsoon system. Palynomorph influx data dovetails the Fe/Ti and planktic $\delta^{18}O$ proxies, most likely indicating a fluvial input of pollen into the study region. High pollen influx prevails in MIS 2 and corresponds with eccentricity minima. The mangrove pollen, *Rhizophora,* is interpreted as an indicator of sea level change, which high abundances in MIS 5 and 1 evidencing sea level rise. Lastly, the Afromontane pollen *Podocarpus,* shows a strong correspondence with precession minima, suggesting alternating dominance of trade wind and monsoon intensity over the 23 ka precessional cycle.

9.4. Future Perspectives

This thesis has extended understanding of late Quaternary West Equatorial African climate change and has advanced understanding of the drivers behind these changes. However, further research is required to test and develop the ideas presented in this study. Future improvements may be accomplished with the following suggestions.

9.4.1 Increasing the Isotopic Resolution of the MD03-2708 Record

Despite presenting regionally and globally comparable data sets, obtaining a higher resolution record of the planktic and benthic $\delta^{18}O$ and $\delta^{13}C$ isotopic stratigraphies was harboured due to a lack of foraminifera present within marine MD03-2708 during MIS 1 and 5. Increasing the $\delta^{18}O$ foraminiferal resolution from 7.7 ka (planktic) and 14.5 ka (benthic) to ≤ 1 ka would allow millennial climatic variability, e.g. Heinrich events and Dansgaard-Oeschger stadials, to be reconstructed and a more robust chronology to be produced. A study from the eastern Gulf of Guinea (Weldeab, 2012) has demonstrated the ability of planktic foraminiferal $\delta^{18}O$ in recording millennial-scale riverine runoff variability, coincident with Northern Hemisphere climatic oscillations, between 75 and 25 ka. High resolution analysis of the MD03-2708 planktic $\delta^{18}O$ record would enable an investigation as to whether the smaller-scale Ogooué River catchment was able to detect such climatic variability and also extend the regional record to 160 ka.

Fine fraction carbonate $\delta^{18}O$ analysis was instrumental in filling in the gaps of the $\delta^{18}O$ foraminiferal record. The fine fraction $\delta^{13}C$ also facilitated the production of Late Quaternary EEA $\Delta\delta^{13}C$ isotopic gradients. Identification of the composition of the MD03-2708 fine fraction carbonate (e.g. foraminiferal remains, coccoliths and/or skeletal carbonate remains) under a scanning electron microscope, would allow for a more accurate $\Delta\delta^{13}C$ reconstruction and understanding of the water masses that operated in the EEA over the time frame.

9.4.2 Extending and Verifying the SST Record

Preliminary Mg/Ca analysis undertaken on the top 8 m of core MD03-2708 evidenced the potential of using the Mg/Ca of *G.ruber* (white variety) in documenting the relationship between Ogooué River runoff and EEA SST variability over the past 30 ka. Extension of the Mg/Ca record across the remainder of the MD03-2708 sequence would facilitate the production of a high-resolution, glacial-interglacial, SST record from the Ogooué margin. Furthermore, the production of a Mg/Ca derived SST record resolves the ambiguities of interpreting temperature variations from the $\delta^{18}O$ isotope record alone.

Whilst implementing additional trace element analysis, the production of a Barium/Calcium (Ba/Ca) stratigraphy, again upon the planktic foraminifera *G. ruber,* would facilitate the production of an independent salinity record. Knowledge of the past salinities of the Ogooué Margin would further inform the previous palaeodischarge interpretation and allow for a more rounded interpretation of surface palaeoceanographic change. Dinoflagellate cyst assemblage analysis offers an additional means of investigating past salinity changes, which would not only compliment the $\delta^{18}O$ and $\delta^{13}C$ records, but also help to resolve any associated uncertainties surrounding the isotopic data.

9.5. Importance of Catchment Scale Climate Reconstructions

Exploration of marine core MD03-2708 has revealed the novel approach of producing regionally and globally comparable climatic palaeo-reconstructions from a small WEA river catchment. Planktic and benthic $\delta^{18}O$ isotope stratigraphies were produced that document regional hydrological variability, that are also synchronous with global $\delta^{18}O$ records. The $\delta^{13}C$ gradients show local productivity changes in the Ogooué margin, whilst also recording shifts in global oceanographic currents. Palynological data

records vegetation biome shifts concurrent with regional hydrological, and global palaeoclimatic changes.

This study has demonstrated the atypical behaviour of the Ogooué River in comparison to the neighbouring Niger, Sanaga and Congo Rivers in response to orbital forcing over the past 156 ka, which may be attributed to latitudinal positioning of the Ogooué catchment, but also catchment size. Whilst recording regionally synchronous vegetation biome shifts from MIS 6 to 5, the MD03-2708 presents a local palynological signal from 100 ka onwards. For example, lowland tropical rainforest taxa prevail as refugia during cooler and drier glacial period MIS 4-2, suggesting a local response and presence of the monsoon system, not documented in other regional records.

These findings evidence the need to examine Late Quaternary climatic change at the catchment scale. This practise will not only be beneficial for furthering knowledge of land-ocean feedbacks and validating climate models, but it will be of huge importance to the current African societies that depend on such highly variable river systems. Finally, this local scale approach can be applied not only to WEA studies, but can be used a sensitive palaeoclimate reconstruction tool across the globe.

Appendix

Appendix 1: Pollen taxa grouped into biomes. Pollen Identified Using: Gosling *et al.* (2003). Pollen grouped using: Sowumni (1981) Dupont *et al.* (1988), Fredoux (1994), Shi and Dupont (1997), and Miller and Gosling (2014).

Genus	Species	Family	Reference
Afromontane			
Diospyros	abyssinica	Ebenaceae	Miller and Gosling (2014)
Erica	arborea	Ericaeae	Shi and Dupont (1997)
Myrica		Myricaceae	Shi and Dupont (1997)
Podocarpus		Podocarpaceae	Shi and Dupont (1997)
Pygeum	africanum	Rosaceae	Shi and Dupont (1997)
Musanga	leo-errerae	Urticaceae	Miller and Gosling (2014)
Coastal Forest			
Illigera	rhodantha	Hernandiaceae	Miller and Gosling (2014)
Ritchiea	capparoides	Capparaceae	Miller and Gosling (2014)
Ritchiea	fragariodora	Capparaceae	Miller and Gosling (2014)
Medusandra	richardsiana	Periscaceae	Miller and Gosling (2014)
Desert & Semi-Desert Vegetation			
Solanum		Solanaceae	Shi and Dupont (1997)
Balanites	aegyptiacus	Zygophyllaceae	Shi and Dupont (1997)
		Caryophyllaceae	Shi and Dupont (1997)
		Chenopodiaceae	Shi and Dupont (1997)
Corchorus	fascicularis	Malvaceae	Fredoux (1994)
Corchous	trilocularis	Malvaceae	Fredoux (1994)
	Plantago	Plantaginaceae	Shi and Dupont (1997)
Scaphopetalum	letestui	Malvaceae	Shi and Dupont (1997)
Tephrosia	nana	Fabaceae	Fredoux (1994)
Piptostigma	mayumbense	Annonaceae	Miller and Gosling (2014)
Aftemanthera	repens	Amaranthaceae	Shi and Dupont (1997)
Cissus	quadrangularis	Vitaceae	Fredoux (1994)
Commelina	africana	Commelinaceae	Fredoux (1994)
Dichrostachys	cinerea	Fabaceae	Fredoux (1994)
Dichrostochys	glomerata	Fabaceae	Fredoux (1994)
Dichrostrachys	unijuga	Fabaceae	Fredoux (1994)
Justicia		Acanthaceae	Shi and Dupont (1997)
Prosopis	africana	Fabaceae	Miller and Gosling (2014)
Prosopis	alpatoco	Fabaceae	Miller and Gosling (2014)
Vigna	luteola	Fabaceae	Fredoux (1994)
Farsetia	stenoptera	Brassicaceae	Shi and Dupont (1997)
Dry Forest and Woodland			
Acanthaceae			Shi and Dupont (1997)
Combretum	aculeatum	Combretaceae	Dupont et al (1998)
Daniella	oliveri	Fabaceae	Miller and Gosling (2014)
Dichostemma		Euphorbiaceae	Sowunmi (1981)
Kirkia	acuminata	Kirkiaceae	Fredoux (1994)
Lannea	humilis	Anacardiaceae	Shi and Dupont (1997)
Parinari		Chrysobalanaceae	Miller and Gosling (2014)
Sclerocarya	birrea	Anacardiaceae	Fredoux (1994)
Strephonema	pseudocola	Combretaceae	Miller (2014)
Sterculia	tragacantha	Malvaceae	Shi and Dupont (1997)
Grassland			
Borassus	aethiopum	Arecaceae	Miller and Gosling (2014)
Guaduella	oblonga	Poaceae	Miller and Gosling (2014)

		Poaceae	Miller and Gosling (2014)
Lowland Rainforest			
Cassipourea	flanaganii	Rhizophoraceae	Fredoux (1994)
Celosia	stuhlmannii	Amaranthaceae	Fredoux (1994)
Adenia		Passifloraceae	Fredoux (1994)
Croton	gratissimus	Euphorbiaceae	Fredoux (1994)
Elaeodendron	buchananii	Celastraceae	Fredoux (1994)
Terminalia	aemula	Combretaceae	Fredoux (1994)
Atroxima	afzeliana	Polygalaceae	Fredoux (1994)
Cola	millenii	Malvaceae	Miller and Gosling (2014)
Hewittia	sublobata	Convolvulaceae	Fredoux (1994)
Triplochiton	scleroxylon	Malvaceae	Miller and Gosling (2014)
Pyschotria		Rubiaceae	Fredoux (1994)
Acacia	clavigera	Fabaceae	Miller and Gosling (2014)
Acacia	egglingii	Fabaceae	Miller and Gosling (2014)
Acacia	senegal	Fabaceae	Miller and Gosling (2014)
	Alchornea	Euphorbiaeeae	Shi and Dupont (1997)
Anthocleista	grandiflora	Gentianaceae	Fredoux (1994)
Bosqueia	manongarivensis	Moraceae	Shi and Dupont (1997)
Calpocalyx	brevibracteatus	Fabaceae	Miller and Gosling (2014)
Cardiospermum	corindum	Sapindaceae	Fredoux (1994)
Commiphora	campestris	Burseraceae	Miller and Gosling (2014)
Commiphora	scheffleri	Burseraceae	Miller and Gosling (2014)
Dialium	guianense	Fabaceae	Miller and Gosling (2014)
Dichapetalum	mossambicense	Dichapetalaceae	Fredoux (1994)
Diospyros	abyssinica	Ebenaceae	Miller and Gosling (2014)
Diospyros	mespiliformis	Ebenaceae	Miller and Gosling (2014)
Entada	pursaetha	Fabaceae	Shi and Dupont (1997)
Erythrococca	bongensis	Euphorbiaceae	Fredoux (1994)
Eugenia	michoacanensis	Myrtaceae	Fredoux (1994)
Funtumia	latifolia	Apocynaceae	Fredoux (1994)
Grewia	bicolo	Malvaceae	Fredoux (1994)
Iodes	ovalis	Icacinaceae	Shi and Dupont (1997)
Maesobotrya		Phyllanthaceae	Shi and Dupont (1997)
Turraeanthus	africana	Meliaceae	Miller and Gosling (2014)
		Moraceae	Shi and Dupont (1997)
Nesogordonia	papaverifera	Malvaceae	Miller and Gosling (2014)
Ormocarpum	sennoides	Fabaceae	Fredoux (1994)
Parkia	bussei	Fabaceae	Miller and Gosling (2014)
Piliostigma	reticulatum	Fabaceae	Miller and Gosling (2014)
Placodiscus	amaniensis	Sapindaceae	Fredoux (1994)
Prunus	africana	Rosaceae	Fredoux (1994)
Fagara	macrophylla	Rutaceae	Fredoux (1994)
Securidaca	longepedunculata	Polygalaceae	Fredoux (1994)
Spondias	mombin	Anacardiaceae	Fredoux (1994)
Xylia	evansii	Fabaceae	Fredoux (1994)
Dracaena	camerooniana	Asparagaceae	Shi and Dupont (1997)
Mangrove			
Avicennia	officinalis	Acanthaceae	Miller and Gosling (2014)
Rhizophora	mangle	Rhizophoraceae	Miller and Gosling (2014)
Swamp			
Ancistrophyllum	laurentii	Arecaceae	Fredoux (1994)
Ancistrophyllum	secundiflorum	Arecaceae	Fredoux (1994)
Crudia	bracteata	Fabaceae	Fredoux (1994)
Raphia	ruffia	Arecaceae	Shi and Dupont (1997)
Crinum	pauciflorum	Amaryllidaceae	Fredoux (1994)
Crinum	powella	Amaryllidaceae	Fredoux (1994)
Anthostema	aubryanum	Euphorbiaceae	Miller and Gosling (2014)
Calamus	erectus	Arecaceae	Fredoux (1994)
Calamus	gracilis	Arecaceae	Fredoux (1994)

	Cyperaceae	Cyperaceae	Fredoux (1994)
Elaeis	guineensis	Arecaceae	Shi and Dupont (1997)
Pandanus	livingstonianus	Pandanaceae	Fredoux (1994)
Dracaena	reflexa	Asparagaceae	Shi and Dupont (1997)
Typha		Typhaceae	Shi and Dupont (1997)
Unclassified			
Calystegia	sepium	Convolvulaceae	
Dielsantha		Campanulaceae	
Acidanthera	brevicollis	Iridaceae	
Uvaria	kirkii	Annonaceae	
Uvariopsis	congensis	Annonaceae	
		Calophyllaceae	
Costus	spectabilis	Costaceae	
Monotes	kerstingii	Dipterocarpacerae	
Sesamum	angustifolium	Pedaliaceae	
		Violaceae	
Agelaea	heterophylla	Connaraceae	
Guibourtia	arnoldiana	Fabaceae	
Napoleona	imperialis	Lecythidaceae	
Odyendea	gabunenesis	Simaroubaceae	
Tylophora	sylvatica	Apocynaceae	
	Urticaceae		
Xyris	montana	Xyridaceae	
Xyris	welwitschii	Xyridaceae	
Sesuvium	sessile	Aizoaceae	Fredoux (1994)
Diodia	scandens	Rubiaceae	Fredoux (1994)

Appendix 2: Non-pollen palynomorph taxa grouped into biomes. NPP identified using: Gelorini *et al.* (2011) and van Geel *et al.* (2011).NPP grouped using: Mudie *et al.* (2010), Gelorini *et al.* (2011), van Geel *et al.* (2011) and Farooqui *et al.* (2014).

Genus	Species	Reference
Algal		
Botryococcus	cf. neglectus	Gelorini et al (2011)
Coelastrum	reticulatum	Gelorini et al (2011)
Pediastrum	angulosum	Gelorini et al (2011)
Scenedesmus		Gelorini et al (2011)
Spirogyra		Gelorini et al (2011)
Aquatic		
Xylariaceae		Gelorini et al (2011)
Nymphaea	nouchali	Gelorini et al (2011)
Fern		
Coniogramme	africana	Gelorini et al (2011)
Grammitis		Gelorini et al (2011)
Monoletes		Gelorini et al (2011)
Pteridium	aquilinum	Gelorini et al (2011)
Trilete spore		
Fungal		
Acroconidiellina	loudetiae	Gelorini et al (2011)
Amphirosellinia		Gelorini et al (2011)
Anthostomella	vestita	Gelorini et al (2011)
Apiosordaria		Gelorini et al (2011)
Ascodesmis		Gelorini et al (2011)
Ascoma		Mudie et al (2007)
Bactrodesmium		Gelorini et al (2011)
Brachydesmiella		Gelorini et al (2011)
Brachysporium		Gelorini et al (2011)
Byssothecium		Gelorini et al (2011)
Canalisporium	pulchrum	Gelorini et al (2011)
Canalisporium	variable	Gelorini et al (2011)
Cercophora		Gelorini et al (2011)
Cirrenalia		Gelorini et al (2011)
Clasterosporium		Gelorini et al (2011)
Coniochaeta		Gelorini et al (2011)
Cookeina		Gelorini et al (2011)
Curvularia		Gelorini et al (2011)
Delitschia		Gelorini et al (2011)
Dictyosporium	cf heptasporum	Gelorini et al (2011)
Diporotheca		Gelorini et al (2011)
Fusarium		Gelorini et al (2011)
Gelasinospora		Gelorini et al (2011)
Glomus		Gelorini et al (2011)
Kretzschmaria	clavus	Gelorini et al (2011)
Lasiodiplodia	theobromae	Gelorini et al (2011)
Meliola		Gelorini et al (2011)
Mitteriella		Gelorini et al (2011)
Phaeosphaeria		Gelorini et al (2011)
Podosporium	rigidum	Gelorini et al (2011)
Rosellinia		Gelorini et al (2011)
Savoryella	curvispora	Gelorini et al (2011)
Savoryella	lignicola	Gelorini et al (2011)
Sordaria		Gelorini et al (2011)
Spegazzinia	tessarthra	Gelorini et al (2011)
Sporidesmium		Gelorini et al (2011)
Sporoschisma		Gelorini et al (2011)
Urocystis		Gelorini et al (2011)

Ustilago		Van Geel et al (2011)
Terrestrial		
Dumbbell		Gelorini et al (2011)
Poaceous Leaf Cuticle		Farooqui et al (2014)
Marine (Excluded from total count)		
Microscopic Zoological Remains		Gelorini et al (2011)
Copepod Egg		Gelorini et al (2011)
Dinoflagellate Cyst		Gelorini et al (2011)
Foraminifera Lining		Farooqui et al (2014)
Unclassified		
Pseudpschizae		Farooqui et al (2014)

References

Abrantes, F. (1991) 'Increased upwelling off Portugal during the last glaciation — diatom evidence', *Marine Micropaleontology*, 17, pp. 285–310.

Abrantes, F. (2003) 'A 340,000 year continental climate record from tropical Africa – news from opal phytoliths from the equatorial Atlantic', *Earth and Planetary Science Letters*, 209(1–2), pp. 165–179. doi: 10.1016/S0012-821X(03)00039-6.

Adegbie, A. T., Schneider, R. R., Röhl, U. and Wefer, G. (2003) 'Glacial millennial-scale fluctuations in central African precipitation recorded in terrigenous sediment supply and freshwater signals offshore Cameroon', *Palaeogeography, Palaeoclimatology, Palaeoecology*, 197(3–4), pp. 323–333. doi: 10.1016/S0031-0182(03)00474-7.

Alizai, A., Clift, P. D., Giosan, L., VanLaningham, S., Hinton, R., Tabrez, A. R. and Danish, M. (2011) 'Pb isotopic variability in the modern-Pleistocene Indus River system measured by ion microprobe in detrital K-feldspar grains', *Geochimica et Cosmochimica Acta*, 75(17), pp. 4771–4795. doi: 10.1016/j.gca.2011.05.039.

Arz, H., Pätzold, J., & Wefer, G. (1998) 'Correlated millennial-scale changes in surface hydrography and terrigenous sediment yield inferred from last-glacial marine deposits off northeastern Brazil', *Quaternary Research*, 50(2), pp. 157–166. doi: 10.1006/qres.1998.1992.

Bakun, A. (1978) 'Guinea current upwelling', *Nature*, 271, pp. 147–150.

Beard, S. (2004) *Late Quaternary land-ocean interaction, western equatorial Africa*. Undergraduate Degree Thesis. Bangor University.

Behling, H. (2002) 'South and southeast Brazilian grasslands during Late Quaternary times: A synthesis', *Palaeogeography, Palaeoclimatology, Palaeoecology*, 177(1–2), pp. 19–27. doi: 10.1016/S0031-0182(01)00349-2.

Bemis, B., Spero, H.J., Bijma, J. and Lea, D.W. (1998) 'Reevaluation of the oxygen isotope composition of planktonic foraminifera: Experimental results and revised paleotemperature results', *Paleoceanography,* 13(2), pp. 150-160.

Beniston, M. (2004) 'The 2003 heat wave in Europe: A shape of things to come? An analysis based on Swiss climatological data and model simulations', *Geophysical Research Letters*, 31(2). doi: 10.1029/2003GL018857.

Bentahila, Y., Hebrard, O., Ben Othman, D., Luck, J.-M., Seranne, M. and Lopez, M. (2006). 'Gulf of Guinea continental slope and Congo (Zaire) deep-sea fan: Sr–Pb isotopic constraints on sediments provenance from ZaiAngo cores' *Marine Geology,* 226(3–4): 323-332.

Berger, A. (1978) 'Long-term variations of caloric insolation resulting from the earth's orbital elements', *Quaternary Research*, 9, pp. 139–167.

Berger, A. and Loutre, M. F. (1991) 'Insolation values for the climate of the last 10 million years', *Quaternary Science Reviews*, 10(4), pp. 297–317. doi: 10.1016/0277-3791(91)90033-Q.

Berger, W. H. and Vincent, E. (1986) 'Deep-sea carbonates: Reading the carbon-isotope signal', *Geologische Rundschau*, 75(1), pp. 249–269. doi: 10.1007/BF01770192.

Berger, W. H., Smetacek, V. and Wefer, G. (1989) 'Ocean productivity and paleoproductivity - An overview', *Productivity of the Ocean: Present and Past*, (April 2015), pp. 1–34. doi: 10013/epic.10860.

Berger, W.H. and Winterer, E. L. (1974) 'Plate stratigraphy and the fluctuating carbonate line', in Hsu, K.J. and Jenkyns, H. C. (ed.) *Pelagic Sediments: on Land and Under the Sea: International Association of Sedimentologists Special Publications*, pp. 11–148.

Berger, W.H., Smetacek, V. and Wefer, G. (1989) *Productivity of the Ocean: Present and Past*. Chichester: Wiley.

Bertrand, S. Hughen, K. and Giosan, L. (2015) 'Limited influence of sediment grain size on elemental XRF core scanner measurements', in Croudace, I.W. and Rothwell, R. G. (ed.) *Micro-XRF Studies of Sediment Cores: Applications of a non-destructive tool for the environmental science*. London: Springer, pp. 473–490.

Bianchi, T. S., Mitra, S. and McKee, B. A. (2002) 'Sources of terrestrially-derived organic carbon in lower Mississippi River and Louisiana shelf sediments: Implications for differential sedimentation and transport at the coastal margin', *Marine Chemistry*, 77(2–3), pp. 211–223. doi: 10.1016/S0304-4203(01)00088-3.

Bickert, T. and Wefer, G. (1996) 'Late Quaternary deep-water circulation in the South Atlantic: Reconstruction from carbonate dissolution and benthic stable isotopes', in Berger, W.H., Wefer, G., and Siedler, G. (ed.) *The South Atlantic: Present and Past Circulation*. Berlin: Springer, pp. 1237–1248.

Binet, D. (1997) 'Climate and pelagic fisheries in the Canary and Guinea currents 1964-1993: The role of trade winds and the southern oscillation', *Oceanologia Acta*, 20, pp. 177–190.

Bird, M. I. and Cali, J. A. (1998) 'A million-year record of fire in sub-Saharan Africa', *Nature*, 394(6695), pp. 767–769. doi: 10.1038/29507.

Biscara, L., Mulder, T., Martinez, P., Baudin, F., Etcheber, H., Jouanneau, J. M. and Garlan, T. (2011) 'Transport of terrestrial organic matter in the Ogooué deep sea turbidite system (Gabon)', *Marine and Petroleum Geology*, 28(5), pp. 1061–1072. doi: 10.1016/j.marpetgeo.2010.12.002.

Biscaye, P. T. (1965) 'Mineralogy and sedimentation of recent deep sea clay in the Atlantic Ocean and adjacent seas and oceans', *Bulletin of the Geological Society of America*, 76, pp. 803–832.

Blaauw, M. (2010) 'Methods and code for "classical" age-modelling of radiocarbon sequences', *Quaternary Geochronology*, 5(5), pp. 512–518. doi: 10.1016/j.quageo.2010.01.002.

Blanchet, C.L., Thouveny, N. and Vidal, L. (2009) 'Formation and preservation of greigite (Fe_3S_4) in sediments from the Santa Barbara Basin: implication for paleoenvironmental changes during the past 35 ka', *Paleoceanography*, 24. doi: 10.1029/2008PA001719.

Blasco, F. (1982) 'Ecosystemes mangroves: fonctionnement, utilite evolution'. *Oceanological Acta*, Proceedings International Symposium on coastal lagoons, SCOR/ IABO/ UNESCO, Bordeaux, France, 8–14 September, 1981, 225–230.

Blott, S. J. and Pye, K. (2001) 'GRADISTAT: a grain size distribution and statistics package for the analysis of unconsolidated sediments', 1248, pp. 1237–1248. doi: 10.1002/esp.261.

Boeckel, B., Baumann, K. H., Henrich, R. and Kinkel, H. (2006) 'Coccolith distribution patterns in South Atlantic and Southern Ocean surface sediments in relation to environmental gradients', *Deep Sea Research Part I: Oceanographic Research Papers*, 53(6), pp. 1073–1099. doi: 10.1016/j.dsr.2005.11.006.

Bonhoure, D., Rowe, E., Mariano, A.J. and Ryan, E. H. (2004) *'The South Equatorial Sys Current.' Ocean Surface Currents*, *Ocean Surface Currents*. Available at: http://oceancurrents.rsmas.miami.edu/atlantic/south-equatorial.html (Accessed: 1 August 2017).

Bouimetarhan, I., Dupont, L., Kuhlmann, H., Pätzold, J., Prange, M., Schefuß, E. and Zonneveld, K. (2015) 'Northern Hemisphere control of deglacial vegetation changes in the Rufiji uplands (Tanzania)', *Climate of the Past*, 11(5), pp. 751–764. doi: 10.5194/cp-11-751-2015.

Boyle, E. A. and Keigwin, L. D. (1985) 'Comparison of Atlantic and Pacific paleochemical records for the last 215,000 years: changes in deep ocean circulation and chemical inventories', *Earth and Planetary Science Letters*, 76(1–2), pp. 135–150. doi: 10.1016/0012-821X(85)90154-2.

Boyle, J.F., Chiverrell, R.C. and Schillereff, D. N. (2015) 'Approaches to water content correction and calibration for µXRF core scanning: comparing x-ray scatter with simple regression of elemental concentrations', in Croudace, I.W. and Rothwell, R. G. (ed.) *Micro-XRF Studies of Sediment Cores: Applications of a non-destructive tool for the environmental science*. London: Springer, pp. 373–392.

Briceno-Zuluaga, F. J., Sifeddine, A., Caquineau, S., Cardich, J., Salvatteci, R., Gutierrez, D., Ortlieb, L., Velazco, F., Boucher, H. and Machado, C. (2016) 'Terrigenous material supply to the Peruvian central continental shelf (Pisco,

14'S) during the last 1000 years: Paleoclimatic implications', *Climate of the Past*, 12(3), pp. 787–798. doi: 10.5194/cp-12-787-2016.

Broecker, W. S. and van Donk, J. (1970) 'Insolation changes, ice volumes, and the O^{18} record in deep-sea cores', *Reviews of Geophysics*, 8(1), pp. 169–198. doi: 10.1029/RG008i001p00169.

Brown, A. (2012) 'Atmospheric science: global implications for Africa', *Nature Climate Change*, (11), p. 769. doi: 10.1038/nclimate1736.

Burckel, P., Waelbroeck, C., Luo, Y., Roche, D. M., Pichat, S., Jaccard, S. L., Gherardi, J., Govin, A., Lippold, J. and Thil, F. (2016) 'Changes in the geometry and strength of the Atlantic meridional overturning circulation during the last glacial (20-50 ka)', *Climate of the Past*, 12(11), pp. 2061–2075. doi: 10.5194/cp-12-2061-2016.

Burgess, P. M. and Hovius, N. (1998) 'Rates of delta progradation during highstands: consequences for timing of deposition in deep-marine systems', *Journal of the Geological Society*, 155(2), pp. 217–222. doi: 10.1144/gsjgs.155.2.0217.

Busseler, K.O, Ball, L., Andrews, J., Cochran, J.K., Hirschberg, D.J., Bacon, M.P., Fleer, A. and Brzezinski M. (2001) 'Upper ocean export of particulate organic carbon and biogenic silica in the Southern Ocean along 170°W', *Deep-Sea Research II,* 48, pp. 4275-4297.

Calvert, S. E. and Pedersen, T. F. (2007) 'Elemental proxies for palaeoclimatic and palaeoceanographic variability in marine sediments: interpretation and application', *Developments in Marine Geology*, 1(7), pp. 567–644. doi: 10.1016/S1572-5480(07)01019-6.

Charnley, H. (1989) *Clay Sedimentology*. Berlin: Springer.

Chmura, G.L., Smirnov, A. and Campbell. (1999) 'Pollen transport through distributaries and depositional transport in coastal waters', *Palaeogeography, Palaeoclimatology and Palaeoecology,* 149(1), pp.257-270.

Cita, M. B., Vergnaud-Grazzini, C., Robert, C., Chamley, H., Ciaranfi, N. and d'Onofrio, S. (1977) 'Paleoclimatic record of a long deep sea core from the eastern Mediterranean', *Quaternary Research*, 8(2), pp. 205–235. doi: 10.1016/0033-5894(77)90046-1.

Clarke, D. W., Boyle, J. F., Chiverrell, R. C., Lario, J. and Plater, A. J. (2014) 'A sediment record of barrier estuary behaviour at the mesoscale: Interpreting high-resolution particle size analysis', *Geomorphology*, 221, pp. 51–68. doi: 10.1016/j.geomorph.2014.05.029.

Craig, H. (1957) 'Isotopic standards for carbon and oxygen correction factors for mass-spectrometric analysis of carbon dioxide', *Geochimica et Cosmochimica Act,* 12(2), pp. 133-149.

Croudace, I.W. and Rothwell, R. G. (2015) *Micro-XRF Studies of Sediment Cores: Applications of a non-destructive tool for the environmental sciences*. Springer.

Curry, B. and Thomas, J. (1987) 'The δ13C of equatorial Atlantic surface waters: Implications for ice age pCO_2 levels', *Paleoceanography*, 2(5), pp. 489–517.

Dalibard, M., Popescu, S. M., Maley, J., Baudin, F., Melinte-Dobrinescu, M. C., Pittet, B., Marsset, T., Dennielou, B., Droz, L. and Suc, J. P. (2014) 'High-resolution vegetation history of West Africa during the last 145 ka', *Geobios*, 47, pp. 183–198. doi: 10.1016/j.geobios.2014.06.002.

Dansgaard, W. (1964) 'Stable isotopes in precipitation', *Tellus*, 16(4), pp. 436–468. doi: 10.3402/tellusa.v16i4.8993.

Davies, M. 'A 52-000 year reconstruction of the past oceanic conditions of the West African Margin during the Late Quaternary Period using a Foraminifera Species Assemblage Approach. Masters Thesis. University of Liverpool.

Delcourt, H.R, Delcourt, P. (1991) *Quaternary Ecology: A Paleoecological Perspective*. Chapman and Hall.

DeMenocal, P., Ortiz, J., Guilderson, T., Adkins, J., Sarnthein, M., Baker, L. and Yarusinsky, M. (2000) 'Abrupt onset and termination of the African Humid Period: Rapid climate responses to gradual insolation forcing', *Quaternary Science Reviews*, 19(1–5), pp. 347–361. doi: 10.1016/S0277-3791(99)00081-5.

De Villiers, S., Greaves, M. and Elderfield, H. (2002) 'An intensity ratio calibration method for the accurate determination of Mg/Ca and Sr/Ca of marine carbonates by ICP-AES', *Geochemistry Geophysics Geosystems*, 3, doi: 10.1029/2001GC000169.

Diekmann, B., Hofmann, J., Heinrich, R., Futterer, D.K., Rohl, U., W. K.-Y. (2008) 'Detrital sediment supply in the southern Okinawa Trough and its relation to sea level and Kurishio dynamics during the late Quaternary', *Marine Geology*, 255, pp. 83–95. doi: 10.1016/j.margeo.2008.08.001.

Dietze, E., Hartmann, K., Diekmann, B., IJmker, J., Lehmkuhl, F., Opitz, S., Stauch, G., Wünnemann, B. and Borchers, A. (2012) 'An end-member algorithm for deciphering modern detrital processes from lake sediments of Lake Donggi Cona, NE Tibetan Plateau, China', *Sedimentary Geology*, 243–244, pp. 169–180. doi: 10.1016/j.sedgeo.2011.09.014.

Dietze, M., and Dietze, E. (2013) 'EMMAgeo: Endmember modelling algorithm and supporting functions for grain-size analysis, R package version 0.9.1'.

Dudley, W. C. and Goodney, D. E. (1979) 'Oxygen isotope content of coccoliths grown in culture', *Deep Sea Research Part A, Oceanographic Research Papers*, 26(5), pp. 495–503. doi: 10.1016/0198-0149(79)90092-X.

Dupont, L., Jahns, S. and Schneider, R. (1999) 'Marine-terrestrial interaction of climate changes in West Equatorial Africa of the last 190,000 years', 26, pp. 1–21.

Duplessy, J. C., Shackleton, N. J., Fairbanks, R. G., Labeyriefi, L. and Oppo, D. (1988) 'Deepwater source variations during the last climatic cycle and their impact on the global deepwater circulation', *Paleoceanography,* 3(3), pp. 343–360.

Dupont, L. M. and Agwu, C. O. C. (1991) 'Environmental control of pollen grain distribution patterns in the Gulf of Guinea and offshore NW-Africa', *Geologische Rundschau*, 80(3), pp. 567–589. doi: 10.1007/BF01803687.

Dupont, L. M and Weinelt, L. M. D. (1996) 'Vegetation history of the savanna corridor between the Guinean and the Congolian rain forest during the last 150,000 years', *Vegetation History and Archaeobotany*, 5, pp. 273–292.

Dupont, L. M., Jahns, S., Marret, F. and Ning, S. (2000) 'Vegetation change in equatorial West Africa: time-slices for the last 150 ka', *Palaeogeography, Palaeoclimatology, Palaeoecology*, 155(1–2), pp. 95–122. doi: 10.1016/S0031-0182(99)00095-4.

Dupont, L. M. and Behling, H. (2006) 'Land–sea linkages during deglaciation: High-resolution records from the eastern Atlantic off the coast of Namibia and Angola (ODP site 1078)', *Quaternary International*, 148(1), pp. 19–28. doi: 10.1016/j.quaint.2005.11.004.

Dupont, L. M., Behling, H., Jahns, S., Marret, F. and Kim, J. H. (2007) 'Variability in glacial and Holocene marine pollen records offshore from west southern Africa', *Vegetation History and Archaeobotany*, 16(2–3), pp. 87–100. doi: 10.1007/s00334-006-0080-8.

Dupont, L. M., Behling, H. and Kim, J.-H. (2008) 'Thirty thousand years of vegetation development and climate change in Angola (Ocean Drilling Program Site 1078)', *Climate of the Past Discussions*, 4(1), pp. 111–147. doi: 10.5194/cpd-4-111-2008.

Dupont, L. (2011) 'Orbital scale vegetation change in Africa', *Quaternary Science Reviews*, 30(25–26), pp. 3589–3602. doi: 10.1016/j.quascirev.2011.09.019.

Dupont, L. M. and Kuhlmann, H. (2017) 'Glacial-interglacial vegetation change in the Zambezi catchment', *Quaternary Science Reviews*, 155, pp. 127–135. doi: 10.1016/j.quascirev.2016.11.019.

Dypvik, H. and Harris, N. B. (2001) 'Geochemical facies analysis of fine-grained siliciclastics using Th/U, Zr/Rb and (Zr+Rb)/Sr ratios', *Chemical Geology*, 181(1–4), pp. 131–146. doi: 10.1016/S0009-2541(01)00278-9.

Elderfield, H. and Gansen, G. (2000) 'Past temperatures and $\delta^{18}O$ of surface ocean waters inferred from foraminiferal Mg/Ca ratios', *Nature,* 405, pp. 442-445.

Elenga, H., Schwartz, D. and Vincens, A. (1994) 'Pollen evidence of late Quaternary vegetation and inferred climate changes in Congo', *Palaeogeography, Palaeoclimatology, Palaeoecology*, 109(2–4), pp. 345–356. doi: 10.1016/0031-0182(94)90184-8.

Emiliani, C. (1955) 'Pleistocene temperatures', *The Journal of Geology*, 63(6), pp. 538–573.

Epstein, S., Buchsbaum, R., Lowenstam, H.A. and Urey, H. C. (1953) 'Revised carbonate-water isotopic temperature scale', *Geological Society of America Bulletin*, 64(11), pp. 1315–1326.

Fairbanks, R. G., Mortlock, R. A., Chiu, T. C., Cao, L., Kaplan, A., Guilderson, T. P., Fairbanks, T. W., Bloom, A. L., Grootes, P. M. and Nadeau, M. J. (2005) 'Radiocarbon calibration curve spanning 0 to 50,000 years BP based on paired 230Th/234U/238U and 14C dates on pristine corals', *Quaternary Science Reviews*, 24(16–17), pp. 1781–1796. doi: 10.1016/j.quascirev.2005.04.007.

Farrell, J. W. and Prell, W. L. (1989) 'Climatic change and $CaCO_3$ preservation: an 800,000 year bathymetric reconstruction from the central equatorial Pacific Ocean', *Paleoceanography*, 4(4), pp. 447–466. doi: 10.1029/PA004i004p00447.

Folk RL, W. W. (1957) 'Brazos River bar: a study in the significance of grain size parameters', *Journal of Sedimentary Petrology*, 27, pp. 3–26.

Frédoux, A. (1994) 'Pollen analysis of a deep-sea core in the Gulf of Guinea: vegetation and climatic changes during the last 225,000 years B.P', *Palaeogeography, Palaeoclimatology, Palaeoecology*, 109(2–4), pp. 317–330. doi: 10.1016/0031-0182(94)90182-1.

Fütterer, D. K. (2006) 'The solid phase of marine sediments', in Schulz, H.D., Zabel, M. (eds.) *Marine Geochemistry*. Berlin: Springer, pp. 1–25.

Garcin, Y., Vincens, A., Williamson, D., Buchet, G. and Guiot, J. (2007) 'Abrupt resumption of the African Monsoon at the Younger Dryas—Holocene climatic transition', *Quaternary Science Reviews*, 26(5–6), pp. 690–704. doi: 10.1016/j.quascirev.2006.10.014.

Gasse, F. (2000) 'Hydrological changes in the African tropics since the Last Glacial Maximum', *Quaternary Science Reviews*, 19(1–5), pp. 189–211. doi: 10.1016/S0277-3791(99)00061-X.

Gasse, F. and Van Campo, E. (1994) 'Abrupt post-glacial climate events in West Asia and North Africa monsoon domains', *Earth and Planetary Science Letters*, 126(4), pp. 435–456. doi: 10.1016/0012-821X(94)90123-6.

Gasse, F., Chalié, F., Vincens, A., Williams, M. a. J. and Williamson, D. (2008) 'Climatic patterns in equatorial and southern Africa from 30,000 to 10,000 years ago reconstructed from terrestrial and near-shore proxy data', *Quaternary Science Reviews*, 27(25–26), pp. 2316–2340. doi: 10.1016/j.quascirev.2008.08.027.

Gelorini, V., Verbeken, A., van Geel, B., Cocquyt, C. and Verschuren, D. (2011) 'Modern non-pollen palynomorphs from East African lake sediments', *Review of Palaeobotany and Palynology*, 164(3–4), pp. 143–173. doi: 10.1016/j.revpalbo.2010.12.002.

Gelorini, V., Ssemmanda, I. and Verschuren, D. (2012) 'Validation of non-pollen palynomorphs as paleoenvironmental indicators in tropical Africa: Contrasting ~200-year paleolimnological records of climate change and human impact',

Review of Palaeobotany and Palynology, 186, pp. 90–101. doi: 10.1016/j.revpalbo.2012.05.006.

Gibbs, H. K., Brown, S., Niles, J. O. and Foley, J. A. (2007) 'Monitoring and estimating tropical forest carbon stocks: Making REDD a reality', *Environmental Research Letters*, 2(4). doi: 10.1088/1748-9326/2/4/045023.

Giorgi, F and Diffenbaugh, N. S. (2012) 'Climate change hotspots in the CMIP5 global climate model ensemble', *Climatic Change*, 114, pp. 813–822.

Giresse, P., Maley, J. and Brenac, P. (1994) 'Late Quaternary palaeoenvironments in the Lake Barombi Mbo (West Cameroon) deduced from pollen and carbon isotopes of organic matter', *Palaeogeography, Palaeoclimatology, Palaeoecology*, 107(1–2), pp. 65–78. doi: 10.1016/0031-0182(94)90165-1.

Gosling, W. D., Miller, C. S. and Livingstone, D. A. (2013) 'Atlas of the tropical West African pollen flora', *Review of Palaeobotany and Palynology*, 199, pp. 1–135. doi: 10.1016/j.revpalbo.2013.01.003.

Govin, A., Holzwarth, U., Heslop, D., Ford Keeling, L., Zabel, M., Mulitza, S., Collins, J. A. and Chiessi, C. M. (2012) 'Distribution of major elements in Atlantic surface sediments (36'N-49'S): Imprint of terrigenous input and continental weathering', *Geochemistry, Geophysics, Geosystems*, 13(1), pp. 1–23. doi: 10.1029/2011GC003785.

Grossman, E. L. (1987) 'Stable isotopes in modern benthic foraminifera; a study of vital effect', *The Journal of Foraminiferal Research*, 17(1), pp. 48–61. doi: 10.2113/gsjfr.17.1.48.

H. Elderfield and Ganssen, G. (2000) 'Past temperature and $\delta^{18}O$ of surface ocean waters inferred from foraminiferal Mg/Ca ratios', *Letters to Nature*, 705(103), pp. 442–445. doi: 10.1038/35013033.

Haneburth, T.J.J and Lantzsch, H. (2008) 'A Late Quaternary sedimentary shelf system under hyperarid conditions: unravelling climatic, oceanographic and sea-level controls (Golfe d'Arguin, Mauritania, NW Africa)', *Marine Geology*, 256, pp. 77–89. doi: 10.1016/j.margeo.2008.10.001.

Harmon, C. (1957) 'Isotopic standards for carbon and oxygen and correction factors for mass-spectrometric analysis of carbon dioxide', *Geochimica et cosmochimica acta*, 12(1), pp. 133–149. doi: 10.1163/_q3_SIM_00374.

Haug, G. H., Hughen, K. a, Sigman, D. M., Peterson, L. C. and Röhl, U. (2001) 'Southward migration of the intertropical convergence zone through the Holocene.', *Science*, 293(5533), pp. 1304–8. doi: 10.1126/science.1059725.

Hayward, B. (2014) *Foraminifera taxon details, World Foraminifera Database. Available at: http://www.marinespecies.org/foraminifera/aphia.php?p=taxdetails&id=765385 (Accessed: 27 January 2017).*

Healey, S. and Thunell, R. (2004) 'Millennial-scale variability in western subtropical North Atlantic surface and deep water circulation during marine isotope stages 11 and 12', *Paleoceanography*, 19(1), pp. 1–16. doi: 10.1029/2003PA000925.

Hebbeln, D., Knusden, K-L., Gyllencreutz, R., Kristensen, P., Klitgaard-Kristensen, D., Backman, J., Scheurle, C., Jiang, H., Gil, I., Smelor, M., Jones, P.D. and Sejrup, H. P. (2006) 'Late Holocene coastal hydrographic and climate changes in the eastern North Sea', *Holocene*, 16, pp. 987–1001. doi: 10.1177/0959683606hl989rp.

Hemleben, C., Spindler, M., Anderson, O. R. (1989) *Modern Planktonic Foraminifera*. New York: Springer.

Henin, C., P. Hisard, and Piton, B. (1986) 'Observations hydrologiques dans l'ocean Atlantique Equatorial', *FOCAL*, 1, pp. 1–191.

Hennekam, R. and de Lange, G. (2012) 'X-ray fluorescence core scanning of wet marine sediments: methods to improve quality and reproducibility of high-resolution paleoenvironmental records', *Limnology and Oceanography: Methods*, 10, pp. 991–1003. doi: 10.4319/lom.2012.10.1991.

Hessler, I. (2011) *Oceanography, climate and vegetation development of tropical Africa during the last glacial: Palynology and geochemistry*. PhD Thesis. Universität Bremen.

Hessler, I., Steinke, S., Groeneveld, J., Dupont, L. and Wefer, G. (2011) 'Impact of abrupt climate change in the tropical southeast Atlantic during Marine Isotope Stage (MIS) 3', *Paleoceanography*, 26(4), pp. 1–11. doi: 10.1029/2011PA002118.

Hessler, I., Dupont, L., Handiani, D., Paul, A., Merkel, U. and Wefer, G. (2012) 'Masked millennial-scale climate variations in South West Africa during the last glaciation', *Climate of the Past*, 8(2), pp. 841–853. doi: 10.5194/cp-8-841-2012.

Hodell, D. A., Channeil, J. E. T., Curtis, J. H., Romero, O. E. and Röhl, U. (2008) 'Onset of "Hudson Strait" Heinrich events in the eastern North Atlantic at the end of the middle Pleistocene transition (~640 ka)?', *Paleoceanography*, 23(4), pp. 1–16. doi: 10.1029/2008PA001591.

Hodell, D. A., Evans, H. F., Channell, J. E. T. and Curtis, J. H. (2010) 'Phase relationships of North Atlantic ice-rafted debris and surface-deep climate proxies during the last glacial period', *Quaternary Science Reviews*, 29(27–28), pp. 3875–3886. doi: 10.1016/j.quascirev.2010.09.006.

Hoffman, .D. I., Fabian, K., Schneider, F., Donner, B. and Bleil, U. (2005) 'A stratigraphic network across the Subtropical Front in the central South Atlantic: multi-parameter correlation of magnetic susceptibility, density, X-ray fluorescence and δ18O records', *Earth and Planetary Science Letters*, 240, pp. 694–709. doi: 10.1016/j.epsl.2005.09.048.

Holtvoeth, J., Wagner, T. and Schubert, C. J. (2003) 'Organic matter in river-influenced continental margin sediments: The land-ocean and climate linkage

at the Late Quaternary Congo fan (ODP Site 1075)', *Geochemistry, Geophysics, Geosystems*, 4(12). doi: 10.1029/2003GC000590.

Holz, C., Stuut, J. W. and Henrich, R. (2004) 'Terrigenous sedimentation processes along the continental margin off NW Africa: implications from grain-size analysis of seabed sediments', *Sedimentology*, 51(5), pp. 1145–1154. doi: 10.1111/j.1365-3091.2004.00665.x.

Holz, C., Stuut, J. B. W., Henrich, R. and Meggers, H. (2007) 'Variability in terrigenous sedimentation processes off northwest Africa and its relation to climate changes: Inferences from grain-size distributions of a Holocene marine sediment record', *Sedimentary Geology*, 202(3), pp. 499–508. doi: 10.1016/j.sedgeo.2007.03.015.

Hooghiemstra, H. and Agwu, C. O. C. (1986) 'Distribution of palynomorphs in marine sediments: A record for seasonal wind patterns over NW Africa and adjacent Atlantic', *Geologische Rundschau*, 75(1), pp. 81–95. doi: 10.1007/BF01770180.

Hooghiemstra, H., Lézine, A.-M., Leroy, S. a. G., Dupont, L. and Marret, F. (2006) 'Late Quaternary palynology in marine sediments: A synthesis of the understanding of pollen distribution patterns in the NW African setting', *Quaternary International*, 148(1), pp. 29–44. doi: 10.1016/j.quaint.2005.11.005.

Hopkins, B. and White, F. (1987) 'Vegetation Map of Africa. The Vegetation of Africa: A Descriptive Memoir to Accompany the Unesco/AETFAT/UNSO Vegetation map of Africa', *The Journal of Ecology*. doi: 10.2307/2260340.

Housen, B.A., Banerjee, S.K. and Moskowitz, B.M. (1996) 'Low-temperature magnetic properties of siderite and magnetite in marine sediments', *Geophysical Research Letters,* 23, 2843-2846.

Ingram, W.C., Meyers, S.R., Brunner, C.A. and Martens, C. S. (2010) 'Late Pleistocene-Holocene sedimentation surrounding an active seafloor gas-hydrate and cold-seep field on the Northern Gulf of Mexico slope', *Marine Geology*, 278, pp. 45–53. doi: 10.1016/j.margeo.200.09.002.

IPCC (2007) *Climate Change 2007 Synthesis Report*, *Intergovernmental Panel on Climate Change [Core Writing Team IPCC]*. doi: 10.1256/004316502320517344.

IPCC (2014) 'Summary for policymakers', *Climate Change 2014: Impacts, Adaptation and Vulnerability - Contributions of the Working Group II to the Fifth Assessment Report*, pp. 1–32. doi: 10.1016/j.renene.2009.11.012.

Itambi, A. C., Von Dobeneck, T., Mulitza, S., Bickert, T. and Heslop, D. (2009) 'Millennial-scale northwest African droughts related to Heinrich events and Dansgaard-Oeschger cycles: Evidence in marine sediments from offshore Senegal', *Paleoceanography*, 24(1), pp. 1–16. doi: 10.1029/2007PA001570.

Itambi, A. C., Dobeneck, T. V. O. N. and Adegbie, A. T. (2010) 'Millennial-scale precipitation changes over Central Africa during the late Quaternary and Holocene: Evidence in sediments from the Gulf of Guinea', 25, pp. 267–279. doi: 10.1002/jqs.

Jacobsen, H. V. (2012) *Sea-surface conditions through the last 25,000 years off the Ogooué River, West Africa.* Undergraduate Degree Thesis. Aarhus University.

Jaeschke, A., Rühlemann, C., Arz, H., Heil, G. and Lohmann, G. (2007) 'Coupling of millennial-scale changes in sea surface temperature and precipitation off northeastern Brazil with high-latitude climate shifts during the last glacial period', *Paleoceanography*, 22(4), pp. 1–10. doi: 10.1029/2006PA001391.

Jahns, S., Hiils, M. and Sarnthein, M. (1998) 'Vegetation and climate history of west equatorial Africa based on a marine pollen record off Liberia (site GIK 16776) covering the last 400,000 years', *Review of Palynology and Palaeobotany,* 102, pp. 277–288.

Jansen, J H F, Van Iperen, J. M. (1991) 'A 220,000-year climatic record for the east equatorial Atlantic Ocean and equatorial Africa: Evidence from diatoms and opal phytoliths in the Zaire (Congo) deep-sea fan', *Paleoceanograaphy,* 6(5), pp. 573–591.

Jansen, J., Van der Gaast, S., Koster, B. and Vaars, A. (1998) 'CORTEX, a shipboard XRF-scanner for element analyses in split sediment cores', *Marine Geology*, 151, pp. 143–153.

Johnsen, S. F. and North Greenland Ice Core Project Members (2004) 'High-resolution record of Northern Hemisphere climate extending into the last interglacial period', *Nature,* 431(7005), 147-151.

Jolly, D., Harrison, S. P., Damnati, B. and Bonnefille, R. (1998) 'Simulated climate and biomes of Africa during the Late Quaternary: Comparison with pollen and lake status data', *Quaternary Science Reviews,* 17(98), pp. 629-657.

Jones, A.; Kilasara, M.; Le Roux, P.; Michéli, E.; Montanarella, L.; Spaargaren, O.; Thiombiano, L.; Van Ranst, E.; Yemefack, M.; Zougmire, R.; Breuning-Madsen, H.; Brossard, M.; Dampha, A.; Deckers, J.; Dewitte, O. .; Gallali, T.; Hallet, S.; Jones, R Jo, R. (2013) 'Soil Atlas of Africa', in Wright, EP and Burgess, W. (ed.) *Jones, A.; Kilasara, M.; Le Roux, P.; Michéli, E.; Montanarella, L.; Spaargaren, O.; Thiombiano, L.; Van Ranst, E.; Yemefack, M.; Zougmire, R.; Breuning-Madsen, H.; Brossard, M.; Dampha, A.; Deckers, J.; Dewitte, O. .; Gallali, T.; Hallet, S.; Jones, R*. 66th edn. London: Geological Society of London, pp. 131–154.

Jonkers, L., Zahn, R., Thomas, A., Henderson, G., Abouchami, W., François, R., Masque, P., Hall, I. R. and Bickert, T. (2015) 'Deep circulation changes in the central South Atlantic during the past 145 kyrs reflected in a combined $^{231}Pa/^{230}Th$, Neodymium isotope and benthic record', *Earth and Planetary Science Letters*, 419, pp. 14–21. doi: 10.1016/j.epsl.2015.03.004.

Jourdin, F., Froidefond, J., Loyer, S., Mayoyas, Y. and Vrignaud, C. (2006) 'Measuring upper ocean turbidity off Congo and Gabon coasts Sao Tome Gabon Congo', *Proceedings of Caracterisation du Milieu Marin*, 6, pp.16-19.

Kallweit, W., Mollenhauer, G. and Zabel, M. (2012) 'Multi-proxy reconstruction of terrigenous input and sea-surface temperatures in the eastern Gulf of Guinea

over the last ~35ka', *Marine Geology*, 319–322, pp. 35–46. doi: 10.1016/j.margeo.2012.06.007.

Kiefer, T., McCave, I. N. and Elderfield, H. (2006) 'Antarctic control on tropical Indian Ocean sea surface temperature and hydrography', *Geophysical Research Letters*, 33(24), pp. 1–5. doi: 10.1029/2006GL027097.

Kim, J. H., Dupont, L., Behling, H. and Versteegh, G. J. M. (2005) 'Impacts of rapid sea-level rise on mangrove deposit erosion: application of taraxerol and Rhizophora records', *Journal of Quaternary Science*, 20(3), pp. 221–225. doi: 10.1002/jqs.904.

Kim, S., Scourse, J., Marret, F. and Lim, D. (2010) 'A 26,000-year integrated record of marine and terrestrial environmental change off Gabon, west equatorial Africa', *Palaeogeography, Palaeoclimatology, Palaeoecology*, pp. 1–11. doi: 10.1016/j.palaeo.2010.08.026.

Kinkel, H., Baumann, K. H. and Cepek, M. (2000) 'Coccolithophores in the equatorial Atlantic Ocean: Response to seasonal and Late Quaternary surface water variability', *Marine Micropaleontology*, 39(1–4), pp. 87–112. doi: 10.1016/S0377-8398(00)00016-5.

Kiriakoulakis, K., Blackbird, S., Ingels, J., Vanreusel, A. and Wolff, G. A. (2011) 'Organic geochemistry of submarine canyons: The Portuguese Margin', *Deep-Sea Research Part II: Topical Studies in Oceanography*, 58(23–24), pp. 2477–2488. doi: 10.1016/j.dsr2.2011.04.010.

Kolla, V., Biscaye, P. E. and Hanley, A. F. (1979) 'Distribution of quartz in late Quaternary Atlantic sediments in relation to climate', *Quaternary Research*, 11(2), pp. 261–277. doi: 10.1016/0033-5894(79)90008-5.

Konfirst, M.A., Kuhn, G., Monien, D. and Scherer, R. P. (2011) 'Correlation of Early Pliocene diatomite to low amplitude Milankovitch cycles in the ANDRILL AND-1B core', *Marine Micropaleontology*, 80, pp. 114–124. doi: 10.1016/j.marmicro.2011.06.005.

Kuijpers, A., Troelstra, S.R., Prins, M.A., Linthout, K., Akjmetzhanov, A., Bouryak, S., Bachmann, M.F., Lassen, S., Rasmussen, S., Jensen, J. B. (2003) 'Late Quaternary sedimentary processes and ocean circulation changes at the Southeast Greenland margin', *Marine Geology*, 195, pp. 109–129. doi: 10.1016/S0025-3227(02)00684-9.

Kutzbach, J. E. (1981) 'Monsoon climate of the early Holocene: climate experiment with the earth's orbital parameters for 9000 years ago', *Science*, 214, pp. 59–61.

Kutzbach, J. E., Bonan, G., Foley, J. and Harrison, S. P. (1996) 'Vegetation and soil feedbacks on the response of the African monsoon to orbital forcing in the early to middle Holocene', *Nature*, 384, pp. 623–626.

Lamb, H., Cohen, A., Schäbitz, F., Asrat, A., Barker, P., Bates, R., Davies, S., Deino, A., Förster, V., Grove, M., Huws, D., Junginger, A., Konrad-Schmolke, M., Lane, C., Leng, M., Mark, D., Martin-Jones, E., Pearce, N., Pearson, E., Ramsey, C., Raub, T., Rethemeyer, J., Roberts, H., Rogass, C., Trauth, M., Viehberg, F., Wagner, B.

and Woldegabriel, G. (2016) 'The Hominin sites and Palaeolakes Drilling Project: testing hypotheses of climate-driven human evolution and dispersal at Chew Bahir, Ethiopia', *Quaternary International*, 404, pp. 2016. doi: 10.1016/j.quaint.2015.08.202.

Lass, H. U., Schmidt, M., Mohrholz, V., and Nausch, G. (2000) 'Hydrographic and current measurements in the area of the Angola-Benguela front', *Journal of Physical Oceanography,* 30, pp. 2589–2609.

Lea, D. W., Martin, P. A., Pak, D. K. and Spero, H. J. (2002) 'Reconstructing a 350 ky history of sea level using planktonic Mg/Ca and oxygen isotope records from a Cocos Ridge core', *Quaternary Science Reviews*, 21(1–3), pp. 283–293. doi: 10.1016/S0277-3791(01)00081-6.

Lear, C. H., Rosenthal, Y. and Slowey, N. (2002) 'Benthic foraminiferal Mg / Ca-paleothermometry : A revised core-top calibration', *Geochimica et Cosmochimica Acta*, 66(19), pp. 3375–3387. doi: 10.1016/S0016-7037(02)00941-9.

Lebreiro, S. M., Voelker, A. H. L., Vizcaino, A., Abrantes, F. G., Alt-Epping, U., Jung, S., Thouveny, N. and Gracia, E. (2009) 'Sediment instability on the Portuguese continental margin under abrupt glacial climate changes (last 60 kyr)', *Quaternary Science Reviews*, 28, pp. 3211–3223. doi: 10.1016/j.quascirev.2009.08.007.

Leroux, M. (2001) *The Meteorology and Climate of Tropical Africa*. Springer: Chichester.

Lezine, A. M. (1991) 'West African paleoclimates during the last climatic cycle inferred from an Atlantic deep-sea pollen record', *Quaternary Research*, 35(3), pp. 456–463. doi: 10.1016/0033-5894(91)90058-D.

Lézine, A. M., Duplessy, J. C. and Cazet, J. P. (2005) 'West African monsoon variability during the last deglaciation and the Holocene: Evidence from fresh water algae, pollen and isotope data from core KW31, Gulf of Guinea', *Palaeogeography, Palaeoclimatology, Palaeoecology*, 219(3–4), pp. 225–237. doi: 10.1016/j.palaeo.2004.12.027.

Lorious, C., Jouzel, J., Ritz, C., Mrlivat, L., Barkov, N, I., Korotkevitch, Y.S. and Vladimir, K. (1985) 'Delta ^{18}O record versus age for 150 ka in ice core VOSTOK. *PANGEA,* doi.org/10.1594/PANGAEA.860950.

Lutze, G. F. and Thiel, H. (1989) 'Epibenthic foraminifera from elevated microhabitats; Cibicidoides wuellerstorfi and Planulina ariminensis', *The Journal of Foraminiferal Research*, 19(2), pp. 153–158. doi: 10.2113/gsjfr.19.2.153.

Mackensen, Andreas; Bickert, T. (1999) 'Stable carbon isotopes in benthic foraminifera: proxies for deep and bottom water circulation and new production.', in Fischer, G. & Wefer, G. (ed.) *Use of Proxies in Paleoceanoraphy - Examples from the South Atlantic*. Berlin: Springer, pp. 229–254.

Mahé, G., Lerique, J., Olivry, J.-C. (1990) 'Le fleuve Ogooué au Gabon: Reconstitution des débits manquants et mise en évidence des variations climatiques à l'équateur', *Hydrologie Continentale*, 5(2), pp. 105–124.

Mahé, G. and Olivry, J.-C. (1995) 'Variations des précipitations et des écoulements en Afrique de l'Ouest et centrale de 1951 à 1989', *Sécheresse*, 1(6), pp. 109–117.

Maiklem, W.R. (1968) 'Some hydraulic properties of bioclastic carbonate grains', *Sedimentology,* 10, pp. 101-109.

Marret, F., Scourse, J., Jansen, J.H.F. and Schneider, R. (1999) 'Change and palaeoceanographic changes in west Central Africa during the last deglaciation: palynological investigation', *Earth and Planetary Science Series IIa,* 329(10), 721-726.

Marret, F., Scourse, J. D., Versteegh, G., Fred Jansen, J. H. and Schneider, R. (2001) 'Integrated marine and terrestrial evidence for abrupt Congo River palaeodischarge fluctuations during the last deglaciation', *Journal of Quaternary Science*, 16(8), pp. 761–766. doi: 10.1002/jqs.646.

Marret, F., Maley, J. and Scourse, J. (2006) 'Climatic instability in west equatorial Africa during the Mid- and Late Holocene', *Quaternary International*, 150(1), pp. 71–81. doi: 10.1016/j.quaint.2006.01.008.

Marret, F., Scourse, J., Kennedy, H., Ufkes, E. and Jansen, J. H. F. (2008) 'Marine production in the Congo-influenced SE Atlantic over the past 30,000 years: A novel dinoflagellate-cyst based transfer function approach', *Marine Micropaleontology*, 68(1–2), pp. 198–222. doi: 10.1016/j.marmicro.2008.01.004.

Marret, F., Kim, S.-Y. and Scourse, J. (2013) 'A 30,000 yr record of land–ocean interaction in the eastern Gulf of Guinea', *Quaternary Research*, 80(1), pp. 1–8. doi: 10.1016/j.yqres.2013.04.003.

Marsh, R., Mills, R.A., Green, D.R.H., Salter, I. and Taylor, S. (2007) 'Controls on sediment geochemistry in the Crozet region', *Deep Sea Research Part II: Topical Studies in Oceanography*, 54, pp. 2260–2274.

Martinson, D. G., Pisias, N. G., Hays, J. D., Imbrie, J., Moore, T. C. and Shackleton, N. J. (1987) 'Age dating and the orbital theory of the ice-ages: development of a high-resolution 0 to 300,000 year chronostratigraphy', *Quaternary Research*, 27(1), pp. 1–29.

Matthewson, A. P., Shimmield, G. B., Kroon, D. and Fallick, A. E. (1995) 'A 300 kyr high-resolution aridity record of the North African continent', *Paleoceanography*, 10(3), pp. 677–692. doi: 10.1029/94PA03348.

McGregor, H.V., Dupont, L., Stuut, J-B. and Kuhlmann, H. (2009) 'Vegetation change, goats, and religion: a 2000-year history of land use in southern Morocco', *Quaternary Science Reviews*, 28, pp. 1434–1448. doi: 10.1016/j.quascirev.2009.02.012.

McIntyre, A., Ruddiman, W. F., Karlin, K. and Mix, A. C. (1989) 'Surface water response of the equatorial Atlantic Ocean to orbital forcing', *Paleoceanography*, 4(1), pp. 19–55. doi: 10.1029/PA004i001p00019.

McIntyre, A. and Molfino, B. (1996) 'Forcing of Atlantic equatorial and subpolar millennial cycles by precession', *Science*, 274, pp. 0–3.

Meehl, G.A. and Tebaldi, C. (2004) 'More intense, more frequent, and longer lasting heat waves in the 21st century', *Science*, 305(August), pp. 994–997.

Meeuwis, J. M. and J. R. E. L. (1990) 'Surface thermal characteristics of the Angola-Benguela front', *South African Journal of Marine Science*, 9, pp. 261–279.

Miller, C. S. and Gosling, W. D. (2014) 'Quaternary forest associations in lowland tropical West Africa', *Quaternary Science Reviews*, 84, pp. 7–25. doi: 10.1016/j.quascirev.2013.10.027.

Mulitza, S., Rühlemann, C., Bickert, T., Hale, W., Pätzold, J. and Wefer, G. (1998) 'Late Quaternary $\delta^{13}C$ gradients and carbonate accumulation in the western equatorial Atlantic', *Earth and Planetary Science Letters*, 155(3–4), pp. 237–249. doi: 10.1016/S0012-821X(98)00012-0.

Mulitza, S., Heslop, D., Pittauerova, D., Fischer, H. W., Meyer, I., Stuut, J.-B., Zabel, M., Mollenhauer, G., Collins, J. a, Kuhnert, H. and Schulz, M. (2010) 'Increase in African dust flux at the onset of commercial agriculture in the Sahel region', *Nature*, 466(7303), pp. 226–8. doi: 10.1038/nature09213.

Muller, J. (1959) 'Palynology of recent Orinoco delta and shelf sediments: reports of the Orinoco shelf expedition; Volume 5', *Micropaleontology*, 5(1), pp. 1–32. doi: 10.2307/1484153.

Müller, P. J. (1977) 'C/N ratios in Pacific deep-sea sediments: Effect of inorganic ammonium and organic nitrogen compounds sorbed by clays', *Geochimica et Cosmochimica Acta*, 41(6), pp. 765–776.

Müller, P.J., Erlenkeuser, H., and von Grafenstein, R. (1983) 'Glacial-interglacial cycles in oceanic productivity inferred from organic carbon contents in eastern North Atlantic sediment cores', in Suess, E., and Thiede, J. (ed.) *Coastal Upwelling: Its Sediment Record (Pt. B.)*. New York: Plenum, pp. 365–398.

Müller, Peter J; Schneider, Ralph R; Ruhland, G. (1994) 'Late Quaternary PCO2 variations in the Angola Current: evidence from organic carbon δ13C and alkenone temperatures', in *Carbon Cycling in the Glacial Ocean: Constraints on the Oceans Role in Global Change*. Berlin: Springer, pp. 343–366.

Murray, J. W. (1991) *Ecology and palaeoecology of benthic foraminifera*. Harlow: Longman.

Myers, N., Mittermeier, R. A., Mittermeier, C. G., Da Fonseca, G. A. and Kent, J. (2000) 'Biodiversity hotspots for conservation priorities', *Nature*, 403, pp. 853–858.

Nicholson, S. E. (1996) 'A review of climate dynamics and climate variability in eastern Africa', in Johnson, T.C., Odada, E. (ed.) *The Limnology, Climatology and Palaeoclimatology of the East African Lakes.*, pp. 25–56.

Nicholson, S. E. (2009) 'A revised picture of the structure of the "monsoon" and land ITCZ over West Africa', *Climate Dynamics*, 32(7–8), pp. 1155–1171. doi: 10.1007/s00382-008-0514-3.

Nizou, J., Haneburth, T. J. J., Heslop, D., Schwenk, T., Palamenghi, L., Stuut, J-B. and Henrich, R. (2010) 'The Senegal River mud belt: A high-resolution archive of palaeoclimatic change and coastal evolution', *Marine Geology*, 278, pp. 150–164. doi: 10.1016/j.margeo.2010.10.002.

Nürnberg, D., Müller, A. and Schneider, R. R. (2000) 'Paleo-sea surface temperature calculations in the equatorial east Atlantic from Mg/Ca ratios in planktic foraminifera: A comparison to sea surface temperature estimates from UK37, oxygen isotopes, and foraminiferal transfer function', *Paleoceanography*, 15(1), pp. 124–134. doi: 10.1029/1999pa000370.

O'Gorman, P. A. and Schneider, T. (2009) 'The physical basis for increases in precipitation extremes in simulations of 21st-century climate change', *Proceedings of the National Academy of Sciences*, 106(35), pp. 14773–14777. doi: 10.1073/pnas.0907610106.

Peltier, W. R. (1994) 'Ice age paleotopography', *Science*, 265, pp. 195–201.

Peter U. Clark, Richard B. Alley, D. P. (1999) 'Northern Hemisphere Ice-Sheet Influences on Global Climate Change', *Science*, 286, pp. 1104–1111.

Peterson, L. C. (2000) 'Rapid changes in the hydrologic cycle of the tropical Atlantic during the last glacial', *Science*, 290(5498), pp. 1947–1951. doi: 10.1126/science.290.5498.1947.

Petit, R. J., Raynaud, D., Basile, I., Chappellaz, J., Ritz, C., Delmotte, M., Legrand, M., Lorius, C. and Pe, L. (1999) 'Climate and atmospheric history of the past 420,000 years from the Vostok ice core, Antarctica', *Nature*, 399, pp. 429–413. doi: 10.1038/20859.

Petschick, R., Kuhn, G. and Gingele, F. (1996) 'Clay mineral distribution in surface sediments of the South Atlantic: sources, transport, and relation to oceanography', *Marine Geology*, 130(3–4), pp. 203–229. doi: 10.1016/0025-3227(95)00148-4.

Piecuch, C.G., Bittermann, K., Kemp, A.C., Ponte, R.M., Little, C.M., Englehart, .S.E. and Lentz, S.J. (2018) 'River-discharge effects on United States Atlantic and Gulf coast sea-level changes', *PNAS,* 115(30), 7729-7734.

Pierre, C., Saliege, J. F., Urrutiaguer, M. J. and Giraudeau, J. (2001) 'Stable Isotope Record of the Last 500Ky At Site 1087 (Southern Cape Basin)', *Proceedings of the Ocean Drilling Program, Scientific Results*, 175(April), pp. 1–22.

Pisias, N. G., D. G. Martinson, T. C. Moore Jr., N. J. Shackleton, W. Prell, J. Hays, and G. B. (1984) 'High resolution strati- graphic correlation of benthic oxygen

isotope records spanning the last 300,000 years', *Marine Geology*, 56, pp. 119–136.

Prahl, F. G., Ertel, J. R., Goni, M. A., Sparrow, M. A. and Eversmeyer, B. (1994) 'Terrestrial organic carbon contributions to sediments on the Washington margin', *Geochimica et Cosmochimica Acta*, 58(14), pp. 3035–3048. doi: 10.1016/0016-7037(94)90177-5.

Prell, W. L., J. Imbrie, D. G. Martinson, J. J. Morley, N. G. Pisias, N. J. Shackleton, and H. F. (1986) 'Graphic correlation of oxygen isotope stratigraphy: Application to the Late Quaternary', *Paleoceanography*, 1, pp. 137–162.

Ravelo, A. C. (1991) *Reconstructing the tropical Atlantic seasonal thermocline using planktonic foraminifera*. Columbia University.

Ravelo, A. C. and Hillaire-Marcel, C. (2007) 'Chapter Eighteen The Use of Oxygen and Carbon Isotopes of Foraminifera in Paleoceanography', *Developments in Marine Geology*, 1(7), pp. 735–764. doi: 10.1016/S1572-5480(07)01023-8.

Raymond, P. A. and Bauer, J. E. (2001) 'DOC cycling in a temperate estuary : A mass balance approach using natural 14 C and C isotopes', *Program*, 46(3), pp. 655–667. doi: 10.4319/lo.2001.46.3.0655.

Reimer, P., Bard, E., Bayliss, A., Beck, J., Blackwell, P., Ramsey, C., Buck, C., Cheng, H., Edwards, R., Friedrich, M., Grootes, P., Guilderson, T., Haflidason, H., Hajdas, I., Hatté, C., Heaton, T., Hoffmann, D., Hogg, A., Hughen, K., Kaiser, K., Kromer, B., Manning, S., Niu, M., Reimer, R., Richards, D., Scott, E., Southon, J., Staff, R., Turney, C. and van der Plicht, J. (2013) 'Intcal13 and marine13 radiocarbon age calibration curves 0 – 50,000 years cal bp', *Radiocarbon*, 55(4), pp. 1869–1887. doi: 10.2458/rc.v51i4.3569.

Roberts, N., Jones, M. D., Benkaddour, A., Eastwood, W. J., Filippi, M. L., Frogley, M. R., Lamb, H. F., Leng, M. J., Reed, J. M., Stein, M., Stevens, L., Valero-Garcés, B. and Zanchetta, G. (2008) 'Stable isotope records of Late Quaternary climate and hydrology from Mediterranean lakes: the ISOMED synthesis', *Quaternary Science Reviews*, 27(25–26), pp. 2426–2441. doi: 10.1016/j.quascirev.2008.09.005.

Romero, O. E., Kim, J. H. and Donner, B. (2008) 'Submillennial-to-millennial variability of diatom production off Mauritania, NW Africa, during the last glacial cycle', *Paleoceanography*, 23(3), pp. 1–17. doi: 10.1029/2008PA001601.

Rossignol-Strick, M. (1983) 'African monsoons, an immediate climate response to orbital insolation', *Nature*, 304(5921), pp. 46–49. doi: 10.1038/304046a0.

Rothwell, R.G., Hoogakker, B., Thomson, J., Croudace, I.W. and Frenz, M. (2006) 'Turbidite emplacement on the southern Balearic Abyssal Plain (western Mediterranean Sea) during the Marine Isotope Stages 1-3: an application of ITRAX XRF scanning of sediment cores to lithostratigraphic analysis', in Rothwell, R. G. (ed.) *New Techniques in Sediment Core Analysis2*. Geological Society of London, pp. 79–98. doi: 10.1144/GSL.SP.2006.267.01.06.

Rothwell, R.G. and Croudace, I. W. (2015) 'Twenty Years of XRF Core Scanning Marine Sediments: What Do Geochemical Proxies Tell Us?', in : Croudace, I.W.

and Rothwell, R. G. (ed.) *Micro-XRF Studies of Sediment Cores: Applications of a non-destructive tool for the environmental science*. London: Springer, pp. 25–102.

Ruhlemann, C., Frank, M., Hale, W., Mangini, A., Mulitza, S., Muller, P. J. and Wefer, G. (1996) 'Late Quaternary productivity changes in the western equatorial Atlantic: Evidence from 230Th-normalized carbonate and organic carbon accumulation rates', *Marine Geology*, 135, pp. 127–152.

Sarnthein, M., Tetzlaff, G., Koopmann, B., Wolter, K. and Pflaumann, U. (1981) 'Glacial and interglacial wind regimes over the eastern subtropical Atlantic and North-West Africa', *Nature*, 293, pp. 193–196. doi: 10.1038/293193a0.

Sarnthein, M., Erlenkeuser, H., von Grafenstein, R. and Schröder, C. (1984) 'Stable-isotope stratigraphy for the last 750,000 years; "Meteor" core 13519 from the eastern equatorial Atlantic', *Meteor-Forschungsergebnisse*, 38, pp. 9–24.

Sarnthein, M., Winn, K., Duplessy, J. -C and Fontugne, M. R. (1988) 'Global variations of surface ocean productivity in low and mid latitudes: Influence on CO2 reservoirs of the deep ocean and atmosphere during the last 21,000 years', *Paleoceanography*, 3(3), pp. 361–399. doi: 10.1029/PA003i003p00361.

Scheffel, Richard L. and Wernet, S. J. (1982) *Natural Wonders of the World.* Reader's Digest Association, Inc.

Schefuβ, E., Schouten, S. and Schneider, R. R. (2005) 'Climatic controls on central African hydrology during the past 20,000 years', *Nature*, 437(7061), pp. 1003–6. doi: 10.1038/nature03945.

Schillereff, D. N. (2015) *Lake sediment records of flood frequency and magnitude.* PhD Thesis. University of Liverpool.

Schillereff, D. N., Chiverrell, R. C., Macdonald, N. and Hooke, J. M. (2016) 'Hydrological thresholds and basin control over paleoflood records in lakes', *Geology*, 44(1), pp. 43–46. doi: 10.1130/G37261.1.

Schmidt, M. W., Chang, P., Hertzberg, J. E., Them II, T. R., Ji, L. and Otto-Bliesner, B. (2012) 'Impact of abrupt deglacial climate change on tropical Atlantic subsurface temperatures', *PNAS*, 109(36), pp. 1–5. doi: 10.1073/pnas.1207806109.

Schmiedl, G. and Mackensen, A. (1997) 'Late Quaternary paleoproductivity and deep water circulation in the eastern South Atlantic Ocean: Evidence from benthic foraminifera', *Palaeogeography, Palaeoclimatology, Palaeoecology*, 130(1–4), pp. 43–80. doi: 10.1016/S0031-0182(96)00137-X.

Schneider, R. R. and Muller, P.J., Wefer, G. (1994) 'Late Quaternary paleoproductivity changes off the Congo deduced from stable carbon isotopes of planktonic foraminifera', *Palaeogeography, Palaeoclimatology, Palaeoecology*, 110, pp. 255–274.

Schneider, R. R. and Moller, P. J. (1995) 'Late Quaternary surface circulation in the east equatorial South', *Paleoceanography*, 10(2), pp. 197–219.

Schneider, R. R., Price, B., Miiller, P. J., Kroon, D. and Alexander, I. (1997) 'Monsoon related variations in Zaire (Congo) sediment load and influence of fluvial silicate supply on marine productivity in the east equatorial Atlantic during the last 200, 000 years feldspar although', *Paleoceanography,* 12(3), pp. 463–481.

Schumacher, B.A. (2001). *Methods for the determination of total organic carbon (TOC) in soils and sediments*. PhD Thesis. United States Environmental Protection Agency, Las Vegas.

Scourse, J., Marret, F., Versteegh, G. J. M., Jansen, J. H. F., Schefuß, E. and van der Plicht, J. (2005) 'High-resolution last deglaciation record from the Congo fan reveals significance of mangrove pollen and biomarkers as indicators of shelf transgression', *Quaternary Research*, 64(1), pp. 57–69. doi: 10.1016/j.yqres.2005.03.002.

Seranne, M., Bruguier, O. and Moussavou, M. (2008). 'U–Pb single zircon grain dating of Present fluvial and Cenozoic aeolian sediments from Gabon: consequences on sediment provenance, reworking, and erosion processes on the equatorial West African margin' *Bulletin de la Societe Geologique de France* ,179(1): 29-40.

Sexton, P. F., Wilson, P. a. and Pearson, P. N. (2006) 'Microstructural and geochemical perspectives on planktic foraminiferal preservation: "glassy" versus "frosty"', *Geochemistry, Geophysics, Geosystems*, 7(12). doi: 10.1029/2006GC001291.

Shackleton, N. J. (1967) 'Oxygen Isotope Analyses and Pleistocene Temperatures Re-assessed', *Nature*, 215(5096), pp. 15–17. doi: 10.1038/215015a0.

Shanahan, T. M., Overpeck, J. T., Wheeler, C. W., Beck, J. W., Pigati, J. S., Talbot, M. R., Scholz, C. a., Peck, J. and King, J. W. (2006) 'Paleoclimatic variations in West Africa from a record of late Pleistocene and Holocene lake level stands of Lake Bosumtwi, Ghana', *Palaeogeography, Palaeoclimatology, Palaeoecology*, 242(3–4), pp. 287–302. doi: 10.1016/j.palaeo.2006.06.007.

Shanahan, T. M., Beck, J. W., Overpeck, J. T., McKay, N. P., Pigati, J. S., Peck, J. A., Scholz, C. A., Heil, C. W. and King, J. (2012) 'Late Quaternary sedimentological and climate changes at Lake Bosumtwi Ghana: New constraints from laminae analysis and radiocarbon age modeling', *Palaeogeography, Palaeoclimatology, Palaeoecology*, 361–362, pp. 49–60. doi: 10.1016/j.palaeo.2012.08.001.

Shanahan, T. M., Peck, J. A., McKay, N., Heil, C. W., King, J., Forman, S. L., Hoffmann, D. L., Richards, D. A., Overpeck, J. T. and Scholz, C. (2013) 'Age models for long lacustrine sediment records using multiple dating approaches - An example from Lake Bosumtwi, Ghana', *Quaternary Geochronology*, 15, pp. 47–60. doi: 10.1016/j.quageo.2012.12.001.

Siani, G., Colin, C., Michel, E., Carel, M., Richter, T., KIssel, C. and Dewilde, F. (2010) 'Late Glacial to Holocene terrigenous sediment record in the Northern Patgonian margin: Paleoclimte implications', *Palaeogeography, Palaeoclimatology, Palaeoecology*, 297, pp. 26–36. doi: 10.1016/j.paleo.2010.07.011.

Sikes, E.L. and Keigwin, L. D. (1994) 'Equatorial Atlantic sea surface temperature for the last 30 kyr: A comparison of UK37 and 18O foraminiferal assemblage temperature estimates', *Paleoceanography*, 9(1), pp. 31–45.

Scheiter, S. and Higgins S, I. (2008) 'Impacts of climate change on the vegetation of Africa: an adaptive dynamic vegetation modelling approach', *Global Change Biology*, 15(2224–2246).

Shi, N., Schneider, R., Beug, H-J. and Dupont, L.M. (2001) 'Southeast trade wind variations during the last 135 kyr: evidence from pollen spectra in eastern South Atlantic sediments', *Earth and Planetary Science Letters,* 187, pp. 311-321.

Skonieczny, C., Paillou, P., Bory, A., Bayon, G., Biscara, L., Crosta, X., Eynaud, F., Eacute, B. M., Revel, M., Aleman, N., Barusseau, J. P., Vernet, R., Lopez, S. and Grousset, F. (2015) 'African humid periods triggered the reactivation of a large river system in Western Sahara', *Nature Communications*, 6, pp. 1–6. doi: 10.1038/ncomms9751.

Spalding, M.D., Blasco, F. and Field, C. (1997) World Mangrove Atlas. Okinawa, Japan: The International Society for Mangrove Ecosystems.

Spero, H. J. and Lea, D. W. (1993) 'Intraspecific stable isotope variability in the planktic foraminifera Globigerinoides sacculifer: Results from laboratory experiments', *Marine Micropaleontology*, 22(3), pp. 221–234. doi: 10.1016/0377-8398(93)90045-Y.

Spofforth, D.J.A., Palike, H., Green, D. (2008) 'Paleogene record of elemental concentrations in sediments from the Arctic Ocean obtained by XRF analyses', *Paleoceanography*, 23. doi: 10.1029/2007PA001489.

Stoll, H. M. (2005) 'Limited range of interspecific vital effects in coccolith stable isotopic records during the Paleocene-Eocene thermal maximum', *Paleoceanography*, 20(1), pp. 1–10. doi: 10.1029/2004PA001046.

Stoner, J.S. and St-Onge, G. (2007) 'Chapter Three Magnetic Stratigraphy in Paleoceanography: Reversals, Excursions, Paleointensity, and Secular Variation', *Developments in Marine Geology*, 1, pp. 99–138.

Stuiver, M. and Reimer P, J. (1993) 'Extended 14C data base and revised calib 3.0 ^{14}C age calibration program', 35(1), pp. 215–230.

Stuiver, M., Reimer, P.J. and Braziunas, T. F. (1998) 'High-precision radiocarbon age calibration for terrestrial and marine samples', *Radiocarbon,* 40(3), pp. 1127–1151.

Stuut, J. B. W., Prins, M. A., Schneider, R. R., Weltje, G. J., Fred Jansen, J. H. and Postma, G. (2002) 'A 300-kyr record of aridity and wind strength in southwestern Africa: Inferences from grain-size distributions of sediments on Walvis Ridge, SE Atlantic', *Marine Geology*, 180(1–4), pp. 221–233. doi: 10.1016/S0025-3227(01)00215-8.

Subramaniam, A., Mahaffey, C., Johns, W. and Mahowald, N. (2013) 'Equatorial upwelling enhances nitrogen fixation in the Atlantic Ocean', *Geophysical Research Letters*, 40(9), pp. 1766–1771. doi: 10.1002/grl.50250.

Thiéblemont, D., Castaing, C., Billa, M., Bouton, P., & Préat, A. (2009) 'Notice explicative de la carte géologique et des ressources minérales de la République Gabonaise à 1/1000000', *Programme Sysmin*, 384.

Thomson, J., Croudace, I.W. and Rothwell, R. G. (2006) 'A geochemical application of the ITRAX scanner to a sediment core containing eastern Mediterranean sapropel units', in New Techniques in Sediment Core Analysis, pp. 65–77. doi: 10.1144/ GSL.SP.2006.267.01.05.

Thunell, R. C., Tappa, E., Pride, C. and Kincaid, E. (1999) 'Sea-surface temperature anomalies associated with the 1997 – 1998 El Niño recorded in the oxygen isotope composition of planktonic foraminifera', *Geology*, 27, pp. 843–846. doi: 10.1130/0091-7613(1999)027<0843.

Tjallingii, R., Röhl, U., Kölling, M. and Bickert, T. (2007) 'Influence of the water content on X-ray fluorescence corescanning measurements in soft marine sediments', *Geochemistry, Geophysics, Geosystems*, 8(2), pp. 1–12. doi: 10.1029/2006GC001393.

Tjallingii, R., Claussen, M., Stuut, J.-B. W., Fohlmeister, J., Jahn, A., Bickert, T., Lamy, F. and Röhl, U. (2008) 'Coherent high- and low-latitude control of the northwest African hydrological balance', *Nature Geoscience*, 1(10), pp. 670–675. doi: 10.1038/ngeo289.

Tjallingii, R., Stattgger, K., Wetzel, A. and Van Phach, P. (2011) 'Infilling and flooding of the Mekong River incised valley during deglacial sea-level rise', *Quaternary Science Reviews*, 29, pp. 1432–1444. doi: 10.1016/j.quatscirev.2010.02.022.

Upton, K. and O Dochartaigh, B. E. (2016) Africa Groundwater Atlas: Hydrogeology of Gabon. British Geological Survey. Available at: http://earthwise.bgs.ac.uk/index.php/Hydrogeology_of_Gabon (Accessed: 1 May 2017).

Van Campo, E. and Bengo, M. D. (2004) 'Mangrove palynology in recent marine sediments off Cameroon', *Marine Geology*, 208(2–4), pp. 315–330. doi: 10.1016/j.margeo.2004.04.014.

van Geel, B., Gelorini, V., Lyaruu, A., Aptroot, A., Rucina, S., Marchant, R., Damsté, J. S. S. and Verschuren, D. (2011) 'Diversity and ecology of tropical African fungal spores from a 25,000-year palaeoenvironmental record in southeastern Kenya', *Review of Palaeobotany and Palynology*, 164(3–4), pp. 174–190. doi: 10.1016/j.revpalbo.2011.01.002.

Van Hoang, L., Clift, P. D., Schwab, a. M., Huuse, M., Nguyen, D. a. and Zhen, S. (2010) 'Large-scale erosional response of SE Asia to monsoon evolution reconstructed from sedimentary records of the Song Hong-Yinggehai and Qiongdongnan basins, South China Sea', Geological Society, London, Special Publications, 342(1), pp. 219–244. doi: 10.1144/SP342.13.

Verosub, K. L. and Roberts, A. P. (1995) 'Environmental magnetism: Past, present, and future', *Geophysical Research Letters*, 100, pp. 2175–2192. doi: 10.1029/94JB02713.

Versteegh, G. J. ., Schefuß, E., Dupont, L., Marret, F., Sinninghe Damsté, J. S. and Jansen, J. H. F. (2004) 'Taraxerol and Rhizophora pollen as proxies for tracking past mangrove ecosystems', *Geochimica et Cosmochimica Acta*, 68(3), pp. 411–422. doi: 10.1016/S0016-7037(03)00456-3.

Vincens, A., Leźine, A. M., Buchet, G., Lewden, D., Le Thomas, A., Agwu, C. O. C., Azéma, C., Ballouche, a., Baxter, a., Bengo, M. D., Beuning, K., Bolick, M. R., Bonnefille, R., Bousman, C. B., Buchet, N., Bumey, D. a., Caratini, C., Carrion, J. S., Cazet, J. P., Cohen, J., Cooresman, B., Cour, P., Denèfle, M., Dupont, L., Duzer, D., Edorh, T., El Ghazali, G. E. B., El Moslimany, a. P., El Moutaki, S., Elenga, H., Guinet, P., Hamilton, a. C., Hedberg, O., Hooghiemstra, H., Irving, S. J. E., Jahns, S., Jolly, D., Kadomura, H., Kendall, R. L., Lamb, H. F., Laseski, R. a., Leroy, S., Livingstone, D. a., Magioncalda, R., Maley, J., Marchant, R., Marret, F., Matsumoto, K., Meadows, M., Mercuri, a. M., Mohammed, U. M., Morrison, M. E. S., Moscol-Olivera, M. C., Nakimera-Ssemmanda, I., Ntaganda, C., Nyakale, M., Osadtchy, C., Perrott, R. a., Pons, a., Quézel, P., Reynaud-Farrera, I., Riollet, G., Ritchie, J. C., Roche, E., Rucina, S. M., Salzmann, U., Schulz, E., Scott, L., Shi, N., Soulet, G., Sowunmi, M. a., Straka, H., Sugden, J. M., Taylor, D., Tissot, C., Van Campo, E., Van Campo, M., Van Zinderen Bakker, E. M., Vilimumbalo, S., Waller, M. P., Watrin, J. and Ybert, J. P. (2007) 'African pollen database inventory of tree and shrub pollen types', *Review of Palaeobotany and Palynology*, 145(1–2), pp. 135–141. doi: 10.1016/j.revpalbo.2006.09.004.

Waelbroeck, C., Labeyrie, L., Michel, E., Duplessy, J. C., McManus, J. F., Lambeck, K., Balbon, E. and Labracherie, M. (2002) 'Sea-level and deep water temperature changes derived from benthic foraminifera isotopic records', *Quaternary Science Reviews*, 21(1–3), pp. 295–305. doi: 10.1016/S0277-3791(01)00101-9.

Wang, M., Zheng, H., Xie, X., Fan, D., Yang, S., Zhoa, Q. and W. K. (2011) 'A 600-year flood history in the Yangtze River drainage: comparison between a subaqueous delta and historical records', *Chinese Science Bulletin*, 56, pp. 188–195. doi: 10.1007/s11434-010-4212-2.

Watanabe, T., Winter, A. and Oba, T. (2001) 'Seasonal changes in sea surface temperature and salinity during the Little Ice Age in the Caribbean Sea deduced from Mg/Ca and 18O/16O ratios in corals', *Marine Geology*, 173(1–4), pp. 21–35. doi: 10.1016/S0025-3227(00)00166-3.

Wedepohl, P.M., J.R.E. Lurjeharms and J. M. M. (2000) ': Surface drift in the south-east Atlantic Ocean', *South African Journal of Marine Science*, 22, pp. 71–79.

Weldeab, S. (2012) 'Bipolar modulation of millennial-scale West African monsoon variability during the last glacial (75,000-25,000 years ago)', *Quaternary Science Reviews*, 40, pp. 21–29. doi: 10.1016/j.quascirev.2012.02.014.

Weldeab, S., Lea, D. W., Schneider, R. R. and Andersen, N. (2007) '155,000 years of West African monsoon and ocean thermal evolution', *Science*, 316(5829), pp. 1303–7. doi: 10.1126/science.1140461.

Weldeab, S., Friedrich, T., Timmermann, A. and Schneider, R. R. (2016) 'Strong middepth warming and weak radiocarbon imprints in the equatorial Atlantic during Heinrich 1 and Younger Dryas', *Paleoceanography*, 31(8), pp. 1070–1082. doi: 10.1002/2016PA002957.

Weltje, G.J.; Meijer, X.D and de Boer, P. L. (1998) 'Stratigraphic inversion of siliciclastic basin fills: a note on the distinction between supply signals resulting from tectonic and climatic forcing', *Basin Research*, 10(1), p. 129.

Weltje, G. J. and von Eynatten, H. (2004) 'Quantitative provenance analysis of sediments: Review and outlook', *Sedimentary Geology*, 171(1–4), pp. 1–11. doi: 10.1016/j.sedgeo.2004.05.007.

Weltje, G.J. and Tjallingii, R. (2008) 'Calibration of XRF core scanners for quantitative geochemical logging of sediment cores: theory and application', *Earth and Planetary Science Letters*, 247, pp. 423–438.

White, F. (1983) *The Vegetation of Africa*. Paris: UNESCO.

Y.-H. Li and Schoonmaker, J. (2003) 'Chemical composition and mineralogy of marine sediments', *Chemical Composition and Mineralogy of Marine Sediments*, pp. 35.

Yamamuro, M. and Kayanne, H. (1995) 'Rapid direct determination of organic carbon and nitrogen in carbonate-bearing sediments with a Yanaco MT-5 CHN analyzer', *Limnology and Oceanography*, 40(5), pp. 1001–1005. doi: 10.4319/lo.1995.40.5.1001.

Zachos, J. C., Pagani, M., Sloan, L., Thomas, E., and Billups, K. (2001) 'Trends, rhythms, and aberrations in global climate 65 Ma to present', *Science*, 292, pp. 686–693.

Zachos, J. C., Bralower, T. J. and Premoli-silva, I. (2009) 'A Transient Rise in Tropical Sea Surface Temperature During the Paleocene-Eocene Thermal Maximum', *Science*, 302(2003), pp. 1151–1154. doi: 10.1126/science.1090110.

Zaragosi, S., Bourillet, J-F., Eynaud, F., Toucanne, S., Denhard, B., Van Toer, A., Lanfumey, V. (2006) 'The impact of the last European deglaciation on the deep-sea turbidite systems of the Celtic-Armorican margin (Bay of Biscay)', *Geo-Marine Letters*, 26, pp. 17–329. doi: 10.1007/s00367-006-0048-9.

Žarić, S., Donner, B., Fischer, G., Mulitza, S. and Wefer, G. (2005) 'Sensitivity of planktic foraminifera to sea surface temperature and export production as derived from sediment trap data', *Marine Micropaleontology*, 55(1–2), pp. 75–105. doi: 10.1016/j.marmicro.2005.01.002.

Zarriess, M. (2010) 'Bi-polar seesaw in the northeastern tropical Atlantic during Heinrich stadials', *Marine Micropaleontology*, 76, pp. 76–91. doi: 10.1016/j.marmicro.2010.03.001.

Zarriess, M. and MacKensen, A. (2011) 'Testing the impact of seasonal phytodetritus deposition on d13C of epibenthic foraminifer Cibicidoides wuellerstorfi: A 31,000 year high-resolution record from the northwest African continental slope', *Paleoceanography*, 26(2). doi: 10.1029/2010PA001944.

Zhao, M., Dupont, L., Eglinton, G. and Teece, M. (2003) 'n-Alkane and pollen reconstruction of terrestrial climate and vegetation for N.W. Africa over the last 160 kyr', *Organic Geochemistry*, 34(1), pp. 131–143. doi: 10.1016/S0146-6380(02)00142-0.

Ziveri, P., Stoll, H., Probert, I., Klaas, C., Geisen, M., Ganssen, G. and Young, J. (2003) 'Stable isotope "vital effects" in coccolith calcite', *Earth and Planetary Science Letters*, 210(1–2), pp. 137–149. doi: 10.1016/S0012-821X(03)00101-8.